The Equivalent Shear Masonry Model

An Alternative Material Model for Masonry Diagonal Staircase Cracking

by

Evelijn Lisanne Vink

A Thesis Submitted in Partial Fulfilment
of the Requirements for the Degree of

Master of Science

in Structural Engineering,
Faculty of Civil Engineering and Geosciences,
Delft University of Technology

TUDelft Delft University of Technology

Summary

This thesis proposes a new material model for masonry, the Equivalent Shear Masonry Model. It was created as an improvement of the Engineering Masonry Model, a smeared cracking material model that was developed by DIANA FEA BV in collaboration with Delft University of Technology to model existing masonry typical for the earthquake-troubled province of Groningen.

The Engineering Masonry Model is an orthotropic model that evaluates failure in the direction perpendicular to the bed joints (i.e. the local vertical direction) and in the direction perpendicular to the head joints of the masonry (i.e. the local horizontal direction). For tension, the model uses a bi-linear constitutive relationship with secant unloading and reloading. The horizontal tensile strength can optionally be derived from the shear strength of the bed joints, assuming a toothed vertical crack failure mechanism. The compressive behaviour is represented by a non-linear constitutive relationship with a combination of linear and secant unloading, and secant reloading. The shear failure along the bed joints is described by a Coulomb friction criterion, with linear unloading and reloading.

As an alternative to the evaluation of the stresses perpendicular to the head joints, the Engineering Masonry Model can evaluate the stress in the direction normal to the expected diagonal staircase cracks. However, this diagonal crack option does not have its own constitutive relation, it only limits the diagonal normal stress. Thus the deformations normal to the cracks do not directly contribute to any softening. This option works well for cases where the diagonal cracks occur as a result of diagonal tension, for instance with rocking mechanisms in slender walls.

However, diagonal staircase cracks observed in laboratory test of wide shear walls often seem to open up horizontally rather than diagonally, like in Figure 1. Besides, horizontal tensile stress may also cause diagonal staircase cracks. The force-displacement diagrams of severely damaged shear wall tests show a hysteresis loop that is similar to the hysteresis loop of the shear behaviour of the bed joints. Therefore, it is interesting to regard the diagonal staircase crack as a horizontal phenomenon, as a diagonal crack that opens up horizontally under the influence of horizontal forces, see Figure 2, whose behaviour is determined by the shear behaviour of the bed joint.
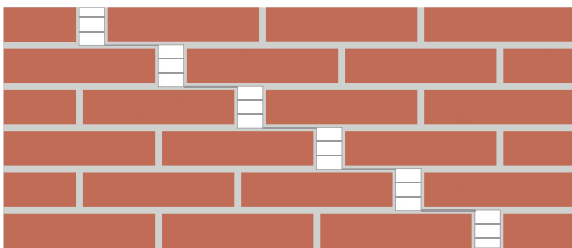
Figure 1: Deformed shape of masonry with a diagonal staircase crack that opens up horizontally.
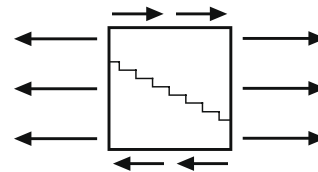
Figure 2: Failure mode considered by the Equivalent Shear Masonry Model: diagonal cracking due to horizontal normal stress and shear stress.

The horizontal opening of a diagonal crack was the inspiration to develop the alternative Equivalent Shear Masonry Model. Its diagonal staircase crack failure criterion is thus derived from horizontal force equilibrium at this crack, between the effects of the load (i.e. the internal stresses) and the resistance of the material (i.e. the shear strength of the bed joint). The criterion combines horizontal normal stress and shear stress as follows:

$$\tau_{xy} + \sigma_{xx} \tan \alpha \leq \tau_{max} \tag{1}$$

where τ_{xy} is (the absolute value of) the masonry shear stress parallel to the bed joint, σ_{xx} is the masonry horizontal tensile stress, $\tan \alpha$ is the height-width ratio of the expected diagonal staircase crack (depending on the type of bond and the brick and mortar dimensions) and τ_{max} is the shear strength

of the bed joints. The left-hand side of Equation 1 is referred to as the equivalent shear stress τ_{eq}. An equivalent measure for the deformation γ_{eq} is formulated as:

$$\gamma_{eq} = \gamma_{xy} + \frac{\varepsilon_{xx}}{\tan\alpha} \tag{2}$$

where γ_{xy} is (the absolute value of) the masonry shear strain parallel to the bed joint and ε_{xx} is the masonry horizontal tensile strain.

The constitutive relation between these two equivalent measures of stress and deformation follows the shear behaviour of the bed joints, see Figure 3. The shear behaviour and the horizontal tensile behaviour are linear and independent of each other as long as their combined equivalent measure does not exceed the material's shear strength. When it does, their combined behaviour is described by the graph in Figure 3. The cumulative equivalent shear strain dictates the softening. Note that the shear unloading behaviour and horizontal tensile unloading behaviour are also linear and independent of each other.
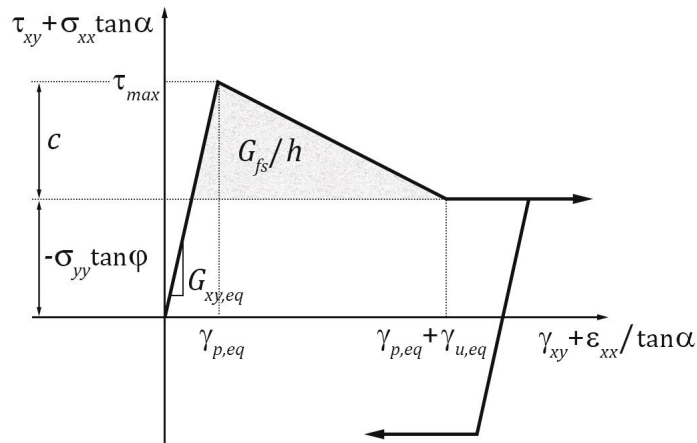
Figure 3: Stress-strain diagram illustrating the equivalent shear behaviour.

Besides the diagonal staircase crack failure described here, the Equivalent Shear Masonry Model evaluates vertical tension, and horizontal and vertical compression, using the same constitutive relations as in the Engineering Masonry Model.

The theoretical description above is implemented as a Fortran subroutine to be used as a user supplied material model in Diana's finite element analysis software. The compiled user supplied material model of the Equivalent Shear Masonry Model is called `usrmat_eqshma.dll`.

The model has first been verified on homogeneously strained single element problems for different load paths. These analyses showed that the user supplied material model works as intended for two-dimensional plane stress elements, for the following load cases: vertical tension and compression loading, unloading and reloading; and for the following load cases while under constant vertical compression: horizontal tensile loading and unloading, shear loading and unloading and three combinations of simultaneous shear loading and/or unloading and horizontal tensile loading and/or unloading. For comparison, the same single element analyses were performed with the Engineering Masonry Model's *Diagonal stair-case cracks* option, but those showed peculiar results, namely sudden drops in the stress-strain diagram and confused crack status output.

After this verification, a validation was made against a masonry unit cell that was analysed with a micro modelling approach in order to approximate the real behaviour of masonry in a detailed manner. The same separate shear and horizontal extension load cases were investigated as for the single element model, as well as three variants of each of the combined shear and horizontal tension load cases. The results showed clear resemblance to the Equivalent Shear Masonry Model's single element model results. For the combined simultaneous shear and horizontal tensile load cases, the resemblance was most clear when the ratio between the extension deformation increment and the shear deformation increment was close to $\tan\alpha$.

Next, the model was validated at structural level, against a shear wall experiment. The shear wall experiment was analysed with a full scale finite element model using the Equivalent Shear Material Model. The experiments modelled are TUD-COMP-47 and TUD-COMP-48, both double clamped shear walls subjected to asymmetric cyclic horizontal loading. The analysis with the Equivalent Shear Masonry Model showed promising characteristics. Though the diagonal cracks were still slightly too steep, their localisation was satisfactory. The force-drift diagram showed linear behaviour in the first cycles, then continued non-linear with some inelastic deformation, and then showed softening and a residual plateau in later cycles. The hysteresis loop had a slight S-shape and a similar width over its entire height. The peak force was slightly reduced with each repetition in each cycle.

Compared to the Engineering Masonry Model's *Diagonal stair-case cracks* option, the model gave smoother results and had less convergence issues. However, it did need more iterations per step. Therefore it is recommended to adjust the 'tangent' shear stiffness returned by the code. The crack direction of the Equivalent Shear Masonry Model is slightly better and its crack localisation is much more realistic. Both models did not reach the experimental peak strength and showed a too steep softening regime, though calibration might be able to improve this. The peak force reduction of the Equivalent Shear Masonry Model was not matched by either the Engineering Masonry Model's *Diagonal stair-case cracks* option or its *Tensile strength head-joint defined by friction* option.

It is recommended to further validate the Equivalent Shear Masonry Model. The behaviour of the material model under other combined load cases should be investigated, for instance the shear behaviour under a varying or even tensile overload. Also other experimental tests should be modelled, for instance slender shear walls that show rocking, window banks that suffer tensile bending failure and wide shear walls that are loaded much further than light damage. Furthermore, some improvements to the theory and the subroutine code are recommended, and eventually expansion to shell elements and three-dimensional solid elements is recommended.

In conclusion, the Equivalent Shear Masonry Model shows promising characteristics to model diagonal staircase cracking in masonry. It produces smooth force-displacement diagrams and has less convergence problems than the Engineering Masonry Model's *Diagonal stair-case cracks* option. It generates cracks that are less steep and more localized. The model is able to represent post-peak behaviour of shear walls and even displays peak force reduction. Therefore, it is recommended that the material model is developed further, so that hopefully one day it can be used in practice to provide more accurate masonry cracking predictions.

Preface

Dear reader,

This thesis report is written as part of the completion of my master study in Civil Engineering at Delft University of Technology. It was written after a difficult time in my life, so completing this thesis has been a rewarding way to put that behind me.

Firstly, I would like to thank Bregje for restoring enough of my confidence to resume my study. Secondly, I would like to express my gratitude to the members of my graduation committee. I would like to thank my professor Jan for creating a save environment for me to reintegrate, without being overwhelmed by regulatory obligations. I would like to thank my supervisor Michele for his patience and his ever positive and constructive comments. They really helped me to push through. I would like to thank Francesco for his critical feedback, that certainly improved the quality of my thesis. I would like to thank Marianthi for introducing me to the user supplied subroutine and for her thorough proofreading. And last but not least, I would like to thank Geert for pointing out any unclear parts and for encouraging me to make my story understandable for uninitiated people.

Furthermore, I would to thank my husband Niels for his considerable IT support and his proofreading. Finally, I would like to thank all my friends and family, whose support and kindness have been instrumental to the successful completion of this thesis.

Evelijn Vink
Delft, 10 October 2019

Contents

List of Symbols

$\mathbf{a}$	vector containing the nodal displacements
$\mathbf{a}^1$	vector containing the nodal displacements after the first iteration
b_{brick}	brick width
b_{crack}	width of a crack segment
b_{joint}	joint width
b_{model}	model width
c	cohesion, or currently remaining cohesion
c_0	initial cohesion
$\mathbf{da}^2$	vector containing the variations of the strain increments of the second iteration
E	normal stiffness
E_0	initial stiffness
E_{linear}	linear stiffness
E_{load}	load stiffness
E_n	stiffness normal to the diagonal staircase crack
$\mathbf{E}_{(n,t)}$	stiffness matrix in the (n,t)-axis system
E_{secant}	secant stiffness
$E_{tangent}$	tangent stiffness
E_{unload}	unload stiffness
E_x	horizontal stiffness, or stiffness normal to the head joint
$\mathbf{E}_{(x,y)}$	stiffness matrix in the (x,y)-axis system
E_y	vertical stiffness, or stiffness normal to the bed joint
$\mathbf{f}$	vector containing the nodal forces
f_c	compressive strength
f_{cx}	horizontal compressive strength
f_{cy}	vertical compressive strength
$\mathbf{f}_e$	vector containing the external nodal forces
$\mathbf{f}_e^t$	vector containing the external nodal forces at time t
$\mathbf{f}_e^{t+\Delta t}$	vector containing the external nodal forces at time $t + \Delta t$
$\mathbf{f}_i$	vector containing the current internal nodal forces
$\mathbf{f}_i^0$	vector containing the current internal nodal forces at the beginning of the step
$\mathbf{f}_i^1$	vector containing the current internal nodal forces after the first iteration
$\mathbf{f}_i^2$	vector containing the current internal nodal forces after the second iteration
$\mathbf{f}_i^t$	vector containing the current internal nodal forces at time t
f_t	tensile strength
f_{tx}	horizontal tensile strength
$f_{tx,j}$	horizontal head joint tensile strength
f_{ty}	vertical tensile strength
$f_{t\alpha}$	diagonal tensile strength

G_{fc}	compressive fracture energy
G_{fcx}	horizontal compressive fracture energy
G_{fcy}	vertical compressive fracture energy
G_{fs}	shear fracture energy
G_{ft}	tensile fracture energy
G_{ftx}	horizontal tensile fracture energy
G_{fty}	vertical tensile fracture energy
G_{nt}	shear stiffness parallel to the diagonal staircase crack
G_{xy}	shear stiffness, or shear stiffness parallel to the bed joint
$G_{xy,eq}$	apparent equivalent shear stiffness at peak
h	crack band width
h_{brick}	brick height
h_{crack}	height of a crack segment
h_{joint}	joint height
h_{model}	model height
$\mathbf{K}$	global stiffness matrix
$\mathbf{K}^0$	global stiffness matrix at the beginning of the step
$\mathbf{K}^1$	global stiffness matrix after the first iteration
$\mathbf{K}^2$	global stiffness matrix after the second iteration
n	factor strain at compressive strength
(n,t)	orthogonal axis system with the n-axis normal to the diagonal staircase crack
$\mathbf{R}$	standard rotation matrix
$\mathbf{r}^1$	vector containing the out-of-balance forces after the first iteration
$\mathbf{r}^2$	vector containing the out-of-balance forces after the second iteration
$\mathbf{R}_\varepsilon$	rotation matrix for strain in vector format
$\mathbf{R}_\sigma$	rotation matrix for stress in vector format
t	time
u_e	prescribed horizontal displacement to create horizontal extension
u_s	prescribed horizontal displacement to create shear shear deformation
u_x	horizontal displacement
$u_x(x,y)$	horizontal displacement field
u_y	vertical displacement
$u_y(x,y)$	vertical displacement field
w_{crack}	crack width
(x,y)	orthogonal axis system with the x-axis parallel to the bed joint
α	angle between the diagonal staircase crack and the bed joint
$\alpha_{c,ref}$	reference compressive strain
$\alpha_{c,ref,x}$	horizontal reference compressive strain
$\alpha_{c,ref,y}$	vertical reference compressive strain
$\alpha_{t,ref}$	reference tensile strain
$\alpha_{t,ref,x}$	horizontal reference tensile strain
$\alpha_{t,ref,y}$	vertical reference tensile strain

β angle between the diagonal staircase crack normal and the bed joint

γ_{cum} cumulative shear strain over the time when $\tau = \tau_{max}$
$\gamma_{cum,eq}$ cumulative equivalent shear strain over the time when $\tau_{eq} = \tau_{max}$
γ_{eq} equivalent shear strain
$\gamma_{eq,cum}$ cumulative equivalent shear strain (over all time)
$\gamma_{eq,elastic}$ elastic part of the equivalent shear strain
$\gamma_{eq,plastic}$ plastic part of the equivalent shear strain
γ_{nt} shear strain parallel to the diagonal staircase crack
$\gamma_{nt,crack}$ crack shear strain parallel to the diagonal staircase crack
$\gamma_{nt,elastic}$ elastic part of the shear strain parallel to the diagonal staircase crack
γ_p shear strain at peak strength
$\gamma_{p,eq}$ equivalent shear strain at peak strength
γ_u ultimate shear strain
$\gamma_{u,eq}$ ultimate equivalent shear strain
γ_{xy} shear strain

$\mathbf{\Delta a}$ vector containing the nodal displacement increments
$\mathbf{\Delta a}^1$ vector containing the nodal displacement increments of the first iteration
$\mathbf{\Delta a}^2$ vector containing the nodal displacement increments of the second iteration
$\mathbf{\Delta f}_e$ vector containing the external nodal force increments
Δt time step
Δu horizontal crack deformation
Δu_e horizontal crack deformation due to horizontal extension
Δu_s horizontal crack deformation due to shear
$\Delta\gamma$ shear strain increment
$\Delta\gamma_{xy}$ shear strain increment
$\Delta\varepsilon$ strain increment
$\mathbf{\Delta\varepsilon}^1$ vector containing the strain increments of the first iteration
$\Delta\varepsilon_{xx}$ horizontal normal strain increment

ε normal strain
$\varepsilon*$ strain value where the third-order part of the compressive constitutive relation connects to its second-order part
ε_0 normal strain before the strain increment
ε_{nn} strain normal to the diagonal staircase crack
$\varepsilon_{nn,crack}$ crack strain normal to the diagonal staircase crack
$\varepsilon_{nn,elastic}$ elastic part of strain normal to the diagonal staircase crack
ε_p strain value at compressive strength
ε_t strain at time t
$\varepsilon_{t,u}$ ultimate tensile strain
ε_{tt} strain tangential to the diagonal staircase crack
ε_{xx} horizontal normal strain

ν Poisson's ratio

λ compressive unloading factor

ρ mass density

σ	normal stress
σ_0	normal stress before the strain increment
$\boldsymbol{\sigma}^1$	vector containing the stresses after the first iteration
$\boldsymbol{\sigma}^2$	vector containing the stresses after the second iteration
$\sigma_{c,ref}$	reference compressive stress
$\sigma_{c,ref,x}$	horizontal reference compressive stress
$\sigma_{c,ref,y}$	vertical reference compressive stress
σ_{nn}	stress normal to the diagonal staircase crack
σ_t	stress at time t
σ_{t-1}	stress at time $t-1$
$\sigma_{t,ref}$	reference tensile stress
$\sigma_{t,ref,x}$	horizontal reference tensile stress
$\sigma_{t,ref,y}$	vertical reference tensile stress
σ_{tt}	stress tangential to the diagonal staircase crack
σ_{xx}	horizontal normal stress, or stress normal to the head joint
$\sigma_{xx,0}$	horizontal normal stress before the strain increments
σ_{yy}	vertical normal stress, or stress normal to the bed joint
τ	shear stress
τ_0	shear stress before the (shear) strain increment(s)
τ_{eq}	equivalent shear stress
$\tau_{eq,l}$	initial linear prediction of the equivalent shear stress
τ_{max}	shear strength, or bed joint shear strength
τ_{nt}	shear stress parallel to the diagonal staircase crack
τ_{xy}	shear stress, or shear stress parallel to the bed joint
φ	friction angle

1

Introduction

1.1. Background

In recent years several mining related earthquakes shook up the northern Dutch province of Groningen. Many buildings were damaged, among which many masonry structures. Some structures were considered to be unsafe and had to be strengthened or rebuild. Other suffered only aesthetic damage, but still had to be restored. Issues arose about who was liable for the damage.

Detailed assessment of masonry behaviour became of interest, not only its ultimate limit state capacity (here, when will a building collapse?), but also its serviceability limit state behaviour (here, when and how will a building start to look damaged?). It became important to be able to asses whether masonry cracks were the result of the earthquakes and thus the liability of the miner, or of other issues such as uneven foundation settlement and thus the responsibility of the building's owner. Therefore, insight into masonry cracking behaviour was desired.

Numerical analysis is often used to gain this understanding of the damage and failing behaviour of structures. Finite element software can be used to model the structures and estimate their behaviour under certain exerted loads. This could provide insight into the occurring crack patterns and accompanying crack widths due to earthquake loads and give an estimate of the residual strength and stiffness afterwards. However, existing material models for masonry were not sufficient to represent the behaviour of the masonry that is typically used in the affected buildings in Groningen. This masonry is slender, unreinforced and has a low bond strength, which leads to cracks forming mainly through the joints, resulting in horizontal cracks, diagonal staircase cracks and vertical toothed cracks. [10]

A special material model for this type of masonry was developed by DIANA FEA BV in collaboration with Delft University of Technology. It is called the Engineering Masonry Model. [6, Section 38.12] This model was developed specifically to be used for cyclic analysis, that represent earthquakes. The model was set out to approximate the initial stiffness, the stiffness at the end of loading, the loading capacity, the energy dissipation and the crack pattern of masonry. The intended applications were flat or curved shear walls under an overload, loaded horizontally at their top.

1.2. Research Objectives

The main research question of this thesis is:

> *Is it possible to improve a Total Strain based constitutive concept like the* Engineering Masonry Model *to better model diagonal cracking in masonry?*

Four research objectives are formulated to answer this question, each with their own sub-questions:

Objective I: *To explain existing ways to model diagonal cracking in masonry, especially the Engineering Masonry Model*

    1. How can masonry be modelled for the finite element analysis?

2. What is the Engineering Masonry Model?

3. How does the Engineering Masonry Model describe the material behaviour?

4. What is the background of the formulas used by the Engineering Masonry Model?

5. What are the advantages and disadvantages of the Engineering Masonry Model?

Objective II: *To create a new material model for masonry that includes a diagonal staircase crack failure mode*

6. Is there another way to view diagonal staircase cracks?

7. What alternative material model could be used?

8. How can this new material model be formulated?

9. How can this new material model be implemented as a user supplied subroutine for DIANA?

Objective III: *To assess the validity of this new material model*

10. Does the user supplied material subroutine work as intended for a single integration point?

11. How does the new material model compare to the Engineering Masonry Model's *Diagonal stair-case cracks* option for a single integration point?

12. How accurately does the material model represent masonry horizontal extension and shear behaviour compared to a masonry micro model?

13. How close are the new material model's approximations to laboratory tests of a real masonry shear wall?

14. How does the new material model compare to the Engineering Masonry Model's *Diagonal stair-case cracks* option for full scale model of a shear wall?

Objective IV: *To review the results of the validity assessment*

15. What aspects of the new material model work well?

16. What aspects of the new material model require improvement?

17. What adaptations could be made to the material model's theory?

18. What adaptations could be made to the material model's code?

19. What further validations are required?

1.3. Report Outline

This report consists of four parts that correspond to the four research objectives stated in Section 1.2. A summary of the report can be found on page iii.

The first part consists of two chapters, one that describes information from literature and one with own work that investigates this information in-depth. Chapter 2 contains a brief description of the finite element method, several fracture models and the DIANA software. It then continues with a detailed description of the Engineering Masonry Model. Chapter 3 provides explanatory derivations behind formulas used in the Engineering Masonry Model, re-derivations of some incorrect formulations found in the Engineering Masonry Model literature and a graphic summary of the failure criteria of the Engineering Masonry Model *Diagonal stair-case cracks* option. Then follows a brief review of the accuracy and efficiency of the Engineering Masonry Model.

The second part consists of three chapters. Chapter 4 shows the features that inspired the creation of the new material model. Chapter 5 contains the theoretical description of the new material model, that is now called the *Equivalent Shear Masonry Model*. Chapter 6 explores the Fortran subroutine code of the Diana user supplied material model that was written for the Equivalent Shear Masonry Model.

The third part aims to asses the validation of the Equivalent Shear Masonry Model. Chapter 7 describes analyses of a single element model with a single integration point to determine whether the code works as intended. It also compares the Equivalent Shear Masonry Model with the Engineering Masonry Model *Diagonal stair-case cracks* option. Chapter 8 describes analyses of a unit cell of micro modelled masonry. This was done to approximately determine the behaviour of real masonry under the same loading conditions that were previously used for the single element model. Chapter 9 contains a finite element model on structural level using the Equivalent Shear Masonry Model, meant to approximate real life masonry laboratory tests of wide double clamped shear walls under cyclic horizontal loading. The results are also compared to an approximation with the Engineering Masonry Model's *Diagonal stair-case cracks* option.

The fourth part consists of the conclusions (Chapter 10) and the recommendations for further work (Chapter 11).

I

Research

2

Literature

This chapter briefly describes the finite element method, several fracture models and the software that was used for this thesis. It then continues with a detailed description of the Engineering Masonry Model.

2.1. The Finite Element Method

The reader is assumed to be familiar with the concept of finite element modelling. For the sake of completeness, a brief introduction into the aspects used in this thesis will be given here.

The finite element method (FEM) is described by Wells as "a numerical method for solving partial differential equations" [19]. More concretely, in structural mechanics it is mainly used to calculate stresses and deformations in structures. For this purpose the continuous material of the structure is represented by a finite number of elements, hence the name finite element method. In general it holds that the smaller these elements are, the more accurate the solution becomes. However, the computational effort increases with the increase in number of elements. Therefore, finite element analysis are often performed on a computer with the help of finite element software.

In this thesis, only plane stress (membrane) elements are used. These are two-dimensional elements that have zero out-of-plane stress components. They are commonly used to model flat structural components, such as walls.

The elements are connected with their neighbouring elements at the nodes, where the forces are transferred. Linear elements have nodes at their corner points. Higher-order serendipity elements have additional nodes at their sides. For example, quadratic (i.e. second-order) elements have one additional node at their sides and cubic (i.e. third-order) have two additional nodes at their sides. At the nodes the user can apply loads (forces or displacements) and define supports (fixed displacements). The finite element method integrates the stress and strain over each element by evaluating their values at specific integration points inside the element. The location and weight factors of these points depend on the integration scheme used. For example, a second-order quadrilateral (i.e. rectangular) element typically has four integration points, though a higher or reduced integration scheme can also be used.

In the finite element method the following equation is solved for a linear structural mechanics problem:

$$\mathbf{Ka} = \mathbf{f} \tag{2.1}$$

where $\mathbf{K}$ is the global stiffness matrix, $\mathbf{a}$ is a vector containing the nodal displacements and $\mathbf{f}$ is a vector containing the nodal forces.

A non-linear problem, however, has to be solved stepwise. The governing equation for each step then becomes:

$$\mathbf{K\Delta a} = \mathbf{f}_e^{t+\Delta t} - \mathbf{f}_i^t \tag{2.2}$$

where $\mathbf{\Delta a}$ is a vector containing the nodal displacement increments, $\mathbf{f}_e^{t+\Delta t}$ is a vector containing the external nodal forces at the end of the increment and $\mathbf{f}_i^t$ is a vector containing the current internal nodal forces.

To solve this equation, the finite element method starts from an equilibrium state at time t when:

$$\mathbf{f}_i^t = \mathbf{f}_e^t \tag{2.3}$$

Then a load increment $\Delta\mathbf{f}_e$ is applied so that:

$$\mathbf{f}_e^{t+\Delta t} = \mathbf{f}_e^t + \Delta\mathbf{f}_e \tag{2.4}$$

The method will then use Equation 2.2 to calculate the corresponding displacement increment:

$$\Delta\mathbf{a} = \mathbf{K}^{-1}\left(\mathbf{f}_e^{t+\Delta t} - \mathbf{f}_i^t\right) \tag{2.5}$$

2.1.1. Iterative Incremental Procedure

Often merely a stepwise (i.e. incremental) solution procedure is not accurate enough, as it tends to drift away from the true solution. Therefore, iterative incremental procedures are used. A common one, the Newton-Raphson method, is pictured in Figure 2.1. The procedure of this method is described below. [17]
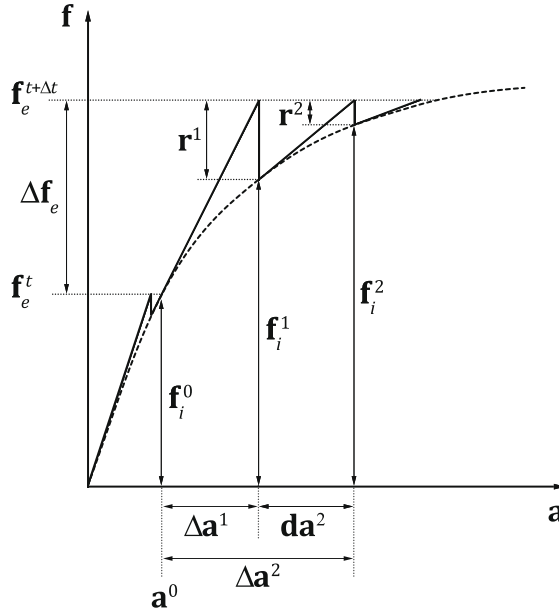
Figure 2.1: Graphical representation of the Newton-Raphson iteration scheme, image based on [17]. The straight, sawtooth shaped line is the path the finite element procedure follows, the dashed line is the true equilibrium path.

The method starts from the initial start point or an equilibrium state, i.e. the final point from the converged previous step called $(\mathbf{a}^0, \mathbf{f}_i^0)$, were $\mathbf{f}_i^0 = \mathbf{f}_e^t$ and the tangent stiffness $\mathbf{K}^0$ is known. The first deformation increment is calculated:

$$\Delta\mathbf{a}^1 = \left[\mathbf{K}^0\right]^{-1}\left(\mathbf{f}_e^t + \Delta\mathbf{f}_e - \mathbf{f}_i^0\right) \tag{2.6}$$

Then an equilibrium check is executed. For this purpose, for each element the displacement increments $\Delta\mathbf{a}^1$ at the nodes are interpolated and differentiated to find the strain increments $\Delta\varepsilon^1$ at each integration point. For each integration point, a material model is used to calculate the stresses σ^1 in the material. Next, these stresses are extrapolated and integrated to obtain the internal forces $\mathbf{f}_i^1$ at the nodes. The material model also provides the information for the current tangent stiffness $\mathbf{K}^1$. Finally, the out-of-balance force is calculated:

$$\mathbf{r}^1 = \mathbf{f}_e^t + \Delta\mathbf{f}_e - \mathbf{f}_i^1 \tag{2.7}$$

If this out-of-balance force is sufficiently small, equilibrium is reached and the step is ended. Otherwise, the procedure continues from this point $\mathbf{a}^1$, $\mathbf{f}_i^1$. A variation of the strain increment is calculated:

$$\mathbf{da}^2 = \left[\mathbf{K}^1\right]^{-1}\mathbf{r}^1 \tag{2.8}$$

which is used to update the total increment:

$$\Delta\mathbf{a}^2 = \Delta\mathbf{a}^1 + \mathbf{da}^2 \tag{2.9}$$

The material model is again used to calculate the stresses $\boldsymbol{\sigma}^2$ at integration point level, which are used to calculated the internal forces $\mathbf{f}_i^2$ at the nodes. Again, the material model also provides the information for the current tangent stiffness $\mathbf{K}^2$. Once more, the out-of-balance force is calculated:

$$\mathbf{r}^2 = \mathbf{f}_e^t + \Delta\mathbf{f}_e - \mathbf{f}_i^2 \tag{2.10}$$

This process is repeated until the out-of-balance forces are so small that the step is considered to be converged.

Overall, the iterative incremental procedure creates a sawtooth shaped path, see Figure 2.1. The slanting parts can be attributed to the main FEM procedure. The calculation is comprised of solving one large linear system of equations for the entire model, with the force, displacement and stiffness data at the nodes. The vertical drops can be attributed to the material model, that calculates the stress and stiffness for each integration point separately.

2.1.2. Stiffness used in the Finite Element Procedure

In the iterative procedure in the previous section, the finite element procedure used the tangent stiffness to calculate the next (variation of the) strain increment. This works fine for materials with a smoothly changing, but always positive stiffness, like in the example in Figure 2.1. However, when the stiffness becomes (almost) zero or even negative, like in Figure 2.2, using the tangent stiffness can become problematic. Also for inelastic materials, whose unloading does not follow the previous equilibrium path, this is less straight forward.

Figure 2.2 shows the stress-strain history of a non-linear material up until a certain point in time. From this bifurcation point the material can go two ways: either unload or continue to load. The stiffness right before this point is the tangent stiffness $E_{tangent}$. If the material continues loading, this is a good approximation of the stiffness E_{load} right after. However, if the material instead continues to unload, it follows a – very different – unload stiffness E_{unload}. Therefore, the stiffness at the bifurcation point is not unique. But only one single value has to be provided for the finite element program to work with.
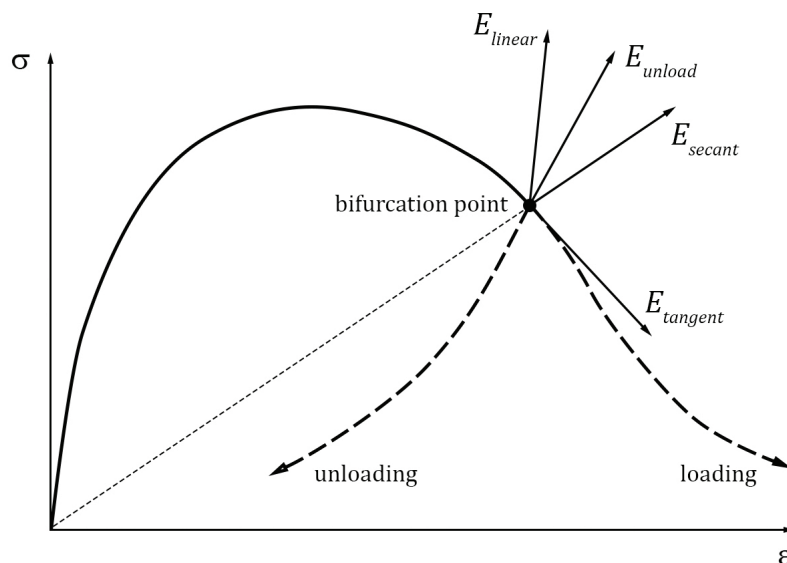
Figure 2.2: The stress-strain history of a fictional non-linear material up to a bifurcation point, where after it may continue to load or start to unload. Several definitions of the stiffness are drawn in at this point. Note that in this case the loading stiffness coincides with the tangent stiffness.

The standard option is to use the tangent stiffness. Since in most analyses materials are mainly loaded, this is usually the best approximation. If the material model is used for cyclic loading, however, this advantage does not hold, as unloading than is just as common as (re)loading.

A bigger problem with the tangent stiffness, is that it can become zero or negative when the material yields horizontally or softens, as is the case in Figure 2.2. A zero stiffness gives problems with inverting

the stiffness matrix in order to solve the linear system of equations from Equation 2.2. Though a single negative entry in a stiffness matrix doesn't give this problem, it can result in (almost) zero values during the assembly of the global stiffness matrix.

Besides the tangent stiffness, two alternatives are pictured in Figure 2.2 and clarified in Equation 2.11. One is the linear stiffness E_{linear}, which is the stiffness the material initially had, the slope of the linear first part of the graph. The other is the secant stiffness E_{secant}, which is slope of the line between the current point and the origin. The advantage of these stiffnesses is that they are never negative. The disadvantage is that they do not always give a good estimate of the material behaviour and thus may need many iterations for the solution to converge.

$$E_{tangent} = \frac{\sigma_t - \sigma_{t-1}}{\Delta \varepsilon}, \qquad E_{linear} = E_0, \qquad E_{secant} = \frac{\sigma_t}{\varepsilon_t} \qquad (2.11)$$

Furthermore, in order for the iteration procedure to work properly, the estimated stiffness has to be a good estimation of the actual stiffness or something larger. If the stiffness is larger than the actual stiffness over the increment, the procedure will always find (a variation of) a deformation increment between the previous deformation and the one searched for. If the stiffness is lower than the actual stiffness over the increment, the iteration procedure will find (a variation of) a deformation increment that goes beyond the searched deformation. If this is still close to the searched value, the procedure might circle back to that and converge. But if this value is to far away, the procedure might not converge.

2.2. Fracture Models

Brittle materials such as masonry are often subject to cracking. There are two ways to model fracture: as discrete cracks or as so-called smeared cracks.

2.2.1. Discrete Cracking: Finite Element Techniques

Discrete crack models feature a line that represents the crack. The displacement field is discontinuous at this crack. This is achieved through special elements or adjustments to the topology. The advantage of discrete crack modelling is that the cracks physically open up, which is closest to what is seen in reality. Four discrete crack models are briefly discussed here. [17]

Nodal Release Technique
The nodal release technique starts out with a common mesh. Once the failure stress is reached in an integration point, an extra node is added at the location of the closest node, so that the elements that were connected at that node now each have their own node and are no longer connected. This means that the topology changes during the analysis, so it requires complicated topology management to tracks these changes. Also, this model is by definition only capable of modelling brittle fracture. The directions of the cracks are fixed, because they can only occur along the mesh lines.

Interface Elements
Another way to achieve a discrete crack is with the help of interface elements. These elements have to be added in advance by the user where he expects cracks to occur. In contrast to the previous crack model, the interface elements preserve the connection between the continuum elements, so they can represent softening and/or sliding. The directions of the cracks are fixed, because they can only occur at the predefined interface elements. In order to minimize added compliance, the interface elements require a high dummy stiffness, which affects the condition of the global stiffness matrix.

Embedded Discontinuity Elements
Embedded discontinuity elements have a crack band added into their shape functions. The large strain increase in case of cracking is assumed to be only in this cracked region, while the other regions remain elastic. The direction of the crack is not fixed. The crack path can be non-continuous, which leads to an overestimation of the crack energy.

eXtended Finite Element Method
The eXtended Finite Element Method (XFEM) uses enhanced elements. In this method a discontinuity in the displacement field is realised with the help of extra degrees of freedom at the existing nodes, multiplied by a Heaviside function. This method gives a continuous crack path whose direction is not

fixed by the mesh. Due to the extra degrees of freedom it does take longer to compute. Also, it only allows for one crack per element and problems arise when the crack gets very close to the nodes.

2.2.2. Smeared Cracking: Material Models

In smeared crack models the cracks are considered to be smeared out over the element. For the smeared cracking approach a special material model is needed. The strain in the crack and strain of the elastic area just around it are averaged, so the crack looks like a stretched band in the results. The displacement field is continuous. The advantage of the smeared crack approach is that cracks can occur anywhere in the model and in any direction, without changing the topology and without using any special elements.

Smeared crack material models are divided into fixed crack models and rotating crack models. Rotating crack models always evaluate the stress in the principle directions. This way, always the lowest softening regime is followed. Fixed crack models evaluate the stress in the principle directions until the integration point reaches the peak stress. After failure, the crack angle is assumed to be fixed in that same direction. This may give too stiff results. [17] Other sources also include a third option, switching from rotating crack to fixed crack after reaching a user defined strain value. [6, Section 38.5]

Total Strain Rotating Crack Model
The Total Strain Rotating Crack Model is a total strain based smeared crack model. Various different constitutive relations for the tensile and the compressive regime can be used. These relations are always isotropic, because the stress is evaluated in the principle directions. [6, Section 38.5]

Rankine-Hill Plasticity Model
The Rankine-Hill model is an anisotropic plasticity model that uses different strength and softening characteristics in orthogonal directions. For masonry, these directions are along the bed joint and perpendicular to the bed joint. The model evaluates the stresses in these two directions only. The constitutive relations are a combination of a Rankine yield criterion for tension that includes softening, with a Hill criterion for compression, that includes hardening and subsequent softening. [6, Section 38.9]

Engineering Masonry Model
The Engineering Masonry Model is a smeared crack model available in *DIANA Finite Element Analysis* that was developed especially for masonry. It is an orthotropic fixed crack model that can evaluate cracking in four directions: normal to the bed joint and either normal to the head joint or normal to two the possible diagonal staircase cracks. This model will be described in detail in Section 2.4.

2.2.3. Masonry Model Scales

Masonry can be modelled with different amounts of detail, see Figure 2.3. The most detailed option is to model the bricks, the mortar and the mortar-brick interface all separately. The bricks and the mortar are then modelled with continuum elements and the mortar-brick interface with interface elements. This is thus a discrete crack model. A model of this scale is often referred to as a *micro model*. The advantage of this scale is that is gives the most accurate results, though it takes some time to model it and it takes a lot of computational effort.

The least detailed option is to model the entire masonry as one homogeneous material. This can be done with a smeared crack material model. A model of this scale is often referred to as a *macro model*. The advantage of this scale is that it is the easiest to model and takes the least computational effort. It is therefore preferred for long analyses like repetitive cyclic loading. Its accuracy is greatly dependent on the material model that is used.

Then there are two in-between options. One is to model the bricks with continuum elements, and to represent the behaviour of the mortar and mortar-brick interface together by interface elements.[1] This is often referred to as *meso model*.

The second in-between option is to model the bricks as they are with continuum elements, and to model the behaviour of the mortar and mortar-brick interface together as joints with continuum elements. These joints are them are then assigned a smeared crack material model. This is sometimes also referred to as a *micro model*.

---

[1]For this model the bricks are usually widened and heightened with the joint thickness.
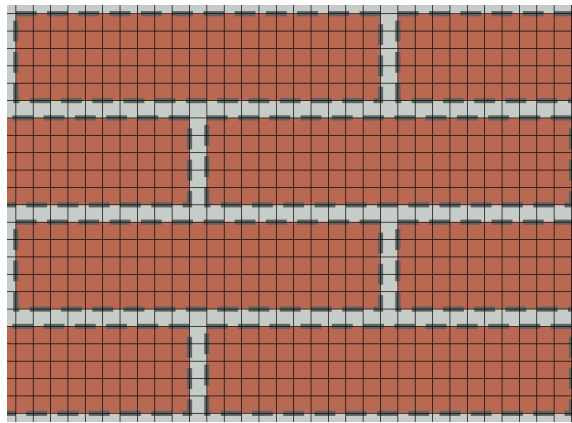
(a) Most detailed micro model: bricks and joints as continuum elements, brick-joint interface as interface elements.
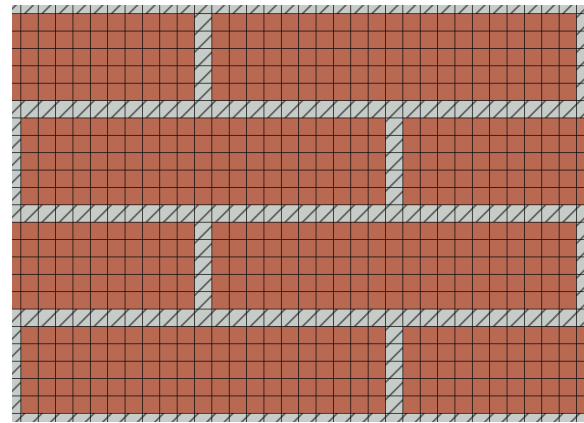
(b) Alternative micro model: bricks as continuum elements, and joints and brick-joint interface together as elements.
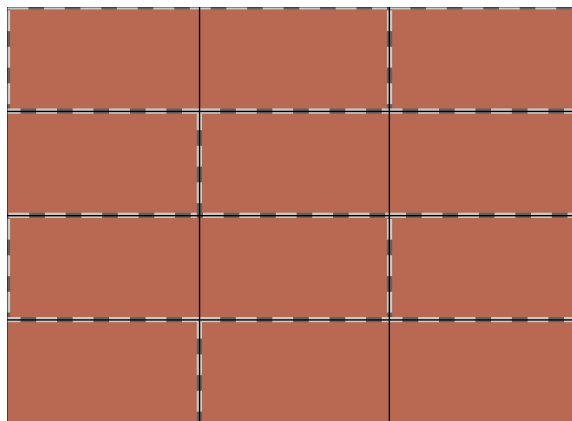
(c) Meso model: bricks as continuum elements, joints and brick-joint interface together as interface elements.
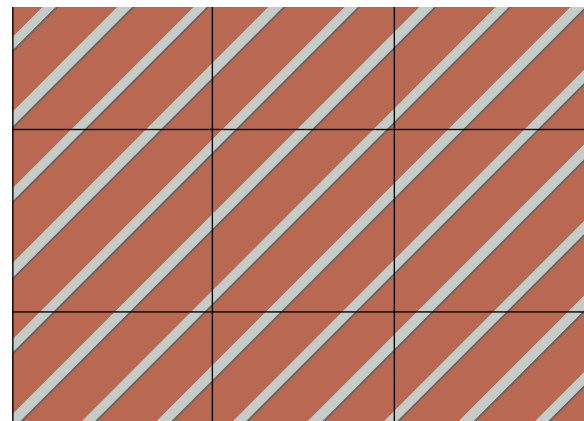
(d) Macro model: bricks, joints and brick-joint interface together as continuum elements.

Figure 2.3: Masonry model scales.

2.3. DIANA Finite Element Analysis

DIANA Finite Element Analysis is a finite element software package by DIANA FEA BV. [4] It is an extensive package, equipped for various analyses, including dynamic analysis and non-linear analysis. It offers a great number of material models, from common models for steel and reinforced concrete to more advanced models for soil and masonry.

The user can create structural models, run analyses and view the results from the graphical user interface *Diana Interactive Environment*. Alternatively, analyses can be run from the *Diana Command Box*. The user must then provide a text file containing the analysis commands with file extension `.dcf` and a text file containing the model data[2] with file extension `.dat`. These files can be lengthy and must satisfy strict syntax requirements. Therefore, it is good practice to first create both the model and the analysis commands as far as possible in the user interface and then export them. This provides a solid starting point to expand on.

2.3.1. User Supplied Material Model

Besides the numerous material models that DIANA provides, it also allows the user to create its own material model. This material model must be written as a Fortran subroutine and compiled to a `.dll`-file that DIANA can read. General information about the user supplied subroutines can be found in Diana's *User's Manual*, *Material Library*, section 13.5 *General User-supplied Material Model*. [5, Section 13.5]

---

[2]This is the description of the model that is to be analysed, containing information about the geometry, elements, material properties, supports, loads etcetera.

More detailed practical instructions can be found in [1] and [20].

As explained in the end of Section 2.1.1, the material model is called each iteration for each integration point to calculate the stress and stiffness. For this purpose, the user supplied subroutine receives information from the DIANA main frame: the stress and strain at the beginning of the step and the applied strain increment, see Figure 2.4. It also receives the material properties as given in the `.dat`-file – which are stored as double precision floating-point numbers in the `USRVAL`-array. In addition, it receives some extra user state parameters – which are stored in two arrays, `USRSTA` for the double precision floating-point numbers and `USRIND` for the integer numbers. These user parameters can be updated by the material model to track the history or describe the current state.[3] At the end, the subroutine must return the stress and stiffness after the increment, and the updated user parameters.
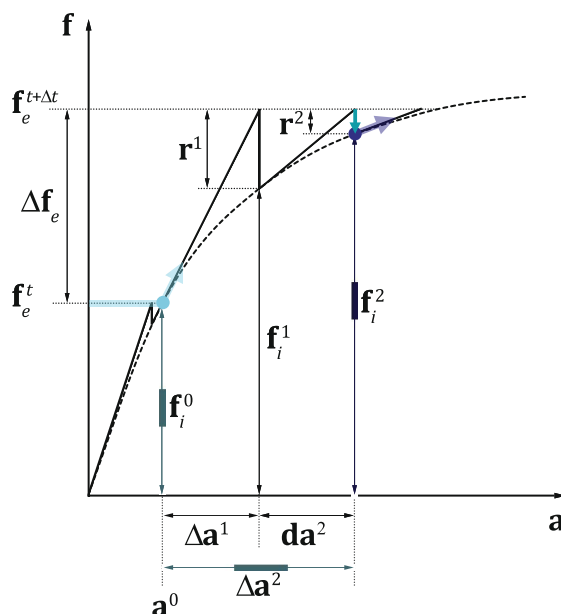
Figure 2.4: The Newton-Raphson iteration scheme that was presented in Figure 2.1, with the user supplied subroutine input marked in blue and the user supplied subroutine output marked in purple, for when the user supplied subroutine is called to perform the part of the iterative procedure marked with the teal arrow.

Once written and compiled, the user supplied material model can be used for finite element analysis. If the material model requires many input parameters, this can best be done by defining those inputs in a `.dat`-file. The `.dat`-file can then be imported into the graphical user interface, or the analysis can be run from the Command Box. In the former case, the location of the `.dll`-file must be specified. In the latter case, the `.dcf`-file must contain two lines to invoke the user supplied subroutine, see line 4 and 5 of Listing C.2 in Appendix C. These lines are `*FORTAN` and `USE "C:\…full directory…\subroutinename.dll"`, or simply `USE "subroutinename.dll"` when the `.dll`-file is located in the working directory.[4] Note that not only the material properties have to be provided, but also two empty arrays (i.e. lists of zeros) for the user state parameters.

2.4. The Engineering Masonry Model

The Engineering Masonry Model is a material model for masonry walls that is available in the finite element software *DIANA Finite Element Analysis*. It was developed especially for cyclic loading. It uses a smeared cracking approach and is a multi-directional fixed crack model. It is compatible with regular plane stress (membrane) elements and curved shell elements. [6, Section 38.12]

To reflect the anisotropy of masonry a horizontal and a vertical stiffness are used. Failure can be considered in four directions: normal to the head joints (in the local x-direction), normal to the bed joints (in the local y-direction) and optionally normal to either of the two expected possible diagonal staircase

---

[3]Their values at input are always those at the beginning of the step, though, not the values at the end of the previous iteration.

[4]The working directory is set by typing `Cd\working directory` in the Command Box.

cracks, see Figure 2.5 and Section 2.4.5 for further description of these directions. When the *Diagonal stair-case cracks* option is not active, the material behaviours in the horizontal and vertical direction are uncoupled.
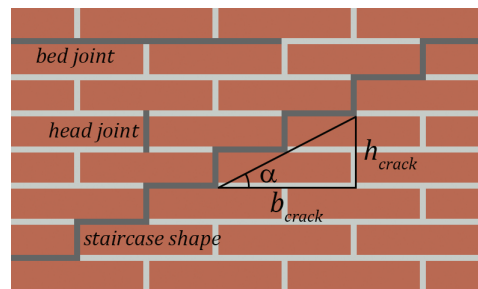
Figure 2.5: A head joint, a bed joint and one possible path of a staircase crack marked in dark grey on a background of a brick wall with a running bond. The height-width ratio of this crack is defined as $\tan \alpha$.

For this section, several sources about the Engineering Masonry Model were consulted, namely:

- The *SAHC* conference paper *Computational modelling of masonry with a view to Groningen induced seismicity*, [14]

- the *DIANA Validation report for Masonry modelling*, [16]

- section 38.12 *Engineering Masonry Model* of the *Theory Manual* in the *DIANA User's Manual*, [6, Section 38.12]

- section 6.5 *Engineering Masonry Model* of the *Material Library* in the *DIANA User's Manual*, [5, Section 6.5]

- the Engineering Masonry Model subroutine `engmas.f`, [15]

- an earlier user supplied subroutine for the Engineering Masonry Model `usrmat_quad2.f`, [2] and

- the graphical user interface *Diana Interactive Environment* of the *Diana* software. [4]

These sources do not all use the same symbols for the same concepts, so an overview of all symbols used by them is given in Appendix A. Sometimes one (or some) of the sources also use a different definition for a similar concept.

2.4.1. Failure Modes Considered

The Engineering Masonry Model can evaluate seven failure modes. The six of them that are applicable to plane stress elements are summarized in Table 2.1.[5] Firstly, the stress in the direction normal to the bed joints is checked for tension (A) and compression (B). The constitutive relations used are discussed in Sections 2.4.3 and 2.4.4. Secondly, shear sliding along the bed joint (C) is considered. This behaviour is described in Section 2.4.2. Finally, for failure in the head joints, the Engineering Masonry Model provides four options:

- The first option does not consider failure in the head joint at all. In the user interface this option is called *Head-joint failure not considered*, in the `.dat`-file it is `HEADTP=NONE`. With this option selected the Engineering Masonry Model checks for failure modes A, B and C from Table 2.1.

- The second option considers the compressive and tensile failure in the head joint similarly to the failure in the bed joint. The user must then provide an explicit value for the horizontal tensile and compressive strengths. In the user interface this option is called *Direct input head-joint tensile strength*,[6] in the `.dat`-file it is `HEADTP=EXPLIC`. With this option selected the Engineering Masonry Model checks for failure modes A, B, C, D and E from Table 2.1.

---

[5] Besides these, the Engineering Masonry Model can also evaluate the out-of-plane shear failure for curved shell elements. This will not be discussed in detail, because this thesis limits itself to flat membrane elements.

[6] It is actually the tensile strength of the masonry as a whole in the direction normal to the head joints that the user supplies.

Table 2.1: Overview of failure modes considered by the Engineering Masonry Model.

A		Vertical tension, i.e. tension normal to the bed joint	$\sigma_{yy} \leq f_{ty}$
B		Vertical compression, i.e. compression normal to the bed joint	$\sigma_{yy} \geq -f_{cy}$
C		Horizontal shear sliding, i.e. shear sliding along the bed joint	$|\tau_{xy}| \leq \tau_{max}$
D		Horizontal tension, i.e. tension normal to the head joint	$\sigma_{xx} \leq f_{tx}$
E		Horizontal compression, i.e. compression normal to the head joint	$\sigma_{xx} \geq -f_{cx}$
F		Diagonal tension, i.e. diagonal staircase crack	$\sigma_{nn} \leq f_{t\alpha}$

- The third option considers the tensile failure normal to the head joint similarly to the failure in the bed joint, but now with a value for the horizontal masonry tensile strength that is derived from friction in the bed joints, see Section 2.4.3. The user must provide information on the masonry topology in the form of the angle α at which a diagonal staircase crack could occur.[7] The user can also provide a minimum horizontal tensile strength. In the user interface this option is called *Tensile strength head-joint defined by friction*,[8] in the `.dat`-file it is `HEADTP=FRICTI`. With this option selected the Engineering Masonry Model checks for failure modes A, B, C and D from Table 2.1.

- The fourth option considers failure in the head joint as part of a diagonal staircase crack. The model does this by evaluating the tensile stress normal to the possible staircase crack. The user must provide the angle α at which this diagonal staircase crack could occur. In the user interface this option is called *Diagonal stair-case cracks*, in the `.dat`-file it is `HEADTP=DIAGON`. With this option selected the Engineering Masonry Model checks for failure modes A, B, C and F from Table 2.1.

2.4.2. Shear Behaviour

The shear behaviour is considered to be dominated by the shear behaviour of the bed joints. The deformed shape of the masonry after shear sliding along the bed joint is depicted in Figure 2.6. The failure criterion to be checked is:

$$|\tau_{xy}| \leq \tau_{max} \tag{2.12}$$

where τ_{xy} is the shear stress and τ_{max} is the shear strength or maximum shear stress. The maximum shear stress is described by the Coulomb friction criterion, known from soil mechanics:

$$\tau_{max} = \max\left(0,\ c - \sigma_{yy} \tan\varphi \right) \tag{2.13}$$

where c is the cohesion, σ_{yy} is the stress normal to the sliding direction, here the local vertical normal stress, and φ is the friction angle.
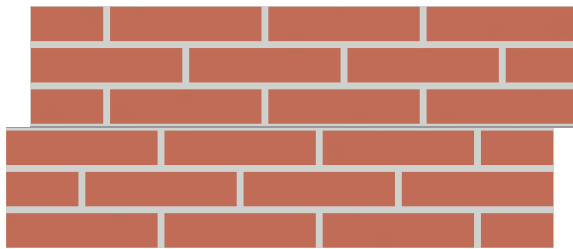
Figure 2.6: Deformed masonry after shear sliding along the bed joint. The crack is a horizontal line, the crack deformation is horizontal.
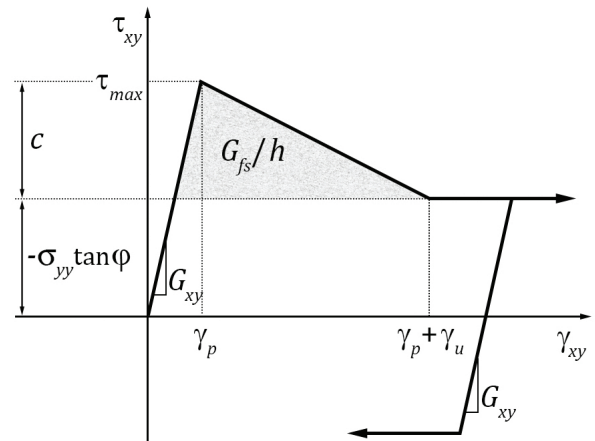
Figure 2.7: Stress-strain diagram of the shear behaviour.

The shear behaviour is pictured in Figure 2.7.[9] Before failure, the material behaves linear elastic. After failure, it softens, followed by sliding under constant stress. Unloading and reloading is linear with

---

[7] This option does not evaluate any diagonal cracking, though.

[8] It is actually not the tensile strength of the head joints, but the horizontal strength of the masonry as a whole that is derived from friction in the bed joints, while assuming that the horizontal tensile strength of the head joints is negligible. See also Sections 2.4.3 and 3.1.2.

[9] In [6, Section 38.12] and [16] the unloading branch is pictured somewhat lower than it should be. After unloading, the stress-strain diagram reaches exactly the inverse of the amount of τ_{max} it still had available when it began to unload.

the initial elastic shear stiffness. This can be summarized as follows:

$$\tau = \begin{cases} -\tau_{max} & \text{for } \tau_0 + G_{xy}\Delta\gamma < -\tau_{max} \\ \tau_0 + G_{xy}\Delta\gamma & \text{for } -\tau_{max} \leq \tau_0 + G_{xy}\Delta\gamma \leq \tau_{max} \\ \tau_{max} & \text{for } \tau_{max} < \tau_0 + G_{xy}\Delta\gamma \end{cases} \tag{2.14}$$

where $\Delta\gamma$ is a shear strain increment, τ is the new shear stress, τ_0 is the shear stress before the shear strain increment and G_{xy} is the shear stiffness.

Should the material be cracked in any direction, the cohesion is reduced to zero immediately. Otherwise, once the material reaches the maximum shear stress, the cohesion is reduced by the following equation:

$$c = c_0 \frac{\gamma_u - \gamma_{cum}}{\gamma_u} \tag{2.15}$$

where c is the current cohesion, c_0 is the initial cohesion, γ_{cum} is the cumulative shear strain over all the time that the shear stress was equal to the maximum shear stress and γ_u is the ultimate shear strain, the cumulative shear strain at which the cohesion is fully gone. This value intrinsically depends on the shear fracture energy and due to the smeared crack approach also depends on the element size, by:[10]

$$\gamma_u = \frac{2G_{fs}}{h \cdot c} - \frac{c}{G_{xy}} \tag{2.16}$$

where G_{fs} is the shear fracture energy and h is the crack band width, which is an approximation of the element width in the direction of the crack opening.

Under cyclic shear loading, energy will be dissipated. The stress-strain diagram will then display a parallelogram shaped hysteresis loop.

2.4.3. Tensile Behaviour
The tensile behaviour is described by a bi-linear stress-strain relation, see Figure 2.8. The material behaviour is linear elastic before failure and after failure it follows a linear softening curve. Unloading and reloading follow a secant line trough the origin and the furthest reached point on the loading curve. This can be summarized as follows:

- If $\varepsilon > \alpha_{t,ref}$ there is new tensile extreme, so:

$$\alpha_{t,ref} = \varepsilon \tag{2.17}$$

  where ε is the current normal strain and $\alpha_{t,ref}$ is the highest reached normal strain value up to this step, or reference tensile strain.

$$\sigma = \begin{cases} E\varepsilon & \text{for } 0 \leq \varepsilon < \dfrac{f_t}{E} \\ \dfrac{E(\varepsilon_{t,u} - \varepsilon)}{E\varepsilon_{t,u} - f_t} \cdot f_t & \text{for } \dfrac{f_t}{E} \leq \varepsilon < \varepsilon_{t,u} \\ 0 & \text{for } \varepsilon_{t,u} \leq \varepsilon \end{cases} \tag{2.18}$$

  where σ is the normal stress, E is the normal stiffness, f_t is the tensile strength, $\varepsilon_{t,u}$ is the ultimate tensile strain, the strain at which the stress is reduced to zero.

$$\sigma_{t,ref} = \sigma \tag{2.19}$$

  where $\sigma_{t,ref}$ is the reference tensile stress, the stress that corresponds to the reference tensile strain.

---

[10][14] uses a different definition of the ultimate shear strain $\gamma_{ult} = \gamma_p + \gamma_u$ and provides the following equation $\gamma_{ult} = 2G_{fs}/h + \sigma_{yy}\tan\varphi/G$, where the division over c is missing in the first term. It incoherently uses this definition of γ_{ult} with the definition of γ_{cum} as given in this section.

- If $\varepsilon \leq \alpha_{t,ref}$ there is tensile unloading or reloading, so:

$$\sigma = \frac{\sigma_{t,ref}}{\alpha_{t,ref}} \cdot \varepsilon \tag{2.20}$$

where $\sigma_{t,ref}$ is the reference tensile stress, the stress that corresponds to the reference tensile strain.

The softening curve is defined by the tensile fracture energy. The ultimate strain depends on the tensile fracture energy, and due to the smeared crack approach also depends on the element size, by:

$$\varepsilon_{t,u} = \frac{2G_{ft}}{h \cdot f_t} \tag{2.21}$$

where G_{ft} is the tensile fracture energy.

Under cyclic tensile loading, zero energy will be dissipated. The stress-strain diagram will then display a straight secant line.
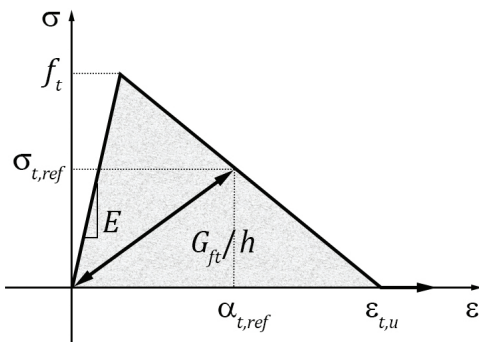
Figure 2.8: Stress-strain diagram of the tensile behaviour.
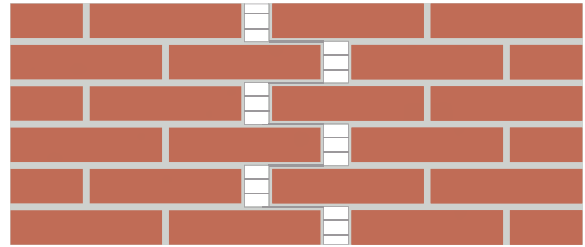
Figure 2.9: Deformed masonry after failure due to horizontal normal stress. The toothed vertical crack opens up horizontally.

Horizontal Tensile Strength

Horizontal tensile failure is only checked when head joint failure option *Direct input head-joint tensile strength* or *Tensile strength head-joint defined by friction* is selected. If the former is selected, f_{tx} is the horizontal tensile strength that was provided by the user.

If the latter option is selected, the horizontal tensile strength is calculated by:

$$f_{tx} = \tau_{max}/\tan\alpha \tag{2.22}$$

where α is the angle at which a diagonal staircase crack could occur, see Equation 2.30.

This formula is based on the concept that masonry horizontal tensile strength is limited by the failure mechanism in Figure 2.9, that depicts a vertical toothed crack. How that concept results in Equation 2.22 will be explained further in Section 3.1.2. For the *Direct input head-joint tensile strength* option, a minimal head joint tensile strength can optionally be provided as minimum value of f_{tx}.[11]

Equation 2.22 is also used to calculate the horizontal tensile strength that is needed to calculate the diagonal tensile strength with the *Diagonal stair-case cracks* option. For that option, a residual tensile strength can provided as minimum value of f_{tx}.

2.4.4. Compressive Behaviour

The compressive loading behaviour is described by a curve that consists of four parts, see Figure 2.10. The first part is a third-order curve, the second part is a second-order curve, then follows a linear softening part, to end with a residual constant stress. Unloading starts with the linear elastic stiffness,

---

[11] This is not a minimal head joint tensile strength, but a minimal tensile strength for the total masonry in the direction normal to the head joints.

then continues secant to the origin.[12] Reloading is secant to the furthest point on the loading curve that was reached. The strain value where the third-order polynomial passes into a second-order polynomial
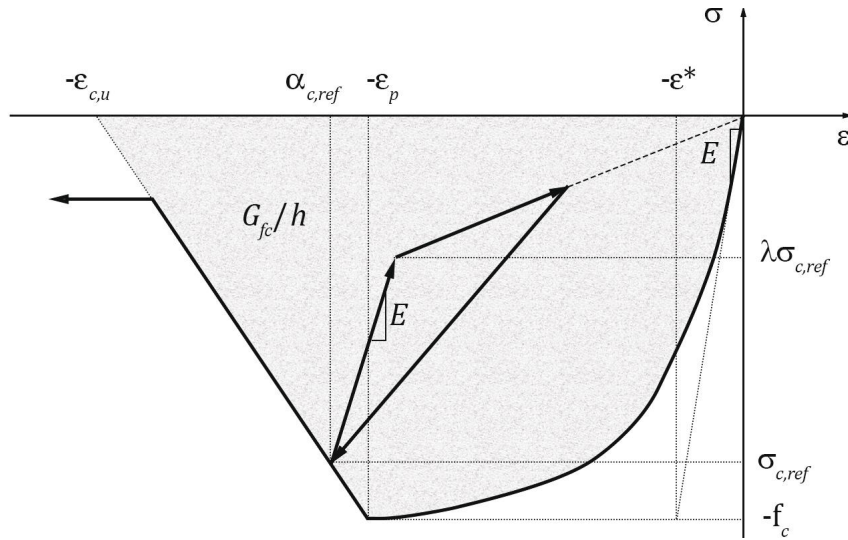
Figure 2.10: Stress-strain diagram of the compressive behaviour.

is:

$$\varepsilon* = \frac{f_c}{E} \tag{2.23}$$

where f_c is the compressive strength.[13] The factor between this value and the strain at the compressive strength is:

$$n = \frac{\varepsilon_p}{\varepsilon*} = \frac{E \cdot \varepsilon_p}{f_c} \tag{2.24}$$

where ε_p is the strain value at the compressive strength. The loading curve in Figure 2.10 can be summarized as follows:

- If $\varepsilon < \alpha_{c,ref}$ there is new compressive extreme, so:

$$\alpha_{c,ref} = \varepsilon \tag{2.25}$$

  where $\alpha_{c,ref}$ is lowest reached normal strain value, or reference compressive strain.

  The stress is given by the constitutive relation in the graph in Figure 2.10. As described in [14], this is a third-order function from the origin until $-\varepsilon*$, then second-order function until $-\varepsilon_p$, where $\sigma = -f_c$, followed a linear softening curve towards the ultimate compressive strain $\varepsilon_{c,u}$, but a maximum[14] value of $-0.10f_c$ is retained. The formula given in [6, Section 38.12], [16], [14] and [2] do not describe this behaviour properly, so the relations where re-derived. These relations are presented in Section 3.1.1. Once the stress σ is known:

$$\sigma_{c,ref} = \sigma \tag{2.26}$$

  where $\sigma_{c,ref}$ is the reference compressive stress, the stress that corresponds to the reference compressive strain.

- If $\varepsilon < \varepsilon_0$ there is compressive reloading, so:

$$\sigma = \sigma_0 + \frac{\Delta\varepsilon}{\alpha_{c,ref} - \varepsilon_0}(\sigma_{c,ref} - \sigma_0) \tag{2.27}$$

---

[12]The stress value at which the linear unloading continues as secant unloading is $\lambda\sigma_{c,ref}$. The value pictured in the compressive stress-strain diagrams in [16] and [6, Section 38.12] is $(1 - \lambda)f_c$, but the text and formulas presented correspond to a value of $\lambda\sigma_{rf}$ instead. The value pictured in the compressive stress-strain diagram in [14] is $(1 - \lambda)\sigma_{ci}$, but the text and formulas presented correspond to a value of $\lambda\sigma_{ci}$ instead.

[13][16] and [6, Section 38.12] alternately use a positive and a negative definition of the compressive strength.

[14]A minimal amount of negative stress, thus a maximum stress.

where σ is the new stress, $\Delta\varepsilon$ is a strain increment, ε_0 is the strain before the strain increment and σ_0 is the stress before the strain increment.

- If $\varepsilon \geq \varepsilon_0$ there is compressive unloading, so:[15]

$$\sigma = \begin{cases} \sigma_{c,ref} + E\left(\varepsilon - \alpha_{c,ref}\right) & \text{for } \varepsilon < \alpha_{c,ref} - \dfrac{(1-\lambda)\sigma_{c,ref}}{E} \\[4mm] \dfrac{\lambda\,\sigma_{c,ref}\,\varepsilon}{\alpha_{c,ref} - \dfrac{(1-\lambda)\sigma_{c,ref}}{E}} & \text{for } \alpha_{c,ref} - \dfrac{(1-\lambda)\sigma_{c,ref}}{E} \leq \varepsilon \end{cases} \tag{2.28}$$

where λ is the compressive unloading factor.[16]

Under cyclic compressive loading, energy will be dissipated. The stress-strain diagram will then display a triangular hysteresis loop.

2.4.5. Diagonal Staircase Crack
If the *Diagonal stair-case cracks* option is checked, the Engineering Masonry Model evaluates the stresses in a rotated axis system.

Definition of the Diagonal Axis System
Figure 2.11 shows how the two axis systems used in the Engineering Masonry Model are defined. The x-axis is defined parallel the bed joint, the y-axis is defined parallel to the head joint. The angle between the staircase crack path and the horizontal axis is called α. A second axis system (n,t) is defined as respectively normal and parallel to the crack. The angle between the n-axis and the horizontal axis is called β. It can be seen that:

$$\beta = \frac{\pi}{2} + \alpha \tag{2.29}$$

where β is the angle between the crack normal and the bed joint and α is the angle between the diagonal staircase crack and the bed joint, both defined in the (x,y)-axis system.
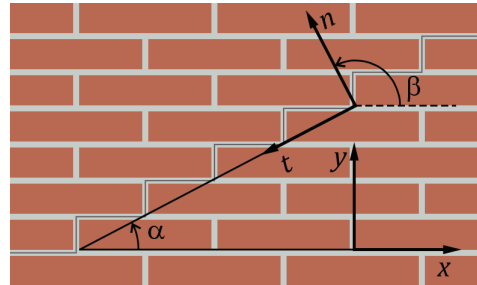
Figure 2.11: The local (x,y)-axis system and the diagonal (n,t)-axis system, to a background of a brick wall with a running bond. The angle that the staircase crack path, given in dark grey, makes with the x-axis is called α. The angle from the x- to the n-axis is called β.

Throughout this thesis all horizontal dimensions of bricks, joints, cracks etcetera will be denoted by the symbol b and all vertical dimensions will be denoted by the symbol h. This is done to distinguish these dimensions from the commonly used crack width or crack opening w and crack length l. The crack angle α of masonry with a common running bond can thus be defined as:

$$\tan\alpha = \frac{h_{crack}}{b_{crack}} = \frac{2 \cdot h_{brick} + 2 \cdot h_{joint}}{b_{brick} + b_{joint}} \tag{2.30}$$

where h_{crack} is the height of a crack segment, b_{crack} is the width of a crack segment, h_{brick} is the brick height, h_{joint} is the joint height, b_{brick} is the brick width and b_{joint} is the joint width.

---

[15]The second formula is incorrectly given as $E\varepsilon\lambda/(1-\lambda)$ in [14], [6, Section 38.12] and [16]. The correct formulae were found in [2].
[16]See also footnote 12.

Note that a brick wall with a running bond has two possible crack angles $\alpha_1 = \alpha$ and $\alpha_2 = -\alpha$. Thus it also has two crack normal directions $\beta_1 = \frac{\pi}{2} + \alpha$ and $\beta_2 = \frac{\pi}{2} - \alpha$ wherein the stress can be evaluated.[17]

Strength Criterion

No separate constitutive relation is given for the diagonal direction. Only a diagonal tensile strength criterion is evaluated:

$$\sigma_{nn} \leq f_{t\alpha} \tag{2.31}$$

where σ_{nn} is the stress normal to the diagonal staircase crack and $f_{t\alpha}$ is the diagonal tensile strength.

The diagonal tensile strength is computed from the horizontal and vertical tensile strengths by the relation:[18]

$$f_{t\alpha} = \frac{f_{tx} \cdot f_{ty}}{\sqrt{f_{tx}^2 \cos^2 \alpha + f_{ty}^2 \sin^2 \alpha}} \tag{2.32}$$

where f_{tx} is the horizontal tensile strength derived with Equation 2.22 and f_{ty} is the vertical tensile strength.[19]

---

[17] In some literature only the angles in the first quadrant (i.e. α and $\beta = \frac{\pi}{2} - \alpha$) are mentioned. Sometimes this is no problem, because in the trigonometric functions used then α_1 and α_2 c.q. β_1 and β_2 are interchangeable, but it is important to realise that α and $\beta = \frac{\pi}{2} - \alpha$ do not correspond to the same crack.

[18] In [16] and [6, Section 38.12] this formula is found in a more extensive but equivalent form, writing $\sin(\frac{\pi}{2} - \alpha)$ instead of $\cos \alpha$ and vice versa. However, α is not defined in the verification report, where instead θ is used for diagonal crack angle.

[19] In [15], f_{ty} is replaced by $\sigma_{t,ref,y}$ once the integration point has been past its vertical tension peak.

3

Analysis of the Engineering Masonry Model

This chapter analyses the Engineering Masonry Model. First, some aspects of the theory behind the model are examined. Then the usability of the Engineering Masonry Model is discussed.

3.1. Analysis of the Theory

Section 2.4 described the theory behind the Engineering Masonry Model as it was found in literature. This section presents own work that examines some aspects of this theory in more detail.

3.1.1. Compressive Behaviour

Because the formula for the constitutive compressive relation found in literature are erroneous, they were re-derived. This derivation starts with assuming that the last segment for $0 > \varepsilon > \varepsilon*$ is described by a third order function $\sigma_1(\varepsilon)$, and the second last segment for $\varepsilon* > \varepsilon > \varepsilon_p$ by a second order function $\sigma_2(\varepsilon)$. The boundary conditions that these functions should comply to are:

$$\text{At } \varepsilon = 0 \begin{cases} \sigma_1 = 0 \\ \dfrac{d\sigma_1}{d\varepsilon} = E \end{cases}, \text{ at } \varepsilon = -\varepsilon* \begin{cases} \sigma_1 = \sigma_2 \\ \dfrac{d\sigma_1}{d\varepsilon} = \dfrac{d\sigma_2}{d\varepsilon} \\ \dfrac{d^2\sigma_1}{d^2\varepsilon} = \dfrac{d^2\sigma_2}{d^2\varepsilon} \end{cases} \text{ and at } \varepsilon = -\varepsilon_p \begin{cases} \sigma_2 = -f_c \\ \dfrac{d\sigma_2}{d\varepsilon} = 0 \end{cases}. \quad (3.1)$$

This yields the third and fourth formulas for the loading curve. As was described in Section 2.4.4, the first segment of the loading curve in Figure 2.10 is a constant value, and the second segment is either this same constant value or a linear interpolation. The first bullet point in Section 2.4.4 can thus be expanded to:

- If $\varepsilon < \alpha_{c,ref}$ there is new compressive extreme, so:

$$\alpha_{c,ref} = \varepsilon \quad (3.2)$$

$$\sigma = \begin{cases} -0.1f_c & \text{for } \varepsilon < -\varepsilon_{c,u} \\[2ex] \min(-0.1f_c, \dfrac{\varepsilon + \varepsilon_{c,u}}{\varepsilon_p - \varepsilon_{c,u}} \cdot f_c) & \text{for } -\varepsilon_{c,u} < \varepsilon \leq -\varepsilon_p \\[2ex] \dfrac{2}{n(3n-2)} \cdot \dfrac{E^2}{f_c} \cdot \varepsilon^2 + \dfrac{4}{3n-2} \cdot E \cdot \varepsilon - \dfrac{-2+n}{3n-2} \cdot f_c & \text{for } -\varepsilon_p < \varepsilon \leq -\varepsilon* \\[2ex] \dfrac{-2+n}{3n-2} \cdot \dfrac{E^3}{f_c^2} \cdot \varepsilon^3 + \dfrac{3n^2 - 6n + 2}{n(3n-2)} \cdot \dfrac{E^2}{f_c} \cdot \varepsilon^2 + E \cdot \varepsilon & \text{for } \varepsilon > -\varepsilon* \end{cases} \quad (3.3)$$

$$\sigma_{c,ref} = \sigma \tag{3.4}$$

As was shown before in Figure 2.10, the area above the loading curve given by Equation 3.3 is defined by the compressive fracture energy and the crack band width. Integration of the loading curve and equalizing the result to G_{fc}/h yields the following formulation for the ultimate strain:

$$\varepsilon_{c,u} = \varepsilon_p + \frac{2G_{fc}}{h \cdot f_c} - \frac{(3n+4) \cdot f_c}{6n \cdot E} - \frac{2(7n^3 - 9n^2 + 2) \cdot f_c}{3n(3n-2) \cdot E} \tag{3.5}$$

where G_{fc} is the compressive fracture energy.

3.1.2. Derivation of the Horizontal Tensile Strength

This section shows the derivation of the formulation for the horizontal tensile strength in Equation 2.22, which is used for the head joint failure options *Direct input head-joint tensile strength* and *Tensile strength head-joint defined by friction*. The horizontal tensile strength is based on the failure mechanism in Figure 3.1. In this failure mechanism tension failure occurs in the head joints and shear sliding occurs in the bed joints.
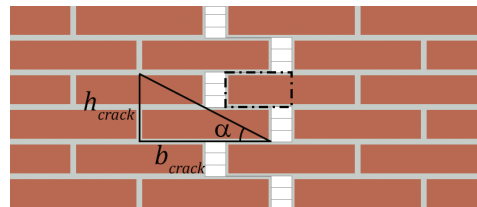
Figure 3.1: Deformed masonry after failure due to horizontal normal stress. The vertical toothed crack opens up horizontally. The dotted-dashed rectangle is the cut-out in Figure 3.2.
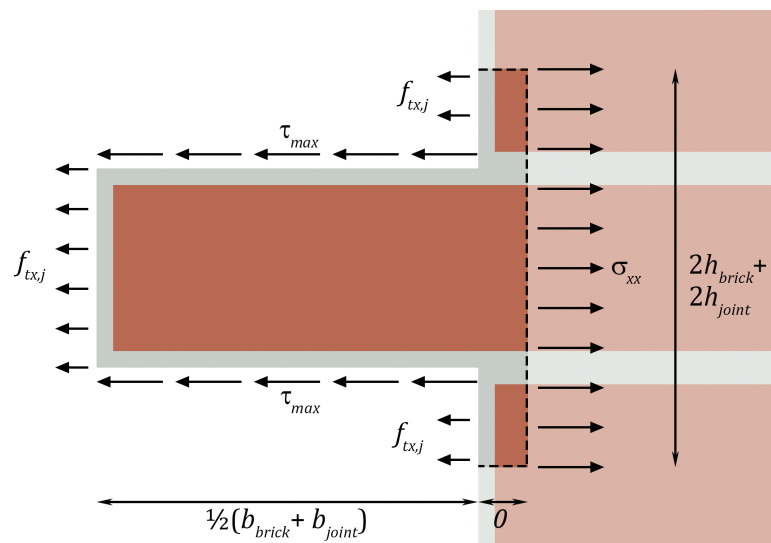
Figure 3.2: Free body diagram of a cut out just right of a vertical toothed crack due to horizontal extension. The horizontal stresses that act upon this body are depicted.

Figure 3.2 shows a free body diagram of the cut-out marked by the dotted-dashed rectangle in Figure 3.1 at the moment of failure due to horizontal extension. Along the cracks, the stresses are equal to the resistance of the material. The shear stress along the cracks through the bed joints is equal to the bed joint shear strength. The stress normal to the cracks in the head joints is equal to the horizontal head joint tensile strength. The stresses inside the intact masonry are the effect of the load, here equal to the horizontal stress due to the horizontal extension. The horizontal force equilibrium reads:

Effect of the load $\leq$ Resistance of the material

$$\sigma_{xx} \cdot 2(h_{brick} + h_{joint}) \leq \tau_{max} \cdot 2 \cdot \frac{1}{2}(b_{brick} + b_{joint}) + f_{tx,j} \cdot 2(h_{brick} + h_{joint})$$

$$\sigma_{xx} \tan \alpha \leq \tau_{max} + f_{tx,j} \tan \alpha \tag{3.6}$$

where σ_{xx} is the average horizontal stress over the cut-out, h_{brick} is the brick height, h_{joint} is the joint height, b_{brick} is the brick width, b_{joint} is the joint width, τ_{max} is the bed joint shear strength,[1] $f_{tx,j}$ is the horizontal head joint tensile strength and α is the angle as defined by Equation 2.30.

The horizontal head joint tensile strength is generally smaller than the bed joint shear strength. [18] Moreover, the tensile behaviour of the head joints is stiffer than the shear behaviour of the bed joints, resulting in head joint cracking long before the shear stresses in the bed joints reach their maximum. The contribution of the head joint strength to the total strength is therefore negligible and Equation 3.6 can be simplified to Equation 2.22.

The Implication of this Concept of Horizontal Strength
The Engineering Masonry Model is defined in a local coordinate system corresponding to the directions of the bed joints and head joints. This gives the impression that the model is valid for masonry with bonds in all possible directions, as long as the local x-axis is defined along the bed joint. However, both the *Tensile strength head-joint defined by friction* and the *Diagonal stair-case cracks* options are based on the idea that the head joints are significantly weaker than the bed joints. With common horizontal masonry, this is due to the fact that the bed joints are compressed by the weight of the bricks on top of them during construction, which is beneficial for the joint strength. The head joints, on the other hand, are barely compressed by the bricks left and right of them, resulting in a lower strength. Thus this idea only holds for horizontal masonry and one should carefully contemplate before using the two options mentioned above for masonry laid in any other direction.

3.1.3. Derivation of the Diagonal Strength
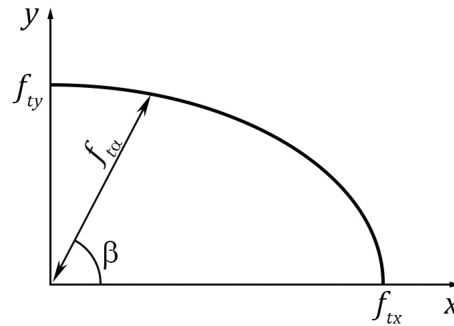
Figure 3.3: The elliptical relation between f_{tx}, f_{ty} and $f_{t\alpha}$.

Figure 3.3 graphically shows the relationship between f_{tx}, f_{ty} and $f_{t\alpha}$. For simplicity, only the first quadrant is pictured, but the equations hold for β-values larger than 90° as well. The curved line is an ellipse described by Equation 3.7. A point on this curve at an angle β from the x-axis has a distance $f_{t\alpha}$ to the origin. The x- and y-coordinates of this point are given by Equations 3.8 and 3.9, where Equation 2.29 is substituted for β. Substituting these coordinates into Equation 3.7 and isolating $f_{t\alpha}$ yields the formulation of the diagonal strength that was displayed in Equation 2.32.

$$\left(\frac{x}{f_{tx}}\right)^2 + \left(\frac{y}{f_{ty}}\right)^2 = 1 \tag{3.7}$$

$$x = f_{t\alpha} \cos \beta = -f_{t\alpha} \sin \alpha \tag{3.8}$$

[1]The bed joint shear strength is the same value as the overall masonry shear strength from Equation 2.13.

$$y = f_{t\alpha} \sin \beta = f_{t\alpha} \cos \alpha \qquad (3.9)$$

The graph in Figure 3.3 clearly shows that when one of the orthogonal strength values is significantly lower than the other, the diagonal strength is mainly governed by that low strength. This happens, for instance, in case of vertical tension. The shear strength τ_{max} and thus the horizontal tensile strength f_{tx} can then easily go to zero, resulting in zero diagonal strength $f_{t\alpha}$. To prevent this, a residual tensile strength can optionally be provided in Diana's user interface.

Furthermore, the Engineering Masonry Model subroutine `engmas.f` uses two additional minimal values for the shear strength. [15] When the shear strength description that is used in this subroutine code (Equation 3.10) is compared to the shear strength criterion as found in all EMM literature (Equation 2.13), it can be seen that a minimal value of the current cohesion and a minimal value of one percent of the "would-be" elastic shear stress are added to the shear strength criterion.

$$\tau_{max} = \max \left(c, \; c - \sigma_{yy} \tan \varphi, \; 0.01|\gamma|G_{xy} \right) \qquad (3.10)$$

3.1.4. Rotation of the Stress and Strain Tensors

The head joint failure option *Diagonal stair-case cracks* of the Engineering Masonry Model evaluates stress in the (n,t)-axis system, see also Figure 2.11 for its definition. [14] gives the relations to compute the stresses and strains in this axis system from those in the (x,y)-axis system, but those relations contain some sign errors. They are therefore recomputed here.

$$\begin{bmatrix} \sigma_{nn} & \sigma_{nt} \\ \sigma_{tn} & \sigma_{tt} \end{bmatrix} = \mathbf{R}^{\mathrm{T}} \cdot \begin{bmatrix} \sigma_{xx} & \sigma_{xy} \\ \sigma_{yx} & \sigma_{yy} \end{bmatrix} \cdot \mathbf{R}, \quad \text{with } \mathbf{R} = \begin{bmatrix} \cos \beta & -\sin \beta \\ \sin \beta & \cos \beta \end{bmatrix} \qquad (3.11)$$

We prefer, however, to write the stress σ as a vector. Expanding Equation 3.11 and rearranging the terms – taking into account that $\tau_{nt} = \sigma_{nt} = \sigma_{tn}$ and $\tau_{xy} = \sigma_{xy} = \sigma_{xy}$ – yields the rotation relationship in vector format:

$$\begin{bmatrix} \sigma_{nn} \\ \sigma_{tt} \\ \tau_{nt} \end{bmatrix} = \mathbf{R}_\sigma \cdot \begin{bmatrix} \sigma_{xx} \\ \sigma_{yy} \\ \tau_{xy} \end{bmatrix}, \quad \text{with } \mathbf{R}_\sigma = \begin{bmatrix} \cos^2 \beta & \sin^2 \beta & 2\sin \beta \cos \beta \\ \sin^2 \beta & \cos^2 \beta & -2\sin \beta \cos \beta \\ -\sin \beta \cos \beta & \sin \beta \cos \beta & \cos^2 \beta - \sin^2 \beta \end{bmatrix} \qquad (3.12)$$

Similarly, the rotation of the strain tensor is:

$$\begin{bmatrix} \varepsilon_{nn} & \varepsilon_{nt} \\ \varepsilon_{tn} & \varepsilon_{tt} \end{bmatrix} = \mathbf{R}^{\mathrm{T}} \cdot \begin{bmatrix} \varepsilon_{xx} & \varepsilon_{xy} \\ \varepsilon_{yx} & \varepsilon_{yy} \end{bmatrix} \cdot \mathbf{R}, \quad \text{with } \mathbf{R} = \begin{bmatrix} \cos \beta & -\sin \beta \\ \sin \beta & \cos \beta \end{bmatrix} \qquad (3.13)$$

This can also be rewritten into vector format, now taking into account that $\gamma_{nt} = \varepsilon_{nt} + \varepsilon_{tn}$ and $\gamma_{xy} = \varepsilon_{xy} + \varepsilon_{yx}$.

$$\begin{bmatrix} \varepsilon_{nn} \\ \varepsilon_{tt} \\ \gamma_{nt} \end{bmatrix} = \mathbf{R}_\varepsilon \cdot \begin{bmatrix} \varepsilon_{xx} \\ \varepsilon_{yy} \\ \gamma_{xy} \end{bmatrix}, \quad \text{with } \mathbf{R}_\varepsilon = \begin{bmatrix} \cos^2 \beta & \sin^2 \beta & \sin \beta \cos \beta \\ \sin^2 \beta & \cos^2 \beta & -\sin \beta \cos \beta \\ -2\sin\beta \cos \beta & 2\sin \beta \cos \beta & \cos^2 \beta - \sin^2 \beta \end{bmatrix} \qquad (3.14)$$

Note that it holds that:

$$\mathbf{R}_\varepsilon^{\mathrm{T}} = \mathbf{R}_\sigma^{-1} \quad \text{and} \quad \mathbf{R}_\sigma^{\mathrm{T}} = \mathbf{R}_\varepsilon^{-1} \qquad (3.15)$$

3.1.5. Rotation of the Stiffness Matrix

When masonry is cracked diagonally, the Engineering Masonry Model subroutine `engmas.f` [15] returns the crack strains normal and tangential to the crack. These crack strains are equal to the total strain, i.e. the fictive smeared strain over the entire element that contains the crack, minus the elastic strain, i.e. the strain of the linear elastic zones inside the element alongside the crack. Therefore it uses the following equations:

$$\varepsilon_{nn,crack} = \left(\varepsilon_{nn} - \varepsilon_{nn,elastic} \right) = \left(\varepsilon_{nn} - \frac{\sigma_{nn}}{E_n} \right) \qquad (3.16)$$

$$\gamma_{nt,crack} = \left(\gamma_{nt} - \gamma_{nt,elastic} \right) = \left(\gamma_{nt} - \frac{\tau_{nt}}{G_{nt}} \right) \qquad (3.17)$$

The Engineering Masonry Model code uses the following approximations of the diagonal normal stiffness and the diagonal shear stiffness:

$$E_n = \max\left(E_x, E_y\right) \tag{3.18}$$

$$G_{nt} = G_{xy} \tag{3.19}$$

It was investigated whether these approximations are realistic by deriving the entire rotated stiffness matrix. In the (x,y)-axis system, the Engineering Masonry Model uses a diagonal stiffness matrix. The Poisson's ratio ν is taken as zero and the constitutive relations in the orthogonal directions are uncoupled.

$$\begin{bmatrix} \sigma_{xx} \\ \sigma_{yy} \\ \tau_{xy} \end{bmatrix} = \mathbf{E}_{(x,y)} \cdot \begin{bmatrix} \varepsilon_{xx} \\ \varepsilon_{yy} \\ \gamma_{xy} \end{bmatrix}, \quad \text{with } \mathbf{E}_{(x,y)} = \begin{bmatrix} E_x & 0 & 0 \\ 0 & E_y & 0 \\ 0 & 0 & G_{xy} \end{bmatrix} \tag{3.20}$$
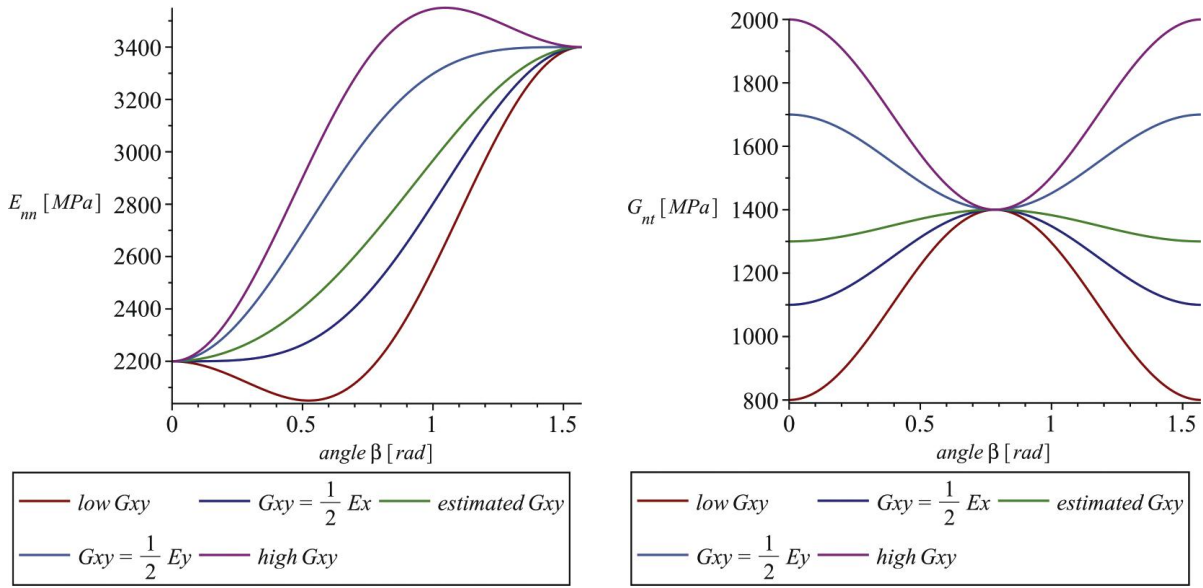
(a) The stiffness normal to the crack E_n

(b) The shear stiffness along the crack G_{nt}

Figure 3.4: Normal stiffness E_n and shear stiffness G_{nt} as a function of the crack normal direction β, for E_x = 2200 MPa, E_y = 3400 MPa and G_{xy} = 800 (low Gxy), 1100 (Gxy=$\frac{1}{2}$Ex), 1300 (estimated Gxy), 1700 (Gxy=$\frac{1}{2}$Ey) and 2000 (high Gxy) MPa. The values of E_x and E_y and the estimated G_{xy} are based on [8, Chapter 5].

The stiffness in the direction normal to the crack can be derived using the rotation formulations of the stresses and the strains. Inverting and substituting Equations 3.12 and 3.14 into Equation 3.20 yields:

$$\mathbf{R}_\sigma^{-1} \cdot \begin{bmatrix} \sigma_{nn} \\ \sigma_{tt} \\ \tau_{nt} \end{bmatrix} = \mathbf{E}_{(x,y)} \cdot \mathbf{R}_\varepsilon^{-1} \begin{bmatrix} \varepsilon_{nn} \\ \varepsilon_{tt} \\ \gamma_{nt} \end{bmatrix}, \tag{3.21}$$

Pre-multiplying both sides with $\mathbf{R}_\sigma$ gives:

$$\begin{bmatrix} \sigma_{nn} \\ \sigma_{tt} \\ \tau_{nt} \end{bmatrix} = \mathbf{R}_\sigma \cdot \mathbf{E}_{(x,y)} \cdot \mathbf{R}_\varepsilon^{-1} \begin{bmatrix} \varepsilon_{nn} \\ \varepsilon_{tt} \\ \gamma_{nt} \end{bmatrix}, \tag{3.22}$$

Or:

$$\begin{bmatrix} \sigma_{nn} \\ \sigma_{tt} \\ \tau_{nt} \end{bmatrix} = \mathbf{E}_{(n,t)} \cdot \begin{bmatrix} \varepsilon_{nn} \\ \varepsilon_{tt} \\ \gamma_{nt} \end{bmatrix}, \quad \text{with } \mathbf{E}_{(n,t)} = \mathbf{R}_\sigma \cdot E_{(x,y)} \cdot \mathbf{R}_\varepsilon^{-1} \tag{3.23}$$

Note that the stiffness matrix $\mathbf{E}_{(n,t)}$ is a fully filled matrix. Though the constitutive relations were uncoupled in the (x,y)-direction, they are coupled in the (n,t)-direction. Because the terms in this matrix are quite extensive, they are not expanded here. To get a sense of the relationship between the two terms used by [15], E_n and G_{nt}, and the material properties E_x, E_y and G_{xy}, they are drawn as a function of β in Figure 3.4. Note that for $\frac{E_x}{2} \leq G_{xy} \leq \frac{E_y}{2}$ it always holds that $E_x \leq E_n \leq E_y$. Note that G_{nt} is always between G_{xy} and $\frac{E_x + E_y}{2}$.

In conclusion, the formulations in Equation 3.16 and 3.17 deviate from the rest of the EMM theory. Firstly, they assume that the constitutive relations in the (n,t)-axis system are uncoupled, which is a direct contradiction with the general EMM assumption that the constitutive relations in the (x,y)-axis system are uncoupled. Secondly, the simplification of the stiffness matrix components that àre used is quite crude compared to the otherwise so detailed material model.

3.1.6. Yield Surface of the *Diagonal stair-case cracks* option

The yield criterion of the *Diagonal stair-case cracks* option consists of several equations. All these equations can be brought together to summarize the yield criterion into one formulation. Substituting Equations 2.13, 2.22, 2.32 and 3.12 into Equation 2.31 yields for both diagonal cracks (i.e. β_i can be $\beta_1 = \frac{\pi}{2} + \alpha$ or $\beta_2 = \frac{\pi}{2} - \alpha$):

$$\cos^2 \beta_i \cdot \sigma_{xx} + \sin^2 \beta_i \cdot \sigma_{yy} + 2\sin\beta_i \cos\beta_i \cdot \tau_{xy} \leq \max\left(0, \frac{\dfrac{(c - \sigma_{yy}\tan\varphi)}{\tan\alpha} \cdot f_{ty}}{\sqrt{\dfrac{(c - \sigma_{yy}\tan\varphi)^2}{\tan^2\alpha}\cos^2\alpha + f_{ty}^2 \sin^2\alpha}}\right)$$

$$(3.24)$$

Together with the vertical tensile failure criterion $\sigma_{yy} \leq f_{ty}$, the vertical compressive failure criterion $\sigma_{yy} \geq -f_{cy}$ and the shear failure criterion $|\tau_{xy}| \leq \tau_{max}$, they form a three-dimensional yield surface, see Figure 3.5.[2]
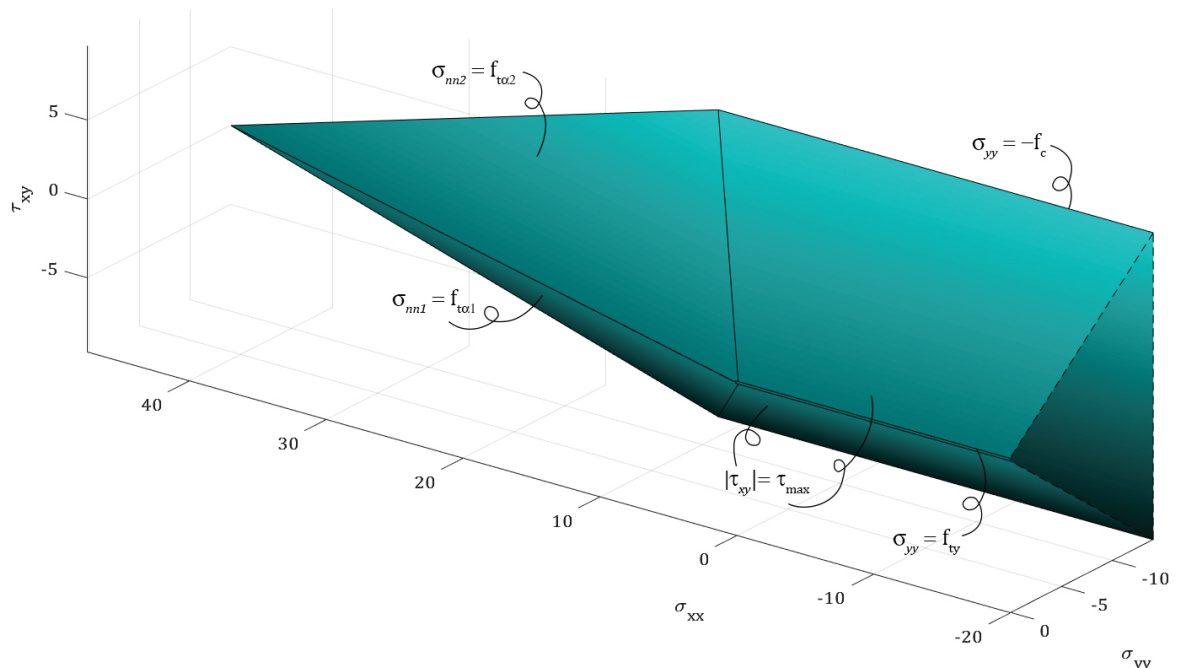
Figure 3.5: The yield surface of the Engineering Masonry Model with the *Diagonal stair-case cracks* option. The top and bottom are symmetric, the back side is a flat surface. Stresses in MPa, for material properties $\alpha = 0.5$ rad, $\varphi = 0.6$ rad, $c = 0.15$ MPa, $f_{ty} = 0.10$ MPa and $f_c = 14$ MPa.

---

[2] This yield surface follows from the theoretical description and does not include the deviations in the `engmas.f`-code mentioned in Section 2.4.5 and Equation 3.10.

There is no horizontal compressive bound, so the yield surface continues infinitely for $\sigma_{xx} \to -\infty$. There is no separate horizontal tensile bound, so horizontal tensile stresses much larger than f_{tx} are possible in combination with vertical compression. Only reaching the top, bottom, front or back surface (i.e. the maximum positive shear, negative shear, vertical tension or vertical compression, respectively) will lead to softening, reaching the left (i.e. the two maximum diagonal stresses) will not.

3.2. Analysis of the Usability

The Engineering Masonry Model is a great addition to the available masonry crack models. Nevertheless, it does not always yield the results desired. [13] Here some remarks on the accuracy and efficiency of the Engineering Masonry Model (EMM) are listed.

Advantages of the Engineering Masonry Model

- The EMM is a smeared cracking approach. Compared to the discrete micro model approach, this makes it easier for the user to mesh a model and less material parameters have to be provided. Therefore, the EMM takes less computational effort, so it is suitable for longer analyses like cyclic analysis. [10]

- The EMM is an orthogonal model. Different strength and stiffness properties can be used for the directions along and perpendicular to the bed joints. In contrast to the isotropic Total Strain Rotating Crack model, this represents the nature of masonry more accurately.

- On top of failure in the two orthogonal directions, the Engineering Masonry Model provides the option *Diagonal stair-case cracks* to consider diagonal cracks by evaluation of the stress in the direction normal to the expected staircase crack. Besides the horizontal and vertical direction, these directions are the most frequent directions of cracks observed in unreinforced masonry typical to the Groningen region. [10] In contrast to the Rankine-Hill Plasticity model, this option does include all the most relevant crack directions.

- The EMM shows better energy dissipation under in-plane cyclic loading (hysteresis) than the Total Strain Rotating Crack model. [16]

- The EMM is quite accurate in modelling in-plane cyclic horizontal loading of slender shear walls, that display rocking. [16]

- The EMM with the *Tensile strength head-joint defined by friction* option yields good force-drift results for light damage shear walls. [9]

Disadvantages of the Engineering Masonry Model

- When the *Diagonal stair-case cracks* option is used, only the stress in the diagonal direction is limited. There is no separate constitutive relation in this direction, so deformation in this direction does not directly contribute to softening.

- The EMM tensile behaviour has secant unloading and reloading, which dissipates zero energy.

- The horizontal tensile behaviour can be partly based on the vertical toothed crack failure mode. The horizontal tensile strength is then derived from the shear strength of the bed joints, but the rest of the tensile behaviour is inconsistently not derived from this same failure mode.

- Analyses using the EMM often have convergence issues and are even known to diverge.

- The crack patterns found in analyses with the EMM is more smeared out than in experimental results.

- Diagonal cracks found in analyses with the EMM are steeper than in experimental results. [9]

- The EMM underestimates the energy dissipation when used for modelling wide shear walls under cyclic horizontal loading. [16]

II
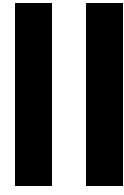
Creation of a Novel Material Model

4

Inspiration

This chapter describes three aspects of masonry shear walls and diagonal staircase cracks that formed the inspiration for the proposed material model, namely the deformation of diagonal staircase cracks in shear walls, the crack pattern of horizontal tensile failure and the shape of the hysteresis loop of shear walls under cyclic loading.

4.1. Deformation of a Diagonal Staircase Crack

The Engineering Masonry Model's diagonal cracking failure criterion evaluates the normal stress in a rotated axis system, normal to the possible staircase crack. See also failure mode F in Table 2.1. When the material cracks due to this diagonal tensile stress, the crack is expected to open up in the same direction as the tensile stress, as in Figure 4.1.
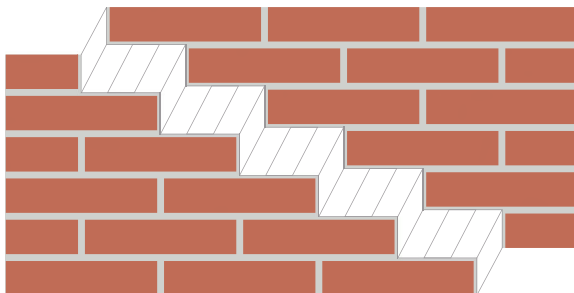
Figure 4.1: Failure mechanism of a diagonal crack that opens up diagonally.
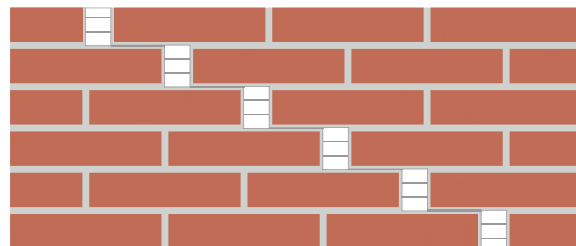
Figure 4.2: Failure mechanism of a diagonal crack that opens up horizontally.

However, in experimental observations of diagonally cracked masonry, like Figure 4.4, the crack seems to open up horizontally rather than diagonally. This phenomenon looks similar to the illustration in Figure 4.2. The diagonal staircase crack seems to be a combination of tensile failure of the head joints and shear sliding along the bed joint. It looks like a hybrid version of the failure mechanisms in Figures 2.6 and 2.9, plain shear sliding along the bed joint and the vertical toothed crack due to horizontal loading.

It is unknown at which point during the experiment the photo in Figure 4.4 was taken. It could be taken after the sideways loading was removed. Although the uncracked middle of the hourglass shaped part suggests otherwise, there could have been a vertical component to the crack opening the moment the material reached its peak strength and the crack just started to form. To be thorough, more detailed Digital Image Correlation (DIC) imagery of another laboratory test are studied.

Figure 4.3 shows the displacements of *TUD-COMP-48*, a double clamped masonry wall undergoing cyclic horizontal loading of increasing amplitude. The image shows a large staircase crack at the top, some smaller cracks in the middle and a more recent crack at the bottom. At the moment of this image was taken (i.e. $t = 486$ s), the top displacement just reached a new extreme of 2.09 mm. The bottom crack is now propagating upwards, so at the very top of this crack material is observed that has just
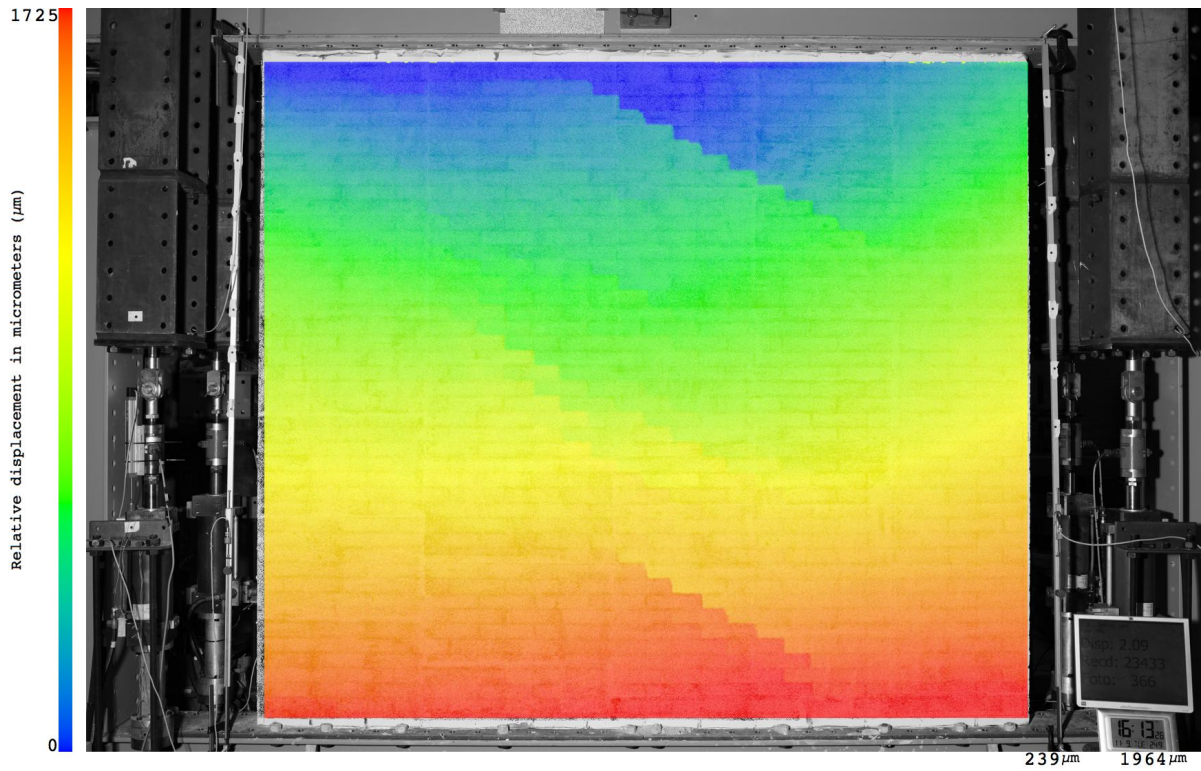
(a) the horizontal displacements.
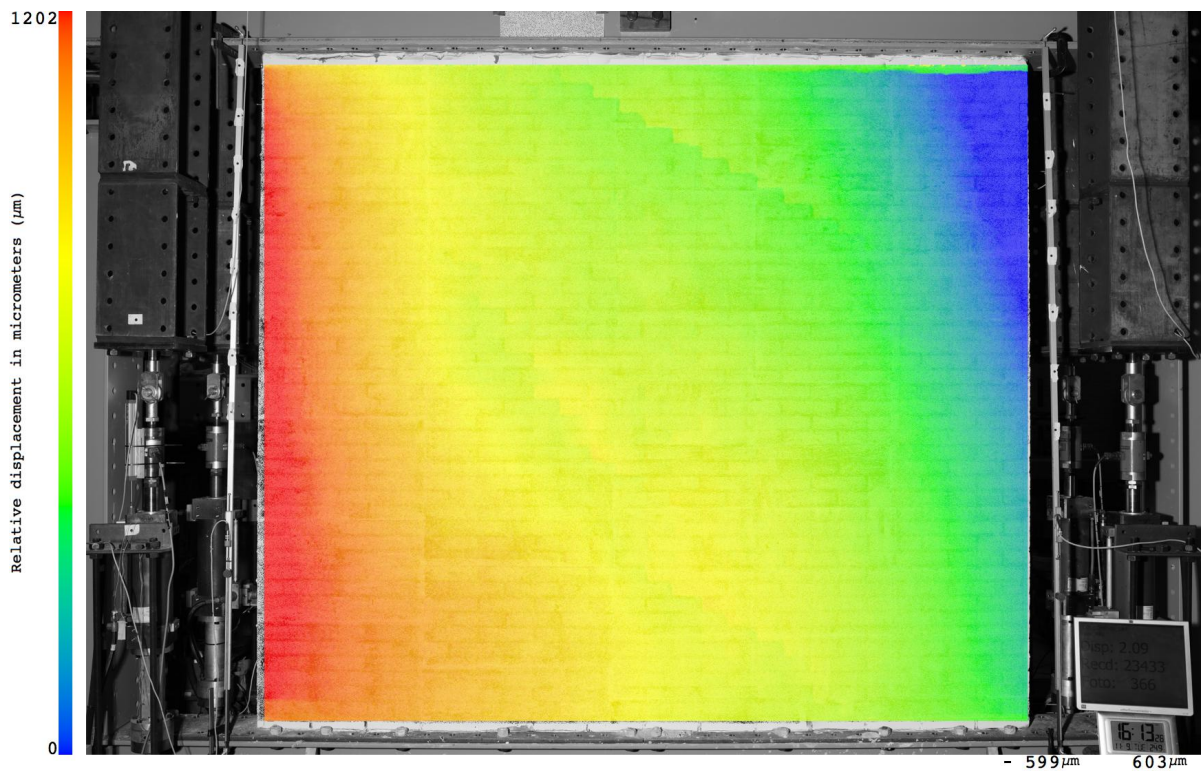
(b) the vertical displacements.

Figure 4.3: Digital images of the horizontal and vertical displacements of test *TUD-COMP-48* at t=486 s, at a new horizontal top displacement extreme. Images courtesy of [9].
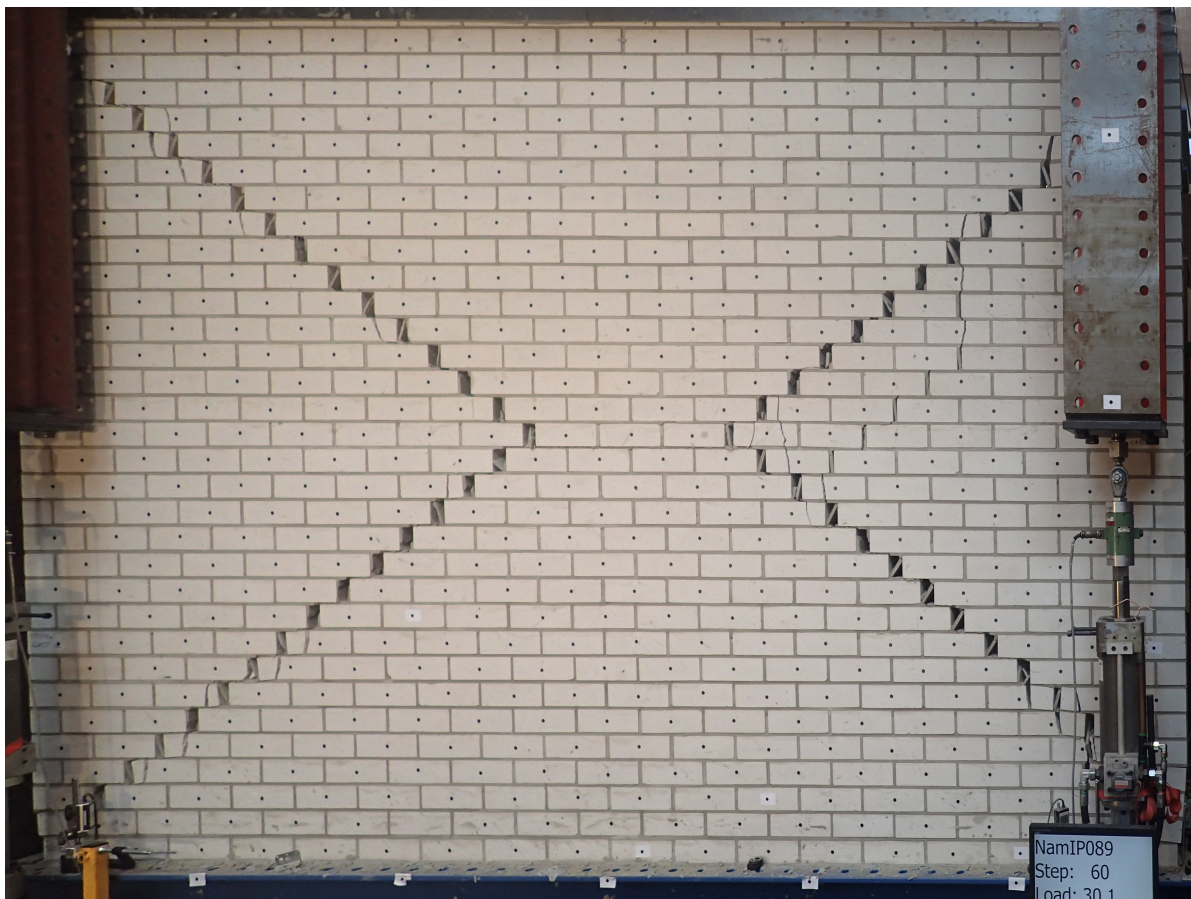
Figure 4.4: Observed crack pattern during the *TUD-COMP-4Q* test, a double clamped shear wall under cyclic horizontal loading of the top. Photo courtesy of [12].

started to crack. Notice the sharp discontinuity of colour in the horizontal displacement in Figure 4.3(a) and the absence of such a discontinuity in the vertical displacement in Figure 4.3(b).[1] This indicates that this crack is opening up horizontally.

In conclusion, these two examples have shown that some diagonal cracks in shear walls open up horizontally rather than diagonally.

4.2. Crack Pattern of Horizontal Tensile Failure

[7] reports tests performed to determine the material properties of masonry. Several shear and compressive test were executed, but for practical reasons no axial tensile test was conducted. What was performed is a horizontal in-plane bending test in order to determine the tensile fracture energy. This four-point bending test is the best alternative source of information for a uni-axial tensile stress test.

In the middle field of a four-point bending test of a slender beam, the shear force is zero, see Figure 4.5. This middle field is a constant moment zone. The stresses that are present in this zone are normal stresses due to bending: horizontal tensile stresses at the bottom and horizontal compressive stresses at the top. One could thus say that any crack occurring in this zone is the result of horizontal tensile stresses.

As Figure 4.6 shows, the crack patterns that occurred during the four point bending tests in [7] consist mainly of cracks through the bed and head joints inside the constant moment zone.[2] Some parts of these patterns show resemblance to the vertical toothed crack we saw in Figure 2.9. Most,

---

[1]Some other diagonal staircase cracks do clearly have a vertical crack opening component, for instance the one at the top. That said, this particular piece of crack, does not.

[2]Only one expected weak zone (i.e. head joint) lies at each extremity in the constant moment zone. Thus it is considered a logical consequence that the cracks also begin or end just outside of the constant moment zone, or even go straight through the brick, due to spatial variation in the material properties.
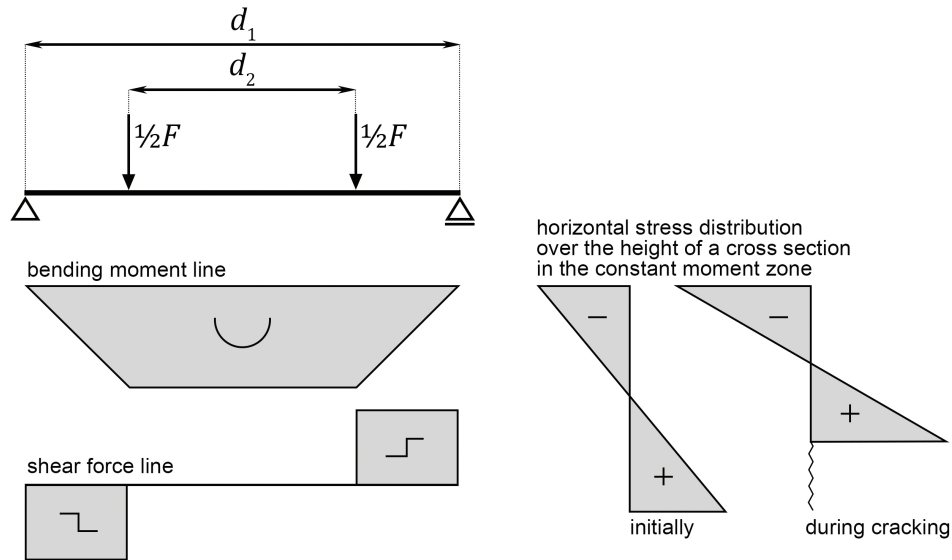
Figure 4.5: Schematic display of a slender beam subjected to four point bending, with its moment line and its shear force line below. The horizontal stress distribution over a cross section in the constant moment zone is given on the right, both initially and once the bottom of the cross section has started to crack.

TUD-MAT-34a

TUD-MAT-34b/c

TUD-MAT-34d

TUD-MAT-34e/f/g
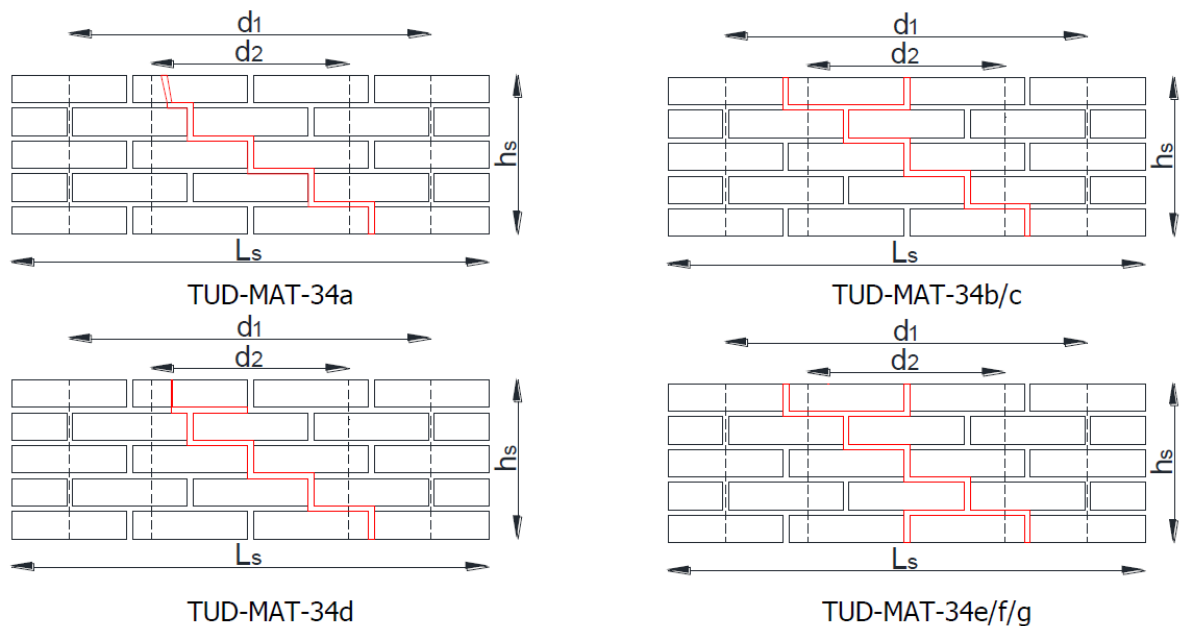
Figure 40 - Crack pattern for single wythe masonry specimens subjected to in-plane bending (IP).

Figure 4.6: Crack patterns of single wythe masonry specimens subjected to a horizontal in-plane four-point bending test, where d_1 is the distance between the supports and d_2 is the distance between the loads. Image courtesy of [7].

however, look more like a diagonal staircase crack.

This example shows that horizontal stress can cause a diagonal staircase crack, too, not only a vertical toothed crack. The crack simply starts in a head joint and then continues to form along a segment of bed joint, be it left or right of the head joint. The crack then goes up the nearest head joint, continues along another segment of bed joint, and so on. Because the middle field is a constant moment zone – and thus the horizontal bending stresses are also constant –, the choice to go left or right is theoretically arbitrary. In practice it is determined by local strength deviations in the material. Nevertheless, whether the total crack pattern will look like a staircase or toothed is arbitrary.

4.3. Shape of the Force Displacement Diagram of a Double Clamped Shear Wall under Cyclic Loading

Figure 4.7 shows the force-displacement diagram of the *TUD-COMP-4Q* test, the shear wall that was portrayed in Figure 4.4. The diagram shows a parallelogram shaped hysteresis loop that looks similar to the parallelogram shaped unloading-reloading loop of the shear behaviour of the bed joints. This similarity suggests that it could be beneficial to exploit the shear behaviour of the bed joints for the overall material behaviour.
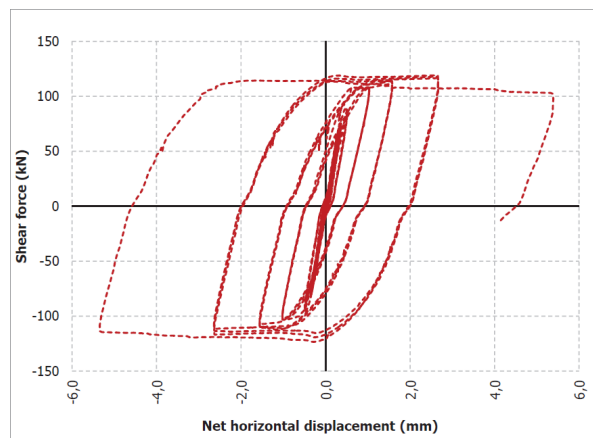
Figure 4.7: Measured horizontal force versus horizontal top displacement of the *TUD-COMP-4Q* experiment. Image courtesy of [12].

4.4. Conclusion

The examples in the previous paragraphs suggest that it could be interesting to regard the diagonal staircase crack as a horizontal phenomenon, as a crack that opens up horizontally under the influence of horizontal forces, see the visual in Table 4.1. It would also be interesting to utilize the shear behaviour of the bed joints for the overall material behaviour. In the next chapter these ideas will be developed into a usable material model.

Table 4.1: Failure mode considered by the proposed material model.
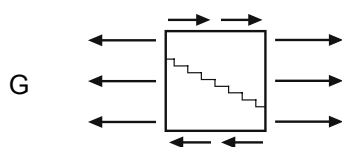
G   Shear and horizontal tension, i.e. horizontally opening diagonal staircase crack

<div style="text-align: right; font-size: 3em;">5</div>

The Equivalent Shear Masonry Model

The Equivalent Shear Masonry Model is an augmentation of the Engineering Masonry Model. It is a similar orthotropic smeared cracking material model, defined in the same (x,y)-axis system with the x-axis (i.e. horizontal axis) parallel the bed joint. It considers the horizontal and vertical compression behaviour as in Section 2.4.4, the vertical tensile behaviour as in Section 2.4.3 and additionally a combined shear-horizontal tension behaviour. This combined behaviour uses the concept of *Equivalent Shear* that will be described in this chapter.

5.1. The Equivalent Shear Failure Criterion

Consider a brick wall at the moment a horizontally opening diagonal crack occurs, like the one in Figure 5.1. For schematization purposes, the crack is assumed to form in the centre of the joints. Now let's zoom in to investigate the forces in play at the onset of failure, similar to what was done to determine the friction based horizontal tensile strength in Section 3.1.2.
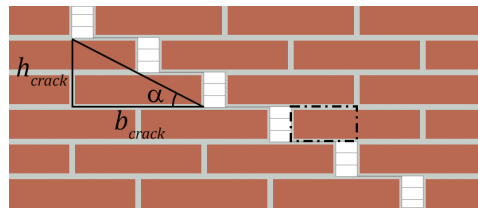
Figure 5.1: Deformed masonry after failure due to horizontal normal stress and shear stress. The crack is a diagonal staircase shape, the crack opening is horizontal. The dotted-dashed rectangle is the cut-out in Figure 5.2.

Figure 5.2 shows the cut-out that is marked with the dotted-dashed rectangle in Figure 5.1 and shows all horizontal stresses involved at the onset of failure. The shear stress τ_{xy} and the horizontal normal stress σ_{xx} due to the load act on the intact edges of this cut out, i.e. the top and the right side. These stresses are the average internal stresses over the masonry cut-out. Stresses equal to the material resistance can be found on the edges that coincide with the newly forming crack, i.e. the bottom and the left side. These stresses are a shear stress equal to the maximum bed joint shear strength τ_{max}[1] and a horizontal stress equal to the horizontal head joint tensile strength $f_{tx,j}$, respectively. The horizontal force equilibrium reads:

Effect of the load $\leq$ Resistance of the material

$$\tau_{xy} \cdot \frac{1}{2}(b_{brick} + b_{joint}) + \sigma_{xx} \cdot (h_{brick} + h_{joint}) \leq \tau_{max} \cdot \frac{1}{2}(b_{brick} + b_{joint}) + f_{tx,j} \cdot (h_{brick} + h_{joint})$$

$$\tau_{xy} + \sigma_{xx} \tan \alpha \leq \tau_{max} + f_{tx,j} \tan \alpha \tag{5.1}$$

where h_{brick} is the brick height, h_{joint} is the joint height, b_{brick} is the brick width, b_{joint} is the joint width and $\tan \alpha$ is the height-width ratio of the diagonal staircase crack as defined by Equation 2.30.

---

[1] The bed joint shear strength is the same value as the overall masonry shear strength from Equation 2.13.
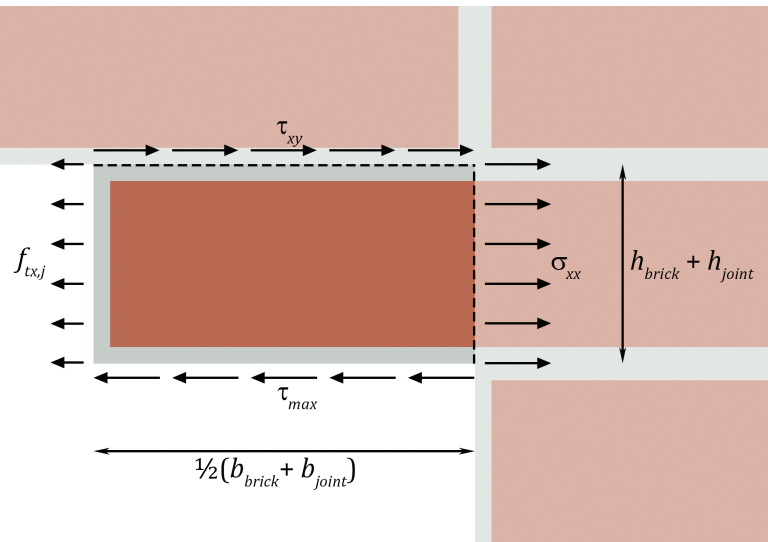
Figure 5.2: Free body diagram of half a brick and its adjacent joints, at the moment a staircase crack forms along its bottom and left side. The horizontal stresses that act upon this body are depicted.

As was explained in Section 3.1.2, the contribution of the head joint strength to the resistance can be neglected for horizontally laid masonry. This yield the failure criterion proposed in this thesis:

$$\tau_{xy} + \sigma_{xx} \tan \alpha \leq \tau_{max} \tag{5.2}$$

Note that the failure criterion in Equation 5.2 also serves for negative shear. Besides, it only applies to horizontal tensile stress, not to compression. Therefore, a more universal formulation of the failure criterion is:

$$|\tau_{xy}| + \max(\sigma_{xx}, 0) \tan \alpha \leq \tau_{max} \tag{5.3}$$

The left-hand side of this equation will be referred to as equivalent shear stress τ_{eq}:

$$\tau_{eq} = |\tau_{xy}| + \max(\sigma_{xx}, 0) \tan \alpha \tag{5.4}$$

In absence of horizontal tension Equation 5.3 can be reduced to Equation 2.12. In absence of shear stress it can be reduced to:

$$\sigma_{xx} \leq \frac{\tau_{max}}{\tan \alpha} \tag{5.5}$$

The failure criterion in Equation 5.3 defines the stress state (or rather, stress states) up until which the material behaviour is linear elastic and beyond which the post-peak behaviour begins. The pre-peak linear elastic shear and horizontal behaviour can be regarded separately. Their post-peak behaviour on the other hand, is coupled and path dependent, meaning that the shear and horizontal tensile stress depend on both the shear and horizontal extension strain state and their histories. Therefore, the deformation of the considered failure mechanism should be further investigated and especially how this can be described as a strain state.

5.2. Kinematic Relations

Once more the failure mechanism depicted in Figure 4.2 is considered. Now imagine a rectangular element that is two bricks and two head joints wide and four bricks and four bed joints high. First, it is assumed that the element includes half of the bed joint at the top, half of the bed joint at the bottom, no head joint at the left, but the entire head joint at the right, see Figure 5.3. Since the crack is assumed to occur in the joint centre, this means the left two corner points are located in the darker triangle on the left side of the crack. The right two corner points, on the other hand, are located in the lighter triangle at the right side of the crack. The deformation of masonry can thus be perceived as a horizontal strain, see Equation 5.6.
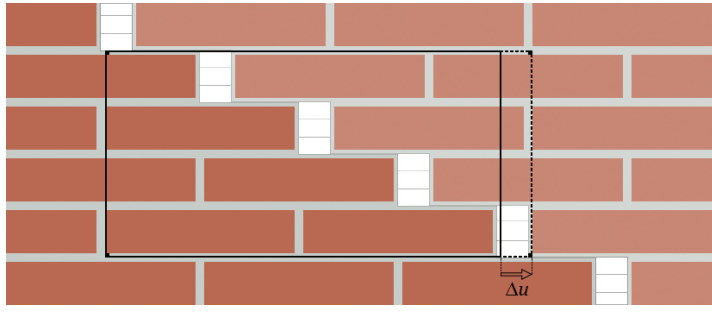
Figure 5.3: Rectangular element that shows horizontal extension, to a background of cracked masonry. The solid line shows the original shape, the dashed line shows deformed shape.

$$\varepsilon_{xx} = \frac{\partial u_x(x,y)}{\partial x} = \frac{\Delta u}{b_{crack}}$$

$$\Delta u = \varepsilon_{xx} \cdot b_{crack} \tag{5.6}$$

where ε_{xx} is the horizontal strain, $u_x(x,y)$ is the horizontal displacement field, x is the horizontal location coordinate, Δu is the horizontal crack deformation and b_{crack} is the horizontal crack dimension.

Alternatively, it can be assumed that the element includes half the head joints on the left, half the head joints on the right, no bed joint at the bottom, but the entire bed joint at the top, see Figure 5.4. In this case, the bottom two corner point are located in the darker triangle left of the crack and the top two corner points are located in the lighter triangle right of the crack. Now, the deformation of the masonry can be perceived as a shear deformation, see Equation 5.7.
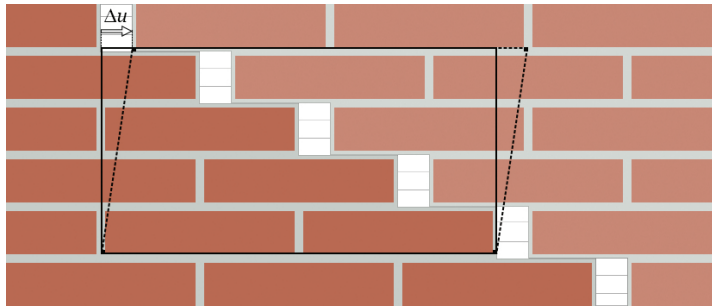
Figure 5.4: Rectangular element that shows shear deformation, to a background of cracked masonry. The solid line shows the original shape, the dashed line shows deformed shape.

$$\gamma_{xy} = \frac{\partial u_x(x,y)}{\partial y} + \frac{\partial u_y(x,y)}{\partial x} = \frac{\Delta u}{h_{crack}} + 0$$

$$\Delta u = \gamma_{xy} \cdot h_{crack} \tag{5.7}$$

where γ_{xy} is the shear strain, $u_y(x,y)$ is the vertical displacement field, y is the vertical location coordinate and h_{crack} is the vertical crack dimension.

Finally, consider the same element as before, but now assume that the corner points are not just inside the rectangle, but exactly at its boundaries, see Figure 5.5. In that case, both the top left and the bottom right corner point are located right on top of the line where the crack will form. After cracking, these nodes can be perceived to be somewhere in the crack opening. Therefore, the deformation can be seen as a combination of extension and shear deformation, see Equation 5.8.
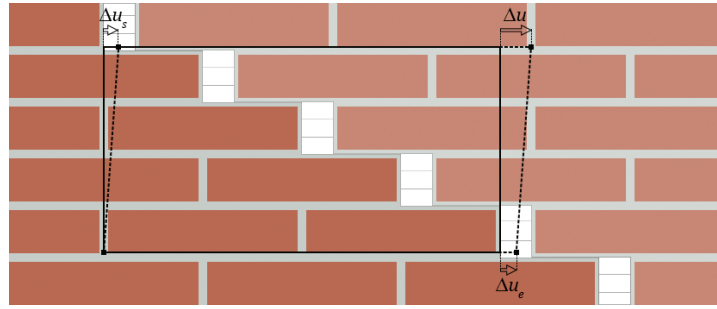
Figure 5.5: Rectangular element that shows a combination of horizontal extension and shear deformation, to a background of cracked masonry. The solid line shows the original shape, the dashed line shows deformed shape.

$$\Delta u = \Delta u_s + \Delta u_e = \gamma_{xy} \cdot h_{crack} + \varepsilon_{xx} \cdot b_{crack} \tag{5.8}$$

where Δu_s is the horizontal crack deformation due to shear and Δu_e is the horizontal crack deformation due to horizontal extension.

The total deformation Δu can be described as a combination of shear strain γ_{xy} and horizontal normal strain ε_{xx}. For this purpose, the amount of γ_{xy} that results in the same deformation Δu as ε_{xx} is derived. Combining Equation 5.6 and 5.7 and eliminating Δu gives:

$$\gamma_{xy,\,equivalent\,to\,\varepsilon_{xx}} \cdot h_{crack} = \varepsilon_{xx} \cdot b_{crack}$$

$$\gamma_{xy,\,equivalent\,to\,\varepsilon_{xx}} = \varepsilon_{xx} \cdot \frac{b_{crack}}{h_{crack}} = \frac{\varepsilon_{xx}}{\tan\alpha} \tag{5.9}$$

The total equivalent deformation can be then described as the equivalent shear strain γ_{eq}:

$$\gamma_{eq} = \gamma_{xy} + \frac{\varepsilon_{xx}}{\tan\alpha} \tag{5.10}$$

Note that the total equivalent deformation in Equation 5.10 also serves for negative shear. Besides, it only applies to horizontal tensile strain, not to compression. Therefore, a more universal formulation of the total equivalent deformation is:

$$\gamma_{eq} = |\gamma_{xy}| + \frac{\max\left(\varepsilon_{xx}, 0\right)}{\tan\alpha} \tag{5.11}$$

5.3. Constitutive Relation

Now the equivalent shear stress and the equivalent shear strain are defined, their relationship is discussed. The resistance of the material to this failure mechanism is governed by the shear sliding behaviour of the bed joints. Therefore, the equivalent shear stress and equivalent shear strain are assumed to behave according to a similar stress-strain diagram as is used for the shear sliding of the bed joints, see Figure 5.6.

As mentioned at the end of Section 5.1, before the combined failure criterion is reached, the shear and extension stress-strain relationships are linear and independent of each other. Note that this part of the graph is not necessarily a straight line, as the two individual strains can increase non-simultaneously, each with their own stiffness. Unloading, too, happens for both shear and extension linearly and independently of each other.

The equations used to describe the behaviour are similar to those that were introduced in Section 2.4.2. The behaviour in Figure 5.6 can be summarized as follows:

$$\tau_{eq} = \begin{cases} -\tau_{max} & \text{for } \tau_{eq,l} < -\tau_{max} \\ \tau_{eq,l} & \text{for } -\tau_{max} \le \tau_{eq,l} \le \tau_{max} \,, \quad \text{with } \tau_{eq,l} = \tau_0 + G_{xy}\Delta\gamma + \left(\sigma_{xx,0} + E_x\Delta\varepsilon_{xx}\right)\tan\alpha \\ \tau_{max} & \text{for } \tau_{eq,l} > \tau_{max} \end{cases} \tag{5.12}$$
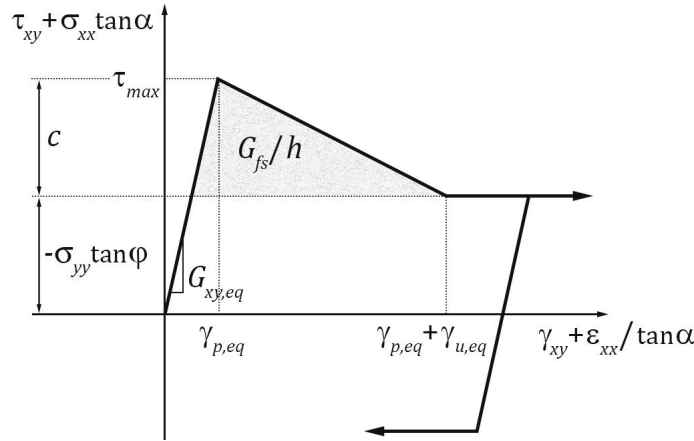
Figure 5.6: Stress-strain diagram illustrating the equivalent shear behaviour.

where τ_{eq} is the new equivalent shear stress, $\tau_{eq,l}$ is the initial linear prediction of the new equivalent shear stress, $\Delta\gamma$ is a shear strain increment, $\Delta\varepsilon_{xx}$ is a simultaneous horizontal normal strain increment, τ_0 is the shear stress before the application of the strain increments, $\sigma_{xx,0}$ is the horizontal normal stress before the strain increments, G_{xy} is the shear stiffness and E_x is the horizontal stiffness.

Should the material be cracked in any direction, the cohesion is reduced to zero immediately. Otherwise, once the material reaches the maximum shear stress, the cohesion is reduced by the following equation:

$$c = c_0 \frac{\gamma_{u,eq} - \gamma_{cum,eq}}{\gamma_{u,eq}} \tag{5.13}$$

where c is the current cohesion, c_0 is the initial cohesion, $\gamma_{cum,eq}$ is the cumulative equivalent shear strain over all the time that the equivalent shear stress was equal to the maximum shear stress, and $\gamma_{u,eq}$ is the equivalent ultimate shear strain, the cumulative equivalent shear strain at which the cohesion is fully gone. This value intrinsically depends on the shear fracture energy and due to the smeared crack approach also depends on the element size, by:

$$\gamma_{u,eq} = \frac{2G_{fs}}{c \cdot h} - \frac{c}{G_{xy,eq}} \tag{5.14}$$

where G_{fs} is the shear fracture energy, c is the cohesion, h is the crack band width and $G_{xy,eq}$ is defined as the apparent equivalent shear stiffness at peak:

$$G_{xy,eq} = \frac{\tau_{max}}{\gamma_{p,eq}} \tag{5.15}$$

5.4. Points of Interest

Equations 5.3 and 5.11 and Section 5.3 almost completely describe the equivalent shear failure mode of the Equivalent Shear Masonry Model. Some aspects require some extra attention, though. They are discussed here separately, because their solutions are not logical extensions of the rest of the theory, but rather artificial choices.

Tensile and Compressive Behaviour Compatibility

In many material models, both compressive and tensile unloading go to the origin. See for instance the compression and tension stress-strain diagrams of the Engineering Masonry Model in Figure 5.7. That way, the tensile and compressive part are always connected.

In the Equivalent Shear Masonry Model, the horizontal tensile behaviour is derived from the shear behaviour of the bed joints. This means that during unloading, negative horizontal normal stress can occur for positive horizontal normal strains, see Figure 5.8. This way, unloading does not go trough the origin and the tensile and compressive part of the stress-strain diagram are not connected.
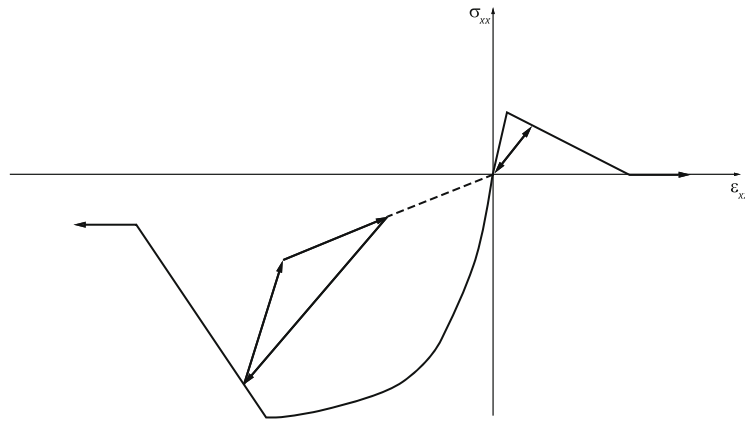
Figure 5.7: Compatibility between the tensile and compressive part of the horizontal stress-strain diagram according to the Engineering Masonry Model, with unloading to the origin.
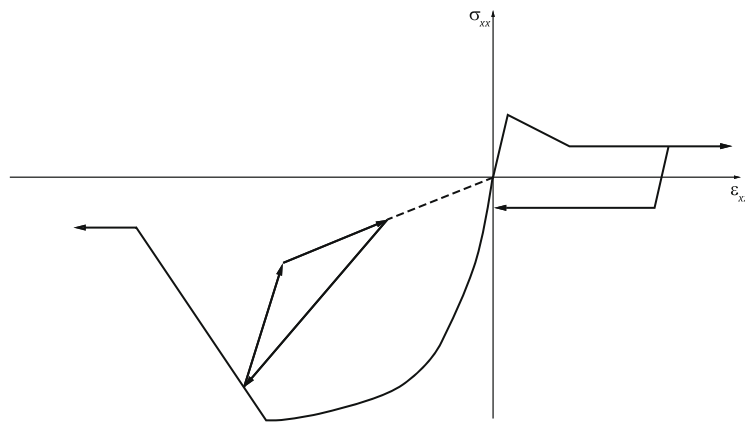
Figure 5.8: Compatibility between the tensile and compressive part of the horizontal stress-strain diagram in the case that the tensile behaviour is derived directly from the shear behaviour of the bed joints.
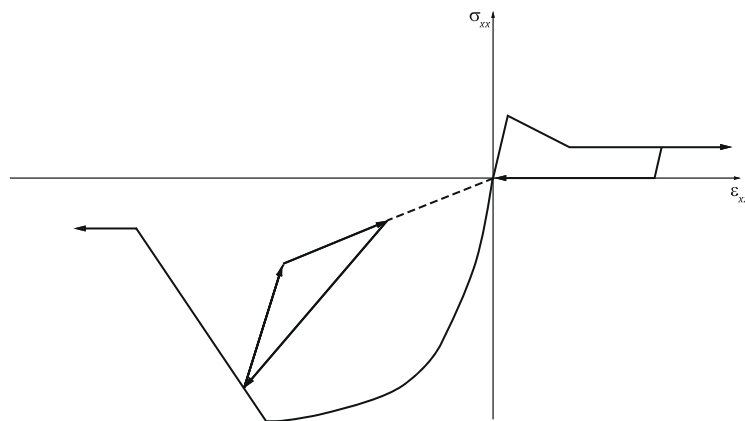
Figure 5.9: Compatibility between the tensile and compressive part of the horizontal stress-strain diagram with tensile unloading adjusted for compatibility.

To resolve this issue, the horizontal tensile behaviour is adapted so that it remains in the first quadrant, see Figure 5.9. To achieve this, a minimal value of zero is assigned to the horizontal tensile stress:

$$\sigma_{xx} \geq 0 \tag{5.16}$$

Equivalent Shear Stress Division into the Shear Stress and the Tensile Stress
The stress-strain diagram in Figure 5.6 and the Equations 5.14 and 5.15 describe the total equivalent shear stress for any given strain state and strain history. They do not, however, give any information on what part of this total equivalent stress should be the shear part, and which should be the normal stress part. To divide the total equivalent shear stress into its two components, it is assumed that the ratio between the two components remains unchanged during softening and further sliding. This assumption is expected to be realistic because with separate (shear) yielding, the stress also stays the same regardless of the (shear) strain increments. For simplicity, this aspect is extended to the softening phase by means of proportionally reducing the shear stress and horizontal tension stress.

5.5. Yield Surface

The yield criterion of equivalent shear $|\tau_{xy}| + \max(\sigma_{xx}, 0)\tan\alpha \leq \tau_{max}$ is combined with the vertical tensile failure criterion $\sigma_{yy} \leq f_{ty}$, the vertical compressive failure criterion $\sigma_{yy} \geq -f_{cy}$ and the horizontal compressive failure criterion $\sigma_{xx} \geq -f_{cx}$ to draw the three-dimensional yield surface of the Equivalent Shear Masonry Model, see Figure 5.10.

Compared to the yield surface of the Engineering Masonry Model's *Diagonal stair-case cracks* option in Figure 3.5, this yield surface is smaller. The horizontal compression stress is limited to the compression strength. The horizontal tensile stress can never be larger than the horizontal tensile strength derived from friction in the bed joints. Reaching any of the surfaces will lead to softening (i.e. shrinkage of the yield surface).
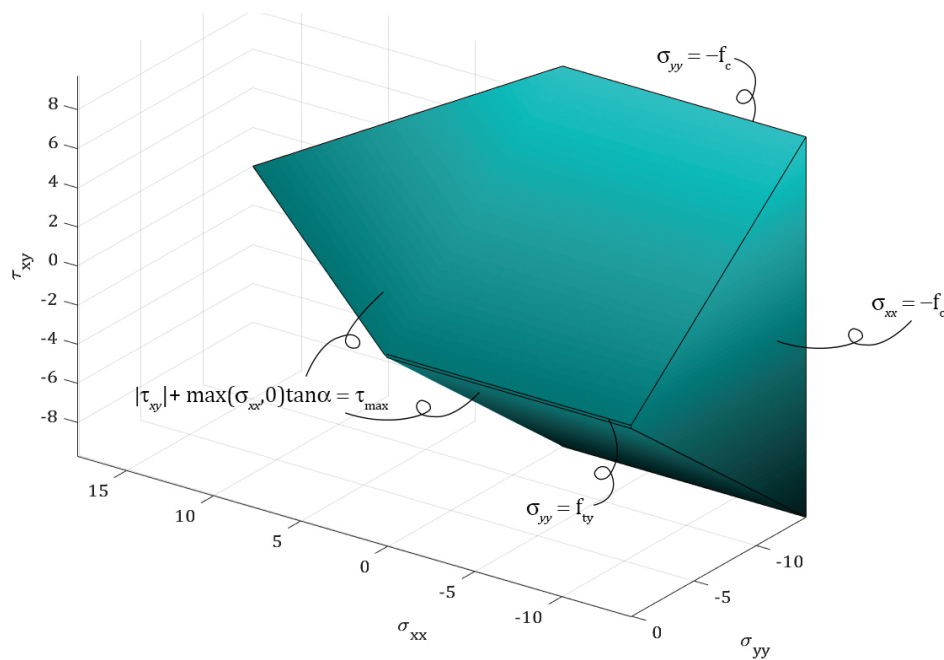
Figure 5.10: The yield surface of the Equivalent Shear Masonry Model. The top and bottom are symmetric, the back side is a flat surface. Stresses in MPa, for material properties $\alpha = 0.5$ rad, $\varphi = 0.6$ rad, $c = 0.15$ MPa, $f_{ty} = 0.10$ MPa and $f_c = 14$ MPa.

6

User Supplied Subroutine Implementation

This chapter explains the Fortran code that was written for the Equivalent Shear Masonry Model user supplied subroutine. Note that this material model is meant for horizontally laid masonry and that the local axis system must be defined such that the x is parallel to the bed joints. Codes snippets of the most interesting parts of the subroutine will be provided and discussed in detail. In addition, the full Fortran code of the User Supplied Subroutine `usrmat_eqshma.f` is given in Appendix B.

6.1. Introduction

The code presented here builds on an earlier user supplied subroutine for the Engineering Masonry Model material model called `usrmat_quad2.f`. The sections `SHEAR RETENTION` and `DIAGONAL CRACK FAILURE CRITERION` were replaced by a new section `FRICTIONAL CRITERION` that describes the combined shear and horizontal extension failure. Also, the formulas that describe the compressive behaviour were adjusted to the formulas in Equation 3.3, because the original equations in the `usrmat_quad2.f`-code did not give the expected stress-strain relationship from the EMM theory and the EMM as implemented in Diana, see also Figure 7.3(c). Besides, some lines were removed or simplified, because the function called in it was not supported by the available function libraries. Other lines were rearranged to a more logical place in the document.

6.2. Front Matter

In the first lines the if statement around the `ATTRIBUTES DLLEXPORT::USRMAT`-command was removed to make the compiling work on a 64 bit Windows pc.

Line 2 to 4 contain the subroutine statement. This statement mirrors the subroutine name `USRMAT` and all its arguments precisely as it should be called in the main frame.

In line 5 to 35 all the dummy arguments that can be used in a user supplied subroutine are explained in comments. The ones that the Equivalent Shear Masonry Model uses are summarized in Table 6.1. Some arguments are only given as input, such as the strain, the strain increment, the iteration number and the user parameters (i.e. among others the material properties). Others are given as input, but must also be updated and returned to the main frame as output. These are the stress, the stiffness, the user state variables and the user state indicators. The other arguments, starting with `N`, inform on the size of the arrays.

The content of the three user arrays is explained by Tables 6.4 to 6.2. The user parameters `USRVAL` are mainly the material properties, complemented with the crack band width. This last one had to be added manually due to the fact that the function used to automatically obtain the crack band width is not supported by the available function library. The user state variables `USRSTA` and users state indicators `USRIND` contain information on the current state of the integration point, such as whether it is crushed or cracked. This is abundantly given in several double precision and integer values, and summarized into one indicator called `FAIMEC`. This indicator is set to zero at the start of the document, and then

Table 6.1: In- and output arguments used by the `usrmat_eqshma.f` user supplied subroutine.

EPS0	double precision array	In	Strain vector at start of step.
DEPS	double precision array	In	Total strain increment.
NS	integer	In	Number of stress components
ITER	integer	In	Current iteration number.
USRVAL	double precision array	In	User parameters.
NUV	integer	In	Number of user parameters.
USRSTA	double precision array	InOut	User state variables at start of step. Should be updated at output.
NUS	integer	In	Number of user state variables.
USRIND	integer array	InOut	User indicators at start of step. Should be updated at output.
NUI	integer	In	Number of user state indicators.
SIGMA	double precision array	InOut	Total stress at start of step. Current stress at output.
STIFF	double precision array	InOut	Previous tangent stiffness. Current tangent stiffness at output.

increased by 1, 2 or 4 etc. when a section on a certain failure mode shows it is cracked or crushed, see also Table 6.3.

Table 6.2: The user indices (integer) as used in the user supplied subroutine in `usrmat_eqshma.f`.

USRIND

1	1 if CRACKD for I=1	1 if cracked in x-direction
2	1 if CRACKD for I=2	1 if cracked in y-direction
3	1 if CRUSHD for I=1	1 if crushed in x-direction
4	1 if CRUSHD for I=2	1 if crushed in y-direction
5	FRCFAI	1 if cracked in shear

Table 6.3: Descriptions of the meaning of the failure mechanism indicator FAIMEC

FAIMEC 0	uncracked
FAIMEC uneven	cracked in x-direction
$\lfloor$FAIMEC/2$\rfloor$ uneven	cracked in y-direction
$\lfloor$FAIMEC/4$\rfloor$ uneven	crushed in x-direction
$\lfloor$FAIMEC/8$\rfloor$ uneven	crushed in y-direction
$\lfloor$FAIMEC/16$\rfloor$ uneven	cracked in shear

The user state variables USRSTA also contains information on the loading history of the integration point in question, such as the maximum reached strains and their corresponding reference stresses and the cumulative post-peak shear strain. Furthermore it contains information that might interest the user as output, like the remaining cohesion, the current shear strength, the current load-resistance ratio and the crack width.

In line 36 to 67 all arguments (i.e. parameters or variables) that are used in the subroutine code are defined. This includes their type, which can be integer (1, 2, ...), double precision (2.20000E+09 and suchlike), parameter (fixed integer value), character (A, B, ...) or logical (true, false). This section also defines the size of the array arguments, for instance EPS0(NS).

Table 6.4: The user parameters (double precision) as used in the user supplied subroutine in `usrmat_eqshma.f`.

USRVAL			
1	`YOUN0(1)`	E_x	Horizontal stiffness
2	`YOUN0(2)`	E_y	Vertical stiffness
3	`SHRM0`	G_{xy}	Shear stiffness
4	`TANPHI`	$\tan\varphi$	Tangent of friction angle
5	`FT(1)`[a]	f_{tx}	Horizontal tensile strength
6	`FT(2)`	f_{ty}	Vertical tensile strength
7	`GFT(1)`[a]	G_{ftx}	Horizontal tensile fracture energy
8	`GFT(2)`	G_{fty}	Vertical tensile fracture energy
9	`FC(1)`	f_{cx}	Horizontal compressive strength
10	`FC(2)`	f_{cy}	Vertical compressive strength
11	`GFC(1)`	G_{fcx}	Horizontal compressive fracture energy
12	`GFC(2)`	G_{fcy}	Vertical compressive fracture energy
13	`UNLFAC`	λ	Compressive unloading factor
14	`COH0`	c	Cohesion
15	`GFS`	G_{fs}	Shear fracture energy
16	`ANLGE0`	α	Diagonal crack angle
17	`EPSCFA(1)`	n	Factor strain at compressive strength, horizontal
18	`EPSCFA(2)`	n	Factor strain at compressive strength, vertical
19	`HCRAC`	h	Crack band width

[a] The values entered for these horizontal tensile properties are not used by the Equivalent Shear Masonry Model. Their presence in the USRVAL-array are merely an inheritance from the `usrmat_quad2.f`-code.

Table 6.5: The user state variables (double precision) as used in the user supplied subroutine in `usrmat_eqshma.f`.

USRSTA			
1	`ALPHA(1)` for `I=1`	$\alpha_{t,ref,x}$	Horizontal tensile extreme strain
2	`ALPHA(1)` for `I=2`	$\alpha_{t,ref,y}$	Vertical tensile extreme strain
3	`ALPHA(2)` for `I=1`	$\alpha_{c,ref,x}$	Horizontal compressive extreme strain
4	`ALPHA(2)` for `I=2`	$\alpha_{c,ref,y}$	Vertical compressive extreme strain
5	`SIGRF(1)` for `I=1`	$\sigma_{t,ref,x}$	Horizontal tensile reference stress
6	`SIGRF(1)` for `I=2`	$\sigma_{t,ref,y}$	Vertical tensile reference stress
7	`SIGRF(2)` for `I=1`	$\sigma_{c,ref,x}$	Horizontal compressive reference stress
8	`SIGRF(2)` for `I=2`	$\sigma_{c,ref,y}$	Vertical compressive reference stress
9	`SHRMAX`	γ_{cum}	Cumulative post-peak shear strain
10	`DBLE(FAIMEC)`		Indicator failure mechanism
11	`COH1`		Remaining cohesion
12	`DBLE(FRCFAI)`		`1.D0` if cracked in shear
13	`TAUEQ/TAUMAX`	τ_{eq}/τ_{max}	Load-resistance ratio
14	`1.D0` if `CRSHED`		`1.D0` if crushed in either direction
15	`DBLE(USRIND(1))`		`1.D0` if cracked in x-direction
16	`DBLE(USRIND(2))`		`1.D0` if cracked in y-direction
17	`TAUMAX`	τ_{max}	Shear strength
18	`SHRMEQ`	$G_{xy,eq}$	Equivalent shear modulus
19	`(EPSHEQ-TAUMAX/ SHRMEQ)*HCRAC`	w_{crack}	Crack width

6.3. Preparation

A piece of code that, among other things, loaded in data about the element type and the crack band width was removed here, because it used functions that were not available. The element type is assumed to be `MEMBRA` (plane stress) throughout the document, so all if statements regarding the element type were removed accordingly. The crack band width has to be provided manually through the user parameters.

In line 68 to 91 the user parameters are loaded into their argument.

A section calculating minimal fracture energy values, ultimate strains and plastic strains was removed here. Its content was moved into the sections about the tensile, compressive and shear behaviour respectively.

In line 92 to 105 the current strain and a first estimate of the current stress are calculated according to Equations 6.1 to 6.3.

$$\varepsilon = \varepsilon_0 + \Delta\varepsilon \tag{6.1}$$

$$\sigma = \sigma_0 + E \cdot \Delta\varepsilon \tag{6.2}$$

$$\tau = \tau_0 + G_{xy} \cdot \Delta\gamma \tag{6.3}$$

In line 106 to 118 all crack indicators, counters and output are initialized.

6.4. Tensile and Compressive Behaviour

In line 119 to 127 a loop is started to execute the next section of code for both the x- and the y-direction. Then all extreme strains and reference stresses are loaded from the user state variables. It is evaluated whether the integration point has been cracked or crushed before using the user state indicators.

Line 128 to 166 handle the tensile behaviour the same as the `usrmat_quad2.f` does. The only difference is that this is only done for `I=2`, i.e. only for the y-direction. If the integration point is under vertical tension, this section returns the current vertical stress and a stiffness.

Line 167 to 248 handle the compressive behaviour. This section is similar to the compressive section in `usrmat_quad2.f` with the difference that the formulas for a new compressive extreme are those in Equation 3.3. If the integration point is in horizontal and/or vertical compression, this section returns the current horizontal and/or vertical stress and respective stiffness.

In line 249 to 268 the crack data are updated. The new extreme strains and reference stresses are written into the user state variables. The loop is then closed.

Stiffness

Though the mainframe asks for the current tangent stiffness as output, this value is not always returned, for reasons explained in Section 2.1.2. The stiffnesses returned be the material model are mostly the secant stiffness, only the tangent stiffness during compressive unloading, but the linear stiffness if it is the first iteration and always a minimum of 0.0001 times the linear stiffness.

6.5. Frictional Criterion

Line 273 to 382 contain the frictional criterion proposed in Chapter 5. In the first lines the values of the cumulative shear strain and the remaining cohesion are loaded in from the user state parameters.

Listing 6.1: Line 273 to 275 of `usrmat_eqshma.f`

```
273 C...   FRICTIONAL CRITERION
274        SHRMAX = USRSTA(9)
275        COH1 = USRSTA(11)
```

Then in line 276 an if statement is started with the condition that the integration point is under horizontal tension. In that case a combination of shear and horizontal tension is evaluated.

Listing 6.2: Line 276 and 277 of `usrmat_eqshma.f`

```
276        IF ( EPS(1) .GT. 0.D0 ) THEN
277 C...     COMBINATION OF SHEAR AND HORIZONTAL TENSION
```

The shear strain and stress are inverted in case of negative shear, so that the rest of this if statement[1]

---

[1]That is the statement following the if condition in line 276, running from line 277 to line 346.

can also be used in case of negative shear. An indicator I is set to register whether or not this inversion has taken place.

Listing 6.3: Line 278 to 286 of `usrmat_eqshma.f`

```
278             IF ( SIGSHR .LT. 0.D0 ) THEN
279                SIGSHR = -SIGSHR
280                SI0SHR = -SI0SHR
281                EPSSHR = -EPSSHR
282                DEPSHR = -DEPSHR
283                I = 1
284             ELSE
285                I = 0
286             END IF
```

The equivalent shear stress is calculated.

Listing 6.4: Line 287 of `usrmat_eqshma.f`

```
287             EPSHEQ = EPSSHR + EPS(1)/TAN(ANGLE0)
```

It is checked whether the shear has reached the maximum shear strength before. This is done by evaluating the 18th entry of the user state parameters, where the equivalent shear stiffness is stored once the peak has been reached. Pre-peak, however, this entry should be zero. If that is the case, the current equivalent shear stiffness is calculated as the current equivalent shear stress divided by the equivalent shear strain. If this equivalent shear strain would be very small, dividing by it would be problematic. Therefore, if it is smaller than 10^6 times the machine precision DPMPAR(1) [2], an alternative approximation of the equivalent shear stiffness is used. Else the integration point has already reached its peak before, so the equivalent shear stiffness is loaded in from the user state parameters.

Listing 6.5: Line 288 to 299 of `usrmat_eqshma.f`

```
288             IF ( USRSTA(18) .EQ. 0.D0 ) THEN
289 C...           PRE-PEAK
290                IF ( EPSHEQ .LT. 1.D+6*DPMPAR(1) ) THEN
291                   SHRMEQ = SHRM0
292                ELSE
293                   SHRMEQ = ( SHRM0*EPSSHR + YOUN0(1)*EPS(1)*TAN(ANGLE0) )
294      $                       / EPSHEQ
295                END IF
296             ELSE
297 C...           POST-PEAK
298                SHRMEQ = USRSTA(18)
299             END IF
```

Next, the ultimate shear strain is calculated according to Equation 5.14. The remaining cohesion is calculated according to Equation 5.13, with a minimum value of zero. When the user supplied a unrealistically small value for the shear fracture energy, the value of the ultimate shear strain can become to small to divide by, or even negative. It was chosen to then still allow the material to reach its peak strength. For this purpose, the cohesion is equal to the initial cohesion before the peak is reached and abruptly lowered to zero after, see Figure 7.4(e) for an illustration of this behaviour. If the integration point is cracked as a result of either horizontal or vertical tension, the cohesion is reduced to zero.

Listing 6.6: Line 300 to 311 of `usrmat_eqshma.f`

```
300             SHRULT = 2.D0*GFS/(HCRAC*COH0)-COH0/SHRMEQ
301             IF ( SHRULT .GT. 1.D+6*DPMPAR(1) ) THEN
302                COH1 = COH0*(SHRULT-SHRMAX)/SHRULT
```

---

[2]For double precision numbers the machine precision is in the order of 10^{-16}, so this small value is about 10^{-10}. The relevant strain values range from 0 to the order 10^{-3}, so 10^{-10} is indeed a very small value in this context.

```
303                    COH1 = MAX( 0.D0, COH1 )
304                ELSE IF ( SHRMAX .EQ. 0.D0 ) THEN
305 C...            GFS TOO SMALL, PRE-PREAK
306                    COH1 = COH0
307                ELSE
308 C...            GFS TOO SMALL, POST-PEAK
309                    COH1 = 0.D0
310                END IF
311                IF ( CRCKED ) COH1 = 0.D0
```

Then the shear strength is calculated according to Equation 2.13. The shear stress is restricted by the shear strength according to Equation 2.12 and the horizontal stress is restricted by the shear strength divided by $\tan\alpha$ according to Equation 5.5. Subsequently, the two stresses are combined into the equivalent shear stress according to Equation 5.4.

Listing 6.7: Line 312 to 315 of `usrmat_eqshma.f`

```
312                TAUMAX   = MAX(0.D0, COH1-SIGMA(2)*TANPHI)
313                SIGSHR   = MIN( SIGSHR, TAUMAX )
314                SIGMA(1) = MIN( MAX(SIGMA(1),0.D0) , TAUMAX/TAN(ANGLE0))
315                TAUEQ    = SIGSHR + SIGMA(1)*TAN(ANGLE0)
```

Now we have reached the combined failure criterion. If the equivalent shear strain is larger than the current shear strength, the failure mechanism indicator `FAIMEC` is increased with 16 to indicate shear failure, see also Table 6.3 for more information.

Listing 6.8: Line 316 and 317 of `usrmat_eqshma.f`

```
316                IF ( ABS(TAUEQ) .GE. TAUMAX ) THEN
317                    FAIMEC = FAIMEC + 16
```

Then there are three possible loading situations. The first is shear loading and simultaneous tensile unloading. This is the case when the tensile strain increment is negative. The horizontal tensile stress is assumed to unload with its linear stiffness, and it is kept the same as the first estimate by Equation 6.2. The shear stress is then assumed to be responsible for the rest of the equivalent shear stress.

Listing 6.9: Line 318 to 320 of `usrmat_eqshma.f`

```
318                    IF ( DEPS(1) .LT. 0.D0 ) THEN
319 C...                SHEAR LOADING, TENSILE UNLOADING
320                        SIGSHR = TAUMAX - SIGMA(1)*TAN(ANGLE0)
```

The second possible loading situation is tensile loading and simultaneous shear unloading. This is the case when the shear strain increment is negative[3]. This time, the shear stress is assumed to unload with its linear stiffness, and is kept the same as its first estimate by Equation 6.3. The horizontal tensile stress is now assumed to be responsible for the rest of the equivalent shear stress.

There is one special case, though, and that is when the shear unloading goes to zero shear. That is the case when the shear stress at the start of the increment and the first estimate of the shear stress do not have the same sign, so their product is negative. Then the shear stress is assumed to be zero and the horizontal tensile stress is thus assumed to be responsible for all equivalent shear stress.

Listing 6.10: Line 321 to 327 of `usrmat_eqshma.f`

```
321                    ELSE IF ( SIGSHR*SI0SHR .LT. 0.D0 ) THEN
322 C...                SHEAR UNLOADING TO ZERO, TENSILE LOADING
323                        SIGSHR = 0.D0
324                        SIGMA(1) = TAUMAX/TAN(ANGLE0)
325                    ELSE IF ( DEPSHR .LT. 0.D0 )  THEN
326 C...                TENSILE LOADING, SHEAR UNLOADING
327                        SIGMA(1) = (TAUMAX - SIGSHR)/TAN(ANGLE0)
```

---

[3]Or in case of negative shear stress, the shear strain increment is positive, but being inverted in line 282 it has a negative value now.

The third possible loading situation is simultaneous shear and horizontal tensile loading. The ratio between the shear stress and the horizontal tensile stress is then kept the same as at the beginning of the increment, as described in Section 5.4. The `RATIO` is the fraction of the equivalent shear stress that is due to the shear stress. An alternative approximation of this ratio is provided is case the equivalent shear stress at the start of the increment (the denominator for calculating the ratio) is very small in order to prevent problems.

Listing 6.11: Line 328 to 339 of `usrmat_eqshma.f`

```
328                 ELSE
329 C...                 SIMULTANEOUS SHEAR AND TENSILE LOADING
330                      IF ( ( SIG0(1)*TAN(ANGLE0) + SI0SHR )
331        $                             .LT. 1.D+6*DPMPAR(1) ) THEN
332                          RATIO = 0.5D0
333                      ELSE
334                          RATIO = SI0SHR / (SIG0(1)*TAN(ANGLE0) + SI0SHR)
335                      END IF
336 C...                 RATIO BETWEEN SHEAR AND HORIZONTAL TESNION IS MAINTAINED
        DURING SOFTENING AND YIELDING
337                      SIGSHR   = RATIO*TAUMAX
338                      SIGMA(1) = (1.D0 - RATIO)*TAUMAX/TAN(ANGLE0)
339                 END IF
```

The equivalent shear modulus is stored in the user state parameters array. The equivalent shear increment is calculated and added to the cumulative shear strain. The shear crack indicator `FRCFAI` is set to one. The if statement started in line 316 is ended. If the shear stress was negative up until line 278, it is now inverted back to negative.

Listing 6.12: Line 340 to 346 of `usrmat_eqshma.f`

```
340                 USRSTA(18) = SHRMEQ
341 C...             SHRMEQ IS KEPT CONSTANT AFTER PEAK
342                 DEPSEQ = DEPSHR + DEPS(1)/TAN(ANGLE0)
343                 SHRMAX = SHRMAX + ABS( DEPSEQ )
344                 FRCFAI = 1
345             END IF
346             IF ( I .EQ. 1 ) SIGSHR = -SIGSHR
```

Here the if statement started in line 276 continues with an else statement. If there is no horizontal tension, than the code checks for shear without horizontal tension. The equivalent shear stress is now simply the absolute value of the shear stress[4]. The pre-peak equivalent shear modulus is the shear modulus and the post peak shear modulus is what was stored in the user state parameters the first time the shear strength was reached. The ultimate shear strain and the remaining cohesion are calculated as in line 300 to 311.

Listing 6.13: Line 347 to 366 of `usrmat_eqshma.f`

```
347         ELSE
348 C...         SHEAR WITHOUT HORIZONTAL TENSION
349             TAUEQ = ABS(SIGSHR)
350             IF ( USRSTA(18) .EQ. 0.D0 ) THEN
351 C...             PRE-PEAK
352                 SHRMEQ = SHRM0
353             ELSE
354 C...             POST-PEAK
355                 SHRMEQ = USRSTA(18)
356             END IF
```

_____

[4]In this case, the equivalent shear stress is only needed to calculate the load-resistance ratio in line 397.

```
357            SHRULT = 2.D0*GFS/(HCRAC*COH0)-COH0/SHRMEQ
358            IF ( SHRULT .GT. 1.D+6*DPMPAR(1) ) THEN
359               COH1 = COH0*(SHRULT-SHRMAX)/SHRULT
360               COH1 = MAX( 0.D0, COH1 )
361            ELSE IF ( SHRMAX .EQ. 0.D0 ) THEN
362               COH1 = COH0
363            ELSE
364               COH1 = 0.D0
365            END IF
366            IF ( CRCKED ) COH1 = 0.D0
```

The shear strength is again calculated according to Equation 2.13. If the absolute value of shear stress is larger then the shear strength, the integration point is cracked in shear, so the failure mechanism indicator FAIMEC is increased with 16. In that case shear stress is reduced to the current shear strength and the equivalent shear modulus is stored in the user state parameters. The equivalent shear strain is now equal to the absolute value of the shear strain[5]. The cumulative shear strain is increased with the absolute value of the shear strain increment. Finally, the if/else statement from lines 276 and 347 is ended.

Listing 6.14: Line 367 to 378 of usrmat_eqshma.f

```
367            TAUMAX =  MAX(0.D0, COH1-SIGMA(2)*TANPHI)
368            IF      ( ABS(SIGSHR) .GT.  TAUMAX ) THEN
369 C...          IF THE SHEAR STRESS IS LARGER THAN THE LIMIT THE PARAMETER
       FAIMEC IS INCREASED OF 16
370               FAIMEC = FAIMEC + 16
371               IF ( SIGSHR .GT.  TAUMAX ) SIGSHR =  TAUMAX
372               IF ( SIGSHR .LT. -TAUMAX ) SIGSHR = -TAUMAX
373               USRSTA(18) = SHRMEQ
374               EPSHEQ = ABS(EPSSHR)
375               SHRMAX = SHRMAX + ABS( DEPSHR )
376               FRCFAI = 1
377            END IF
378         END IF
```

6.6. Post Processing

At the end of the user subroutine some user state parameters are updated with the current values of the corresponding arguments. If the peak shear stress has been reached, a measure for the horizontal crack opening due to shear sliding in the bed joints is given in line 379. This crack width is the plastic part of the equivalent deformation:

$$w_{crack} = \gamma_{eq,plastic} \cdot h = \left(\gamma_{eq} - \gamma_{eq,elastic} \right) \cdot h = \left(\gamma_{eq} - \frac{\tau_{max}}{G_{xy,eq}} \right) \cdot h \qquad (6.4)$$

Also, the output stiffness matrix is constructed. For the x- and y-direction, these are the stiffnesses as described in Section 6.4. The returned shear stiffness is always equal to the initial linear shear stiffness, because the tangent stiffness is always either that or negative in the softening part, or zero during yielding.

Listing 6.15: Line 379 to 401 of usrmat_eqshma.f

```
379         IF ( USRSTA(18) .NE. 0.D0 ) USRSTA(19) =
380      $                            (EPSHEQ-TAUMAX/SHRMEQ)*HCRAC
381         USRSTA(9)  = SHRMAX
382         USRSTA(11) = COH1
383 C
```

---

[5]In this case, the equivalent shear strain is only used to calculate the crack width due to shear in line 379.

```fortran
384 C
385         CALL RSET( 0.D0, STIFF, NS*NS )
386         STIFF(1,1) = YOUN(1)
387         STIFF(2,2) = YOUN(2)
388         STIFF(3,3) = SHRMOD
389         SIGMA(3)   = SIGSHR
390         CALL RSET( 0.D0, EPSP, 4 )
391         IF ( USRIND(1) .EQ. 1 ) EPSP(2) = MAX( 0.D0, EPS(1)*HCRAC )
392         IF ( USRIND(2) .EQ. 1 ) EPSP(1) = MAX( 0.D0, EPS(2)*HCRAC )
393      USRIND(5) = FRCFAI
394
395      USRSTA(10) = DBLE( FAIMEC )
396      USRSTA(12) = DBLE( FRCFAI )
397      USRSTA(13) = TAUEQ/TAUMAX
398      IF ( CRSHED ) USRSTA(14) = 1.D0
399      USRSTA(15) = DBLE( USRIND(1) )
400      USRSTA(16) = DBLE( USRIND(2) )
401      USRSTA(17) = TAUMAX
```

After line 401 the code concludes with post processing for the crack status in line 402 to 422. This part is the same as in the `usrmat_quad2.f`-file. That file then continues with a similar post processing for the plasticity status, but that part was removed because it again used an unsupported function.

Finally, in line 424, the subroutine command started in line 2 is ended.

III
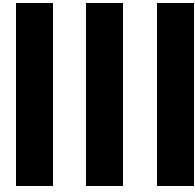
Assesment of the Validity of the Equivalent Shear Masonry Model

7

Single Element Model

A single element model was studied in order to test whether the code of the Equivalent Shear Masonry Model work as it was intended. Several load cases where studied for the Equivalent Shear Masonry Model and also for the Engineering Masonry Model with the *Diagonal stair-case cracks* option from Diana 10.2, for comparison.

7.1. Model Description

Figure 7.1 shows the single element model. It is a four node first-order quadrilateral plane stress element (Q8MEM) 0.1 m wide by 0.1 m heigh with a thickness of 0.1 m. Its local x-axis is horizontally to the right and its local y-axis is vertically upwards. One single integration point is used. This is summarized in Table 7.1.
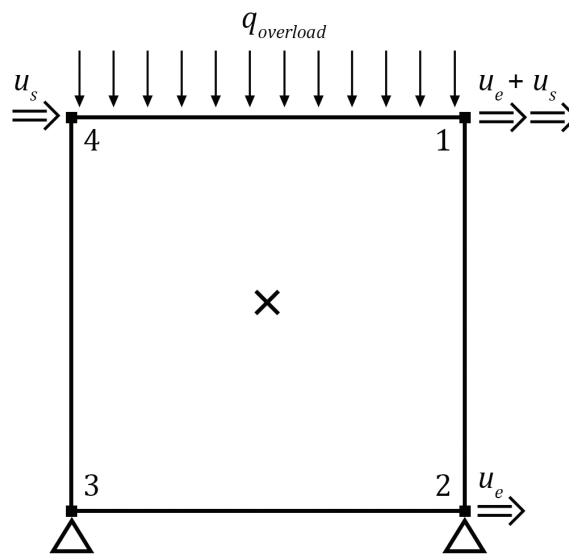
Figure 7.1: The Single Element Model: a four node element with one integration point (the $\times$), loaded by a vertical overload and horizontal prescribed displacements for horizontal extension (u_e) and shear (u_s).

The element is simply supported at the bottom nodes. An overload of 0.40 MPa is applied to the top edge. A prescribed horizontal deformation $u_e = b_{model} = 0.1$ m applied to the bottom right node, and another one $u_s = h_{model} = 0.1$ m to the top left node. These displacements are chosen to correspond to an extension strain and a shear strain respectively of 1.0, and are multiplied by a time dependent function. A FIX-tying ensures that the horizontal displacement of node 1 is equal to the sum of the horizontal displacements of node 2 and 4. The material properties are shown in Table 7.2. As an example, the .dat-file of the single element analysis with the Equivalent Shear Masonry Model for load case G1 is included as Listing C.1 in Appendix C.

Table 7.1: Element properties of the single element model.

Model component	Element type	Integration scheme	Mesh size	Direction of local x-axis	Material Model
The single element	Q8MEM	Reduced, i.e. Gauss 1x1	100x100 mm	Horizontal	*Equivalent Shear Masonry Model* or *Engineering Masonry Model – Diagonal staircase cracks* respectively

Table 7.2: Material properties used in the single element model for both the Equivalent Shear Masonry Model and the Equivalent Shear Masonry Model.

Horizontal stiffness	E_x	2200	MPa
Vertical stiffness	E_y	3400	MPa
Shear stiffness	G_{xy}	1300	MPa
Tangent of friction angle	$\tan\varphi$	0.684137	[-]
Vertical tensile strength	f_{ty}	0.10	MPa
Tensile fracture energy	G_{ft}	5	N/m
Compressive strength	f_c	14	MPa
Horizontal compressive fracture energy	G_{fc}	20000	N/m
Compressive unloading factor	λ	0.3	[-]
Cohesion	c	0.15	MPa
Shear fracture energy	G_{fs}	5	N/m
Diagonal crack angle	α	0.5	rad
Factor strain at compressive strength	n	4	[-]
Crack band width[a]	h	0.1	m
Crack bandwidth specification[b]		*Govindjee*	

[a] Used for the Equivalent Shear Masonry Model only.
[b] Used for the Engineering Masonry Model only.

7.2. Load Cases

Using time dependent functions, several load cases were investigated. The letters refers to the failure modes shown in Tables 2.1 and 4.1.

A   Vertical tensile loading, unloading and reloading.[1]

B   Vertical compressive loading, unloading and reloading.[2]

C1 Shear loading.

C2 Shear loading and unloading halfway through the softening branch.

C3 Shear loading and unloading when a too small value for the shear fracture energy is provided (here G_{fs} = 0.5 N/m).

DE Horizontal tensile loading and unloading to end in compression.

G1 Shear loading and simultaneous horizontal tensile loading that changes to tensile unloading to end with compression.

G2 Horizontal tensile loading and simultaneous positive shear loading that changes to shear unloading to zero.

G3 Horizontal tensile loading and simultaneous negative shear loading that changes during the softening phase to shear unloading to end with positive shear.

---

[1]For this load case, vertical prescribed displacements were applied to the top nodes 1 and 4 instead of the loads shown in Figure 7.1.
[2]See footnote 1.

All load cases were deformation controlled. For load cases C1, C2, C3, DE, G1, G2 and G3 a vertical overload was applied in a separate phase before the deformation load and its accompanying supports and tyings were applied. Horizontal compression was not studied separately because this uses the same code as for vertical compression.

7.3. Analysis Procedure

A non-linear static analysis was performed with prescribed displacement loads that change over time. First the overload was applied in ten load steps. Then the prescribed deformations were applied, in time steps so that $\Delta\varepsilon_{xx}$ and/or $\Delta\gamma_{xy}$ were 10^{-5}. The regular Newton-Raphson iteration method was used, with a maximum number of iterations set at 50. Both the force and the displacement norm had to be satisfied, both with a tolerance of 0.01, though the analysis should continue when convergence was not reached. As an example, the `.dcf`-file of the single element analysis with the Equivalent Shear Masonry Model for load case G1 is included as Listing C.2 in Appendix C.

7.4. Results

Figure 7.2 to 7.8 show the stress-strain diagrams that are the results of the single element model. The Equivalent Shear Masonry Model is shown on the left and the Engineering Masonry Model's *Diagonal stair-case cracks* option on the right.

The lines in the graphs are coloured blue, teal and purple consecutively. This illustrates the loading history and makes it easier to compare the separate graphs in each figure. In Figure 7.2 to 7.5 the blue line represents loading, the teal line unloading and the purple line reloading. In Figure 7.6 to 7.8 the colours correspond to the consecutive parts of the loading protocol given in each subfigure (a).

For each load case the relevant stress-strain diagram(s) is/are given. The non-visualized stresses and deformations are (or should be) zero, with the exception of the vertical compression due to the overload with load cases C1, C2, C3, DE, G1, G2 and G3. This is true for the Equivalent Shear Masonry Model, but not completely for the Engineering Masonry Model's *Diagonal stair-case cracks* option. This model tends to 'invent' small stress and strain values, even though the prescribed displacement of the nodes does not allow any strain in that specific direction. It concerns horizontal stress and strain for the vertical tension and compression and for both the shear load cases. These values are 10^3 to 10^{28} times smaller than the relevant stress and strain values.

For each of the combined load cases an additional stress-strain diagram is given, beside the horizontal and shear diagrams. For the Equivalent Shear Masonry Model, the (fictive) equivalent stress-strain diagram is added, see Figures 7.6(f), 7.7(f) and 7.8(f). The equivalent shear stress is calculated with Equation 5.4 and the equivalent shear strain using Equation 5.11, but then cumulative over the previous steps. These equivalent stress-strain diagrams are added to elucidate how the failure mode works.

For the Engineering Masonry Model's *Diagonal stair-case cracks* option, stress-strain diagram in the n-direction normal to the expected diagonal staircase crack is added, see Figures 7.6(g), 7.7(g) and 7.8(g). The values are calculated with help of Equations 3.12 and 3.14. These diagonal stress-strain diagrams are meant to elucidate what the *Diagonal stair-case crack* option of the Engineering Masonry Model does.
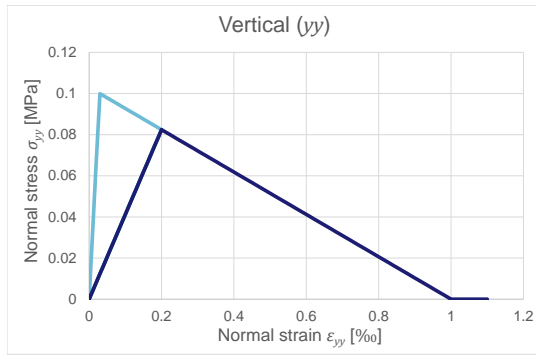
(a) Vertical stress-strain diagram using the Equivalent Shear Masonry Model. Note that the reloading overlaps the secant unloading.
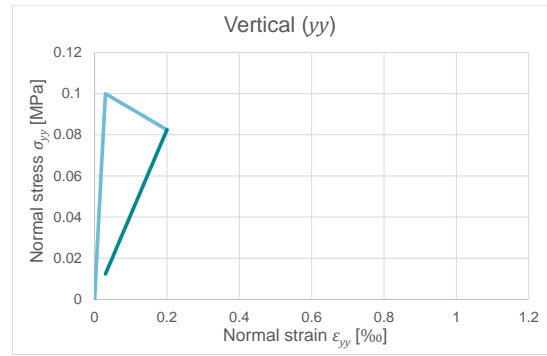
(b) Vertical stress-strain diagram using the Engineering Masonry Model with *Diagonal stair-case cracks* option. Note that the analysis was stopped just before reaching zero strain due to divergence.

Figure 7.2: Results of the single element model for load case A, vertical tensile loading (in blue), unloading (in teal) and reloading (in purple).
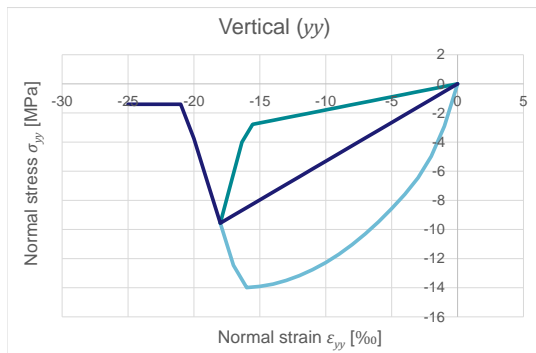
(a) Vertical stress-strain diagram using the Equivalent Shear Masonry Model.
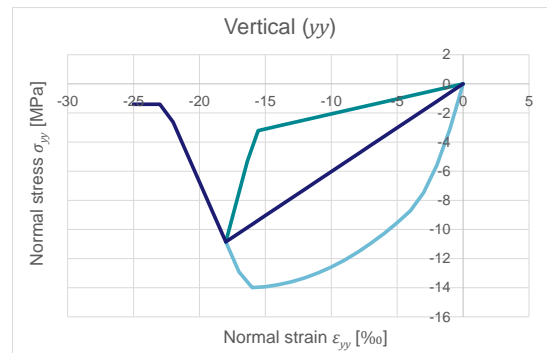
(b) Vertical stress-strain diagram using the Engineering Masonry Model with *Diagonal stair-case cracks* option.
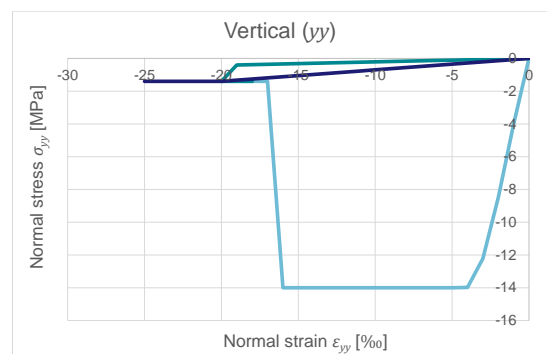
(c) Vertical stress-strain diagram using the `usr-mat_quad2.f`-code of the Engineering Masonry Model.

Figure 7.3: Results of the single element model for load case B, vertical compressive loading (in blue), unloading (in teal) and reloading (in purple).
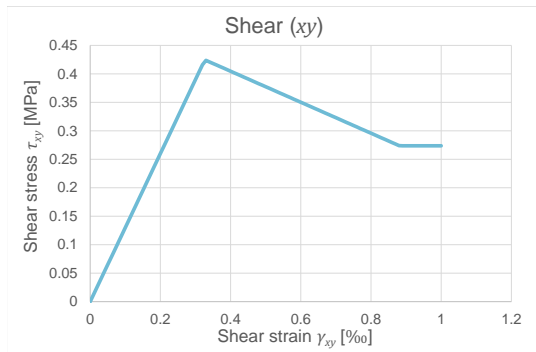
(a) Shear stress-strain diagram for load case C1 using the Equivalent Shear Masonry Model.
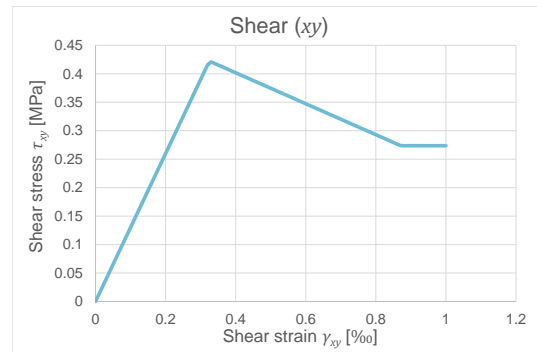
(b) Shear stress-strain diagram for load case C1 using the Engineering Masonry Model with *Diagonal stair-case cracks* option.
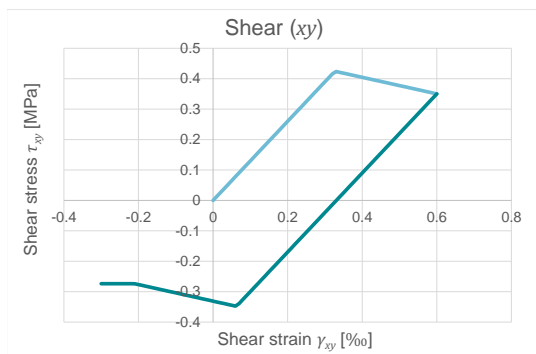
(c) Shear stress-strain diagram for load case C2 using the Equivalent Shear Masonry Model.
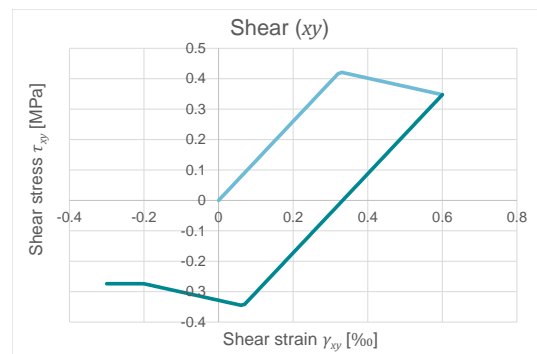
(d) Shear stress-strain diagram for load case C2 using the Engineering Masonry Model with *Diagonal stair-case cracks* option.
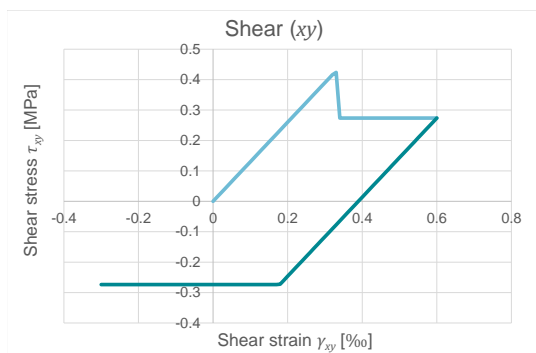
(e) Shear stress-strain diagram for load case C3 using the Equivalent Shear Masonry Model.

Figure 7.4: Results of the single element model for load cases C1 shear loading (in blue), C2 shear loading (in blue) and unloading (in teal) halfway through the softening and C3 shear loading (in blue) and unloading (in teal) for a too low value of the shear fracture energy G_{fs}.
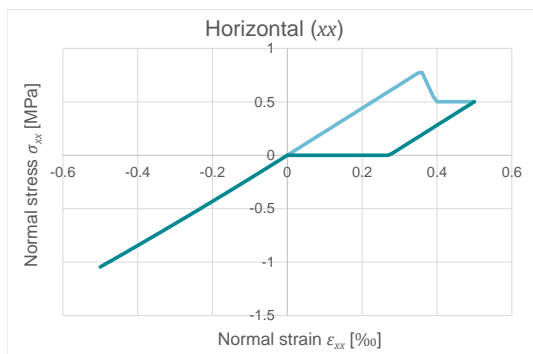
(a) Horizontal stress-strain diagram using the Equivalent Shear Masonry Model.
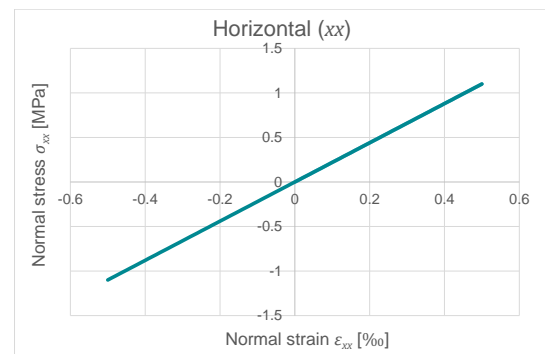
(b) Horizontal stress-strain diagram using the Engineering Masonry Model with *Diagonal stair-case cracks* option. Note that the unloading overlaps the linear loading.

Figure 7.5: Results of the single element model for load case DE, horizontal tensile loading (in blue) and unloading (in teal) to end with compression.
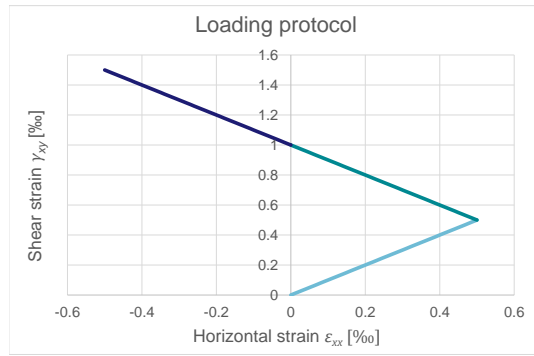
(a) Loading protocol applied for load case G1.
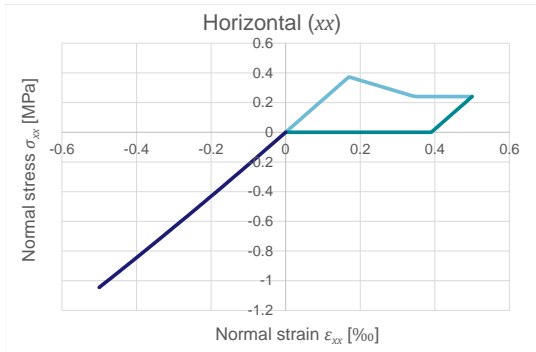
(b) Horizontal stress-strain diagram using the Equivalent Shear Masonry Model.
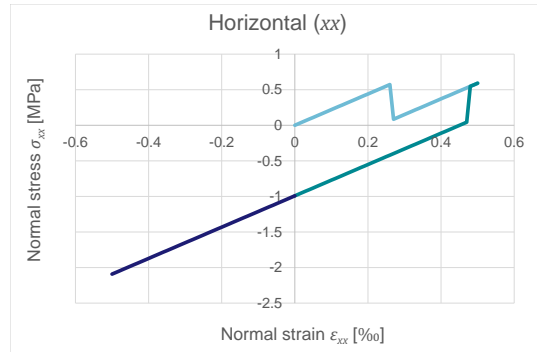
(c) Horizontal stress-strain diagram using the Engineering Masonry Model with *Diagonal stair-case cracks* option.

(d) Shear stress-strain diagram using the Equivalent Shear Masonry Model.
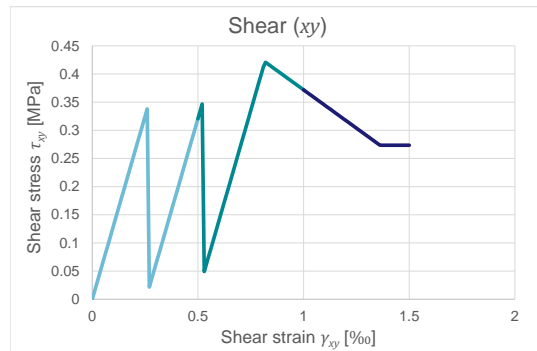
(e) Shear stress-strain diagram using the Engineering Masonry Model with *Diagonal stair-case cracks* option.
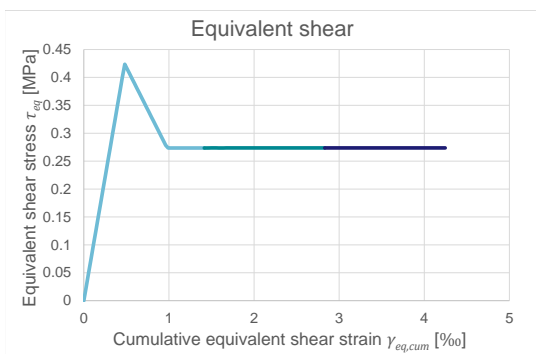
(f) Equivalent shear stress-strain diagram using the Equivalent Shear Masonry Model.

(g) Diagonal stress-strain diagram using the Engineering Masonry Model with *Diagonal stair-case cracks* option, for a crack in direction $-\alpha$.

Figure 7.6: Results of the single element model for load case G1, shear loading and simultaneous horizontal tensile loading and then tensile unloading to end with compression. Colours correspond to the consecutive parts of the loading protocol applied.
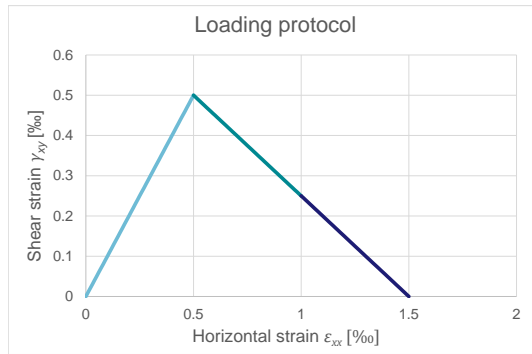
(a) Loading protocol applied for load case G2.
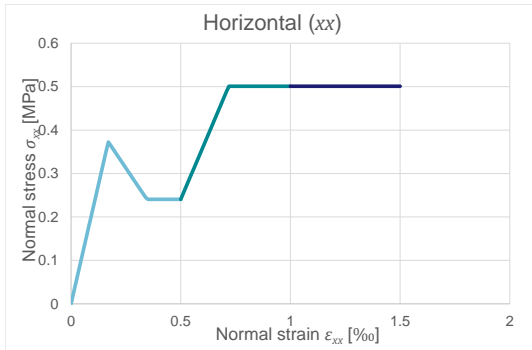
(b) Horizontal stress-strain diagram using the Equivalent Shear Masonry Model.
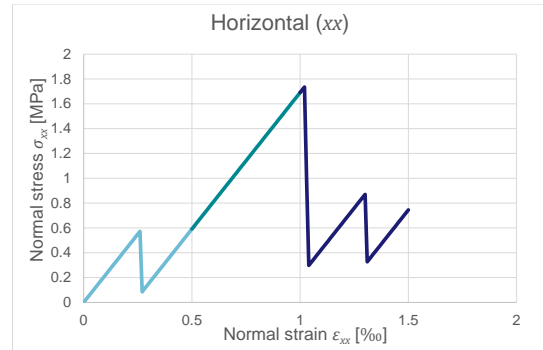
(c) Horizontal stress-strain diagram using the Engineering Masonry Model with *Diagonal stair-case cracks* option.

(d) Shear stress-strain diagram using the Equivalent Shear Masonry Model.
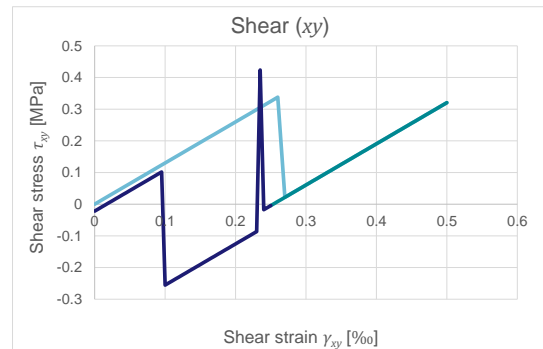
(e) Shear stress-strain diagram using the Engineering Masonry Model with *Diagonal stair-case cracks* option.
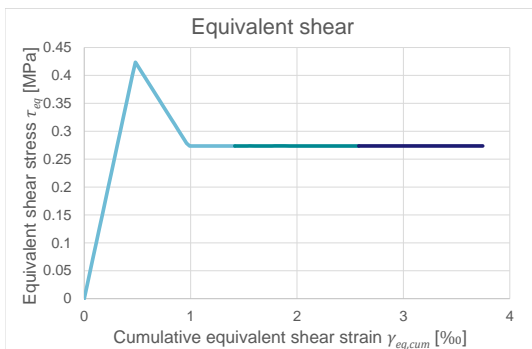
(f) Equivalent shear stress-strain diagram using the Equivalent Shear Masonry Model.

(g) Diagonal stress-strain diagram using the Engineering Masonry Model with *Diagonal stair-case cracks* option, for a crack in direction $-\alpha$.

Figure 7.7: Results of the single element model for load case G2, horizontal tensile loading and simultaneous positive shear loading and then shear unloading to zero. Colours correspond to the consecutive parts of the loading protocol applied.
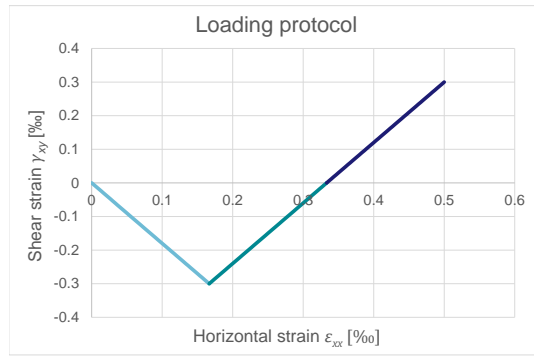
(a) Loading protocol applied for load case G3.
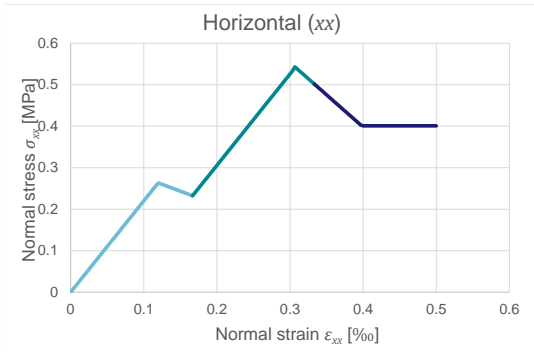
(b) Horizontal stress-strain diagram using the Equivalent Shear Masonry Model.
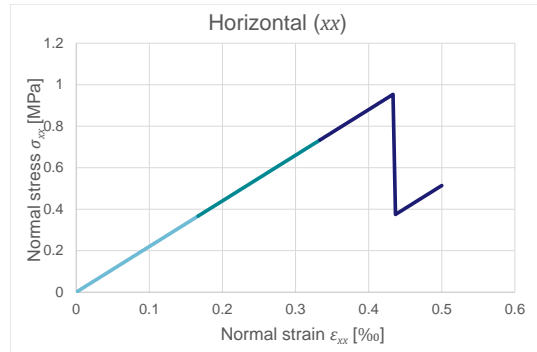
(c) Horizontal stress-strain diagram using the Engineering Masonry Model with *Diagonal stair-case cracks* option.
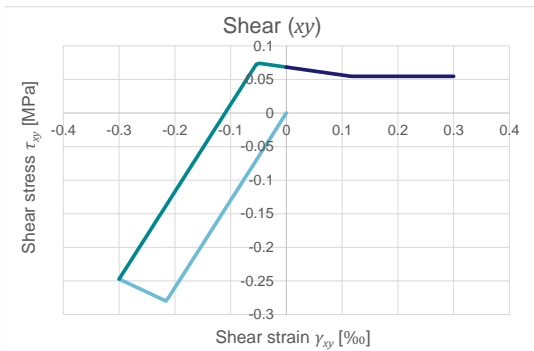
(d) Shear stress-strain diagram using the Equivalent Shear Masonry Model.
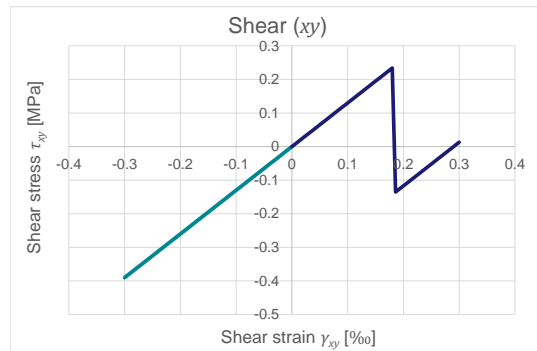
(e) Shear stress-strain diagram using the Engineering Masonry Model with *Diagonal stair-case cracks* option.
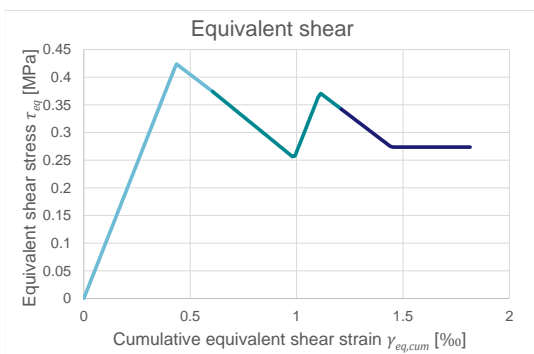
(f) Equivalent shear stress-strain diagram using the Equivalent Shear Masonry Model. Note that the blue line and the teal line for $\sim 0.4 < \gamma_{eq,cum} <\sim 1$ do not have the same slope: the blue line descends due to softening, the teal line descends because of unloading.
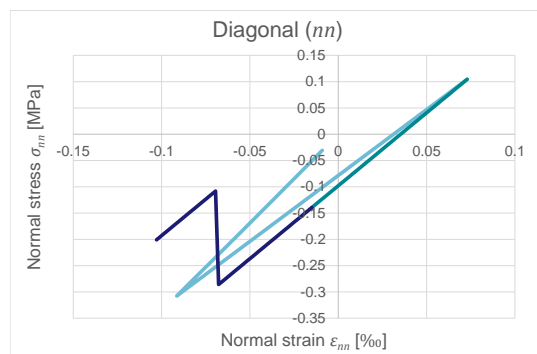
(g) Diagonal stress-strain diagram using the Engineering Masonry Model with *Diagonal stair-case cracks* option, for a crack in direction α.

Figure 7.8: Results of the single element model for load case G3, horizontal tensile loading and simultaneous negative shear loading, then shear unloading during the softening phase to end with positive shear. Colours correspond to the consecutive parts of the loading protocol applied.

7.5. Discussion

Discussion of the Equivalent Shear Masonry Model Results

The previous section presented the stress-strain diagrams of the single element model that display the behaviour of the Equivalent Shear Masonry Model. The vertical curves are all fluent and the behaviour is exactly as intended in the theory. The separate shear and horizontal tension curves both resemble the shear behaviour of the bed joints, except that the horizontal stress does not become negative for positive strain. Figure 7.4(e) shows that the code ensures that the maximum shear strength is reached, even when the user provides a too small value for the shear fracture energy. This does lead to a sudden drop in the shear stress-strain diagram.

The equivalent shear curves in Figures 7.6(f), 7.7(f) and 7.8(f) show that the equivalent shear stress softens and yields according to the shear behaviour of the bed joints. The first two combinations of horizontal tensile stress and shear stress (in Figures 7.6 and 7.7) show that when either one unloads, the other adopts the released capacity. The unloading of direction happens independent of the other and with its own linear stiffness. The third combination (in Figure 7.8) shows that the material model also works for negative shear. It also shows that if one component (here the shear) unloads relatively quickly, the other component (here the horizontal tension) only loads with its own linear stiffness, causing the equivalent shear stress to decrease. Only when the combined equivalent shear once more becomes larger than the shear strength, it continues to soften and yield according to the shear behaviour of the bed joints.

Discussion of the Engineering Masonry Model's *Diagonal stair-case cracks* Option Results

Figures 7.3 and 7.4 show that the analyses with the Engineering Masonry Model's *Diagonal stair-case cracks* option show similar results for the vertical compression and the (separate) shear. Figure 7.3(c) illustrates that the `usrmat_quad2.f`-code's formulas for the compressive behaviour do not represent the desired behaviour, as mentioned in Section 2.4.4. Figure 7.5 shows that the Engineering Masonry Model's *Diagonal stair-case cracks* option uses a linear elastic relation for horizontal tension.

The Engineering Masonry Model's *Diagonal stair-case cracks* option shows unexpected results for the combined load cases G1, G2 and G3. The stress-strain diagrams show sudden drops at the moment the diagonal strength criterion is reached. Instead of the expected plateau, the stress just drops instantly and then continues to increase with the same linear stiffness. Also, the crack status is confused. For example, it says `PARTIALLY OPEN UNLOADING` when loading continues after the first sudden drop in Figures 7.6(c) and (e), 7.7(c) and (e) and 7.8(c) and (e). Also, the vertical tension load case A in Figure 7.2 diverged during the unloading. There seems to be a bug that should be investigated further. For now, the stress-strain diagrams normal to the expected diagonal staircase crack in Figures 7.6(g), 7.7(g) and 7.8(g) can regrettably not elucidate the operation of the Engineering Masonry Model's *Diagonal stair-case cracks* option.

8
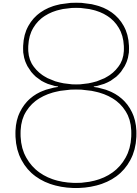
Masonry Unit Cell

A masonry unit cell is studied to observe stress-strain behaviour of a piece of masonry for the same load cases studied in Chapter 7.

8.1. Model Description

The masonry in the unit cell model is modelled the same way as by [9, Chapter 4]. Therefore, a micro-modelling approach was used, where the bricks are modelled as linear elastic plane stress elements; and the mortar and mortar-brick interface are modelled together as plane stress elements whose behaviour is described by the Engineering Masonry Model with the *Direct input head-joint tensile strength*[1]. The joints are thus modelled as a orthotropic material with tensile and compressive behaviour as in Sections 2.4.3 and 2.4.4 and shear behaviour as in Section 2.4.2 parallel to their own orientation. For this purpose, the local x-axis of the joint elements is defined parallel to the joint orientation.

The masonry unit cell is defined as the smallest repeated unit in the masonry pattern. For the running bond, this is a cell that is a single brick plus mortar joint wide and two bricks plus two mortar joints high, see Figure 8.1. The brick dimensions are 210 mm wide and 50 mm high. The joints are 10 mm thick. The thickness of the masonry is 100 mm. The mesh size is 10x10 mm. Second-order eight node quadrilateral plane stress elements (CQ16M) are used. The integration scheme is regular. This is summarized in Table 8.1.

Table 8.1: Element properties used in the masonry unit cell.

Model component	Element type	Integration scheme	Mesh size	Direction of local x-axis	Material Model
Bricks	CQ16M	Regular, i.e. Gauss 2x2	50x50 mm	n.a.	*Linear Elastic Isotropic*
Head joints	CQ16M	Regular, i.e. Gauss 2x2	50x50 mm	Vertical	*Engineering Masonry Model – Direct input head-joint tensile strength*
Bed joints	CQ16M	Regular, i.e. Gauss 2x2	50x50 mm	Horizontal	*Engineering Masonry Model – Direct input head-joint tensile strength*

Figure 8.1(a) shows the loads and boundary conditions that are active during the first phase of the analysis, when the overload is applied. The overload is 0.40 MPa. The bottom of the model is simply supported in the y-direction. The bottom left node is also supported in the x-direction. The vertical displacements of the top nodes of the model are all equal.

Figure 8.1(b) shows the additional loads and boundary conditions that become active during the second phase of the analysis, when the horizontal extension and/or shear loading is applied. This load

---

[1]Remember that this actually means direct input of the tensile strength of the masonry in the direction normal to the head joints.
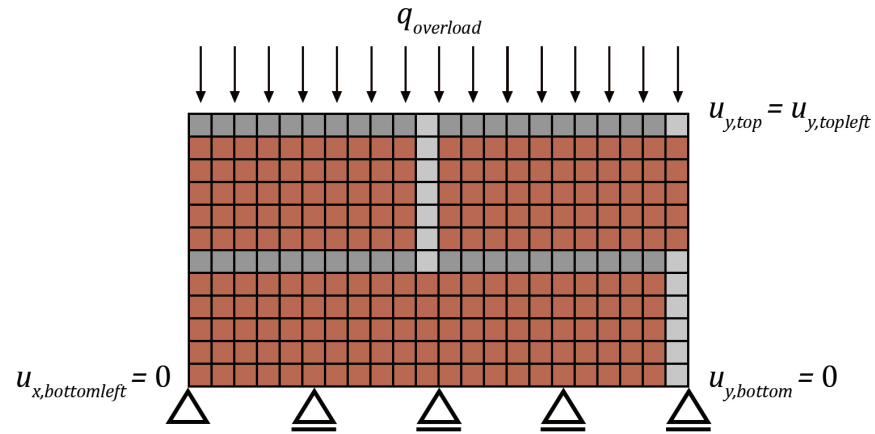
(a) Loads and boundary conditions that are active during the first phase.
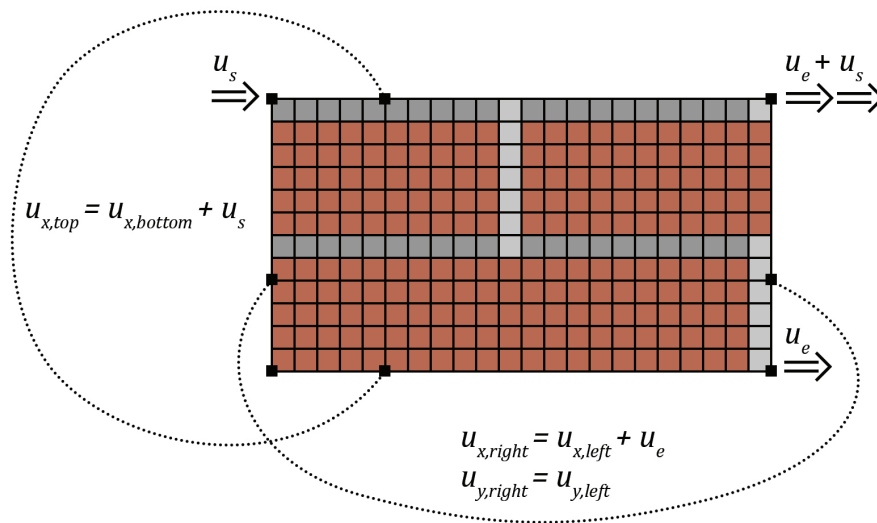
(b) Additional loads and boundary conditions that become active during the second phase. One left-right node pair and one top-bottom node pair are illustrated as examples for the tyings of all node pairs.

Figure 8.1: The masonry unit cell model, with the brick in brown, the bed joints in dark grey and the head joints in light grey.

is applied as prescribed displacements to the corner nodes. Similar to the Single Element Model, a horizontal displacement $u_s = h_{model} = 120$ mm is applied to the top corner nodes, and a horizontal displacement $u_e = b_{model} = 220$ mm is applied to the right corner nodes. These displacements are chosen to represent a shear strain and an extension strain respectively of 1.0, and are multiplied by a time dependent function.

Periodic boundary conditions are defined using `FIX`-tyings, that allow for a displacement to be set as a linear equation of several other displacements, see [3, Section 2.2.7.1]. This tying is not available in Diana's user interface, but can be scripted in the `.dat`-file[2]. Each two nodes on the left and right side that have the same y-coordinate are tied together. For each of these left-right node pairs, the vertical displacement is set equal and the horizontal displacement is defined such that the horizontal displacement of the right node is equal to the sum of the horizontal displacement of the left node and the applied extension displacement u_e. Similarly, each two nodes on the top and bottom side that have the same x-coordinate are tied together. Also for each top-bottom pair, the horizontal displacement of the top node equals the sum of the horizontal displacement of the bottom node and the applied shear

---

[2]Take care that when this `.dat`-file is imported into the user interface, the `FIX`-tyings will work fine at first, but once the model is saved as a `.dpf`-file and reopened, they do not work anymore.

displacement u_s.

The material properties of the bricks are given in Table 8.2 and the material properties of the bed joint are given in Table 8.3. The material properties of the head joints are the same as those of the the bed joint, with the exception that the tensile strength and stiffness are halved.

Table 8.2: Material properties used for the bricks in the masonry unit cell model.

Young's modulus	E	8049	MPa
Poisson's ratio	v	0.16	[-]
Mass density	ρ	1624	kg/m^3

Table 8.3: Material properties used for the bed joints in the masonry unit cell model.

Horizontal Young's modulus	E_x	1050	MPa
Vertical Young's modulus	E_y	1050	MPa
Shear modulus	G_{xy}	453	MPa
Mass density	ρ	1624	kg/m^3
Head-joint tensile strength	f_{tx}	0.08	MPa
Bed-joint tensile strength	f_{ty}	0.08	MPa
Fracture energy in tension	G_{ft}	6.9	N/m
Compressive strength	f_c	3.59	MPa
Fracture energy in compression	G_{fc}	6400	N/m
Factor strain at compressive strength	n	3	[-]
Unloading factor	λ	0	[-]
Friction angle	φ	0.688	rad
Cohesion	c	0.13	MPa
Fracture energy in shear	G_{fs}	3	N/m
Residual tensile strength		[-]	MPa
Crack bandwidth specification		*Govindjee*	

These material properties are adopted from [9, Chapter 4], though the following aspects were changed. The intersection between the head joint and the bed joint is assumed to have the weaker properties of the head joint. These weaker properties consist of not only a lower stiffness, but also a lower strength. Furthermore, the shear fracture energy was reduced from 300 N/m to 3 N/m, so that the softening branch is steep enough for the softening to be visible in the result graphs.

8.2. Load Cases

Of all the load cases studied in Section 7.2, the relevant ones for horizontal extension, shear loading and combinations thereof were studied for the Masonry Unit Cell model, too. They are:

C1 Shear loading.

C2 Shear loading and unloading halfway through the softening branch.

DE Horizontal tensile loading and unloading to end in compression.

G1 Shear loading and simultaneous horizontal tensile loading and then tensile unloading to end with compression.

G2 Horizontal tensile loading and simultaneous positive shear loading and then shear unloading to zero.

G3 Horizontal tensile loading and simultaneous negative shear loading, then shear unloading during the softening phase to end with positive shear.

In addition, two extra variants of load cases G1, G2 and G3 are studied. In these variants the load paths are scaled, so that the ratio between the shear loading and the extension loading is varied. The a-variant is the same as in Chapter 7, for the b-variant the shear loading is doubled and for the c-variant both the shear load is doubled and the extension load is halved.

8.3. Analysis Procedure
A non-linear static analysis was performed with prescribed displacement loads that change over time. First, the overload was applied in ten load steps. Then the prescribed deformations were applied, in time steps so that $\Delta\varepsilon_{xx}$ and/or $\Delta\gamma_{xy}$ were 10^{-5} in the load cases C1, C2, DE, G1a, G2a and G3a. The regular Newton-Raphson iteration method was used, with a maximum number of iterations set at 50. Both the force and the displacement norm had to be satisfied, both with a tolerance of 0.01, though the analysis should continue when convergence was not reached.

8.4. Results
Figure 8.2, 8.4, 8.6, 8.8 and 8.10 show the stress-strain diagrams that are the results of the masonry unit cell model. The horizontal normal stress is the average stress over the left (or right) side of the unit cell and the shear stress is the average shear stress along the top (or bottom) of the unit cell. The horizontal strain is $\varepsilon_{xx} = u_e/b_{model}$ and the shear strain is $\gamma_{xy} = u_s/h_{model}$.

Like in Chapter 7 the lines in the stress-strain graphs are coloured blue, teal and purple consecutively. In Figure 8.2 and 8.4 the blue line represents loading, the green line unloading and the purple line reloading. In Figure 8.6 to 8.10 the colours correspond to the consecutive parts of the loading protocol given in each subfigure (a).

Figure 8.3, 8.5, 8.7, 8.9 and 8.11 show the deformed shapes and the principle strain of al the load cases. These are given either at the end of the load case, or at the end of the first (blue) part of the loading.

(a) Horizontal stress-strain diagram for load case C1.

(b) Shear stress-strain diagram for load case C1.

(c) Horizontal stress-strain diagram for load case C2.

(d) Shear stress-strain diagram for load case C2.
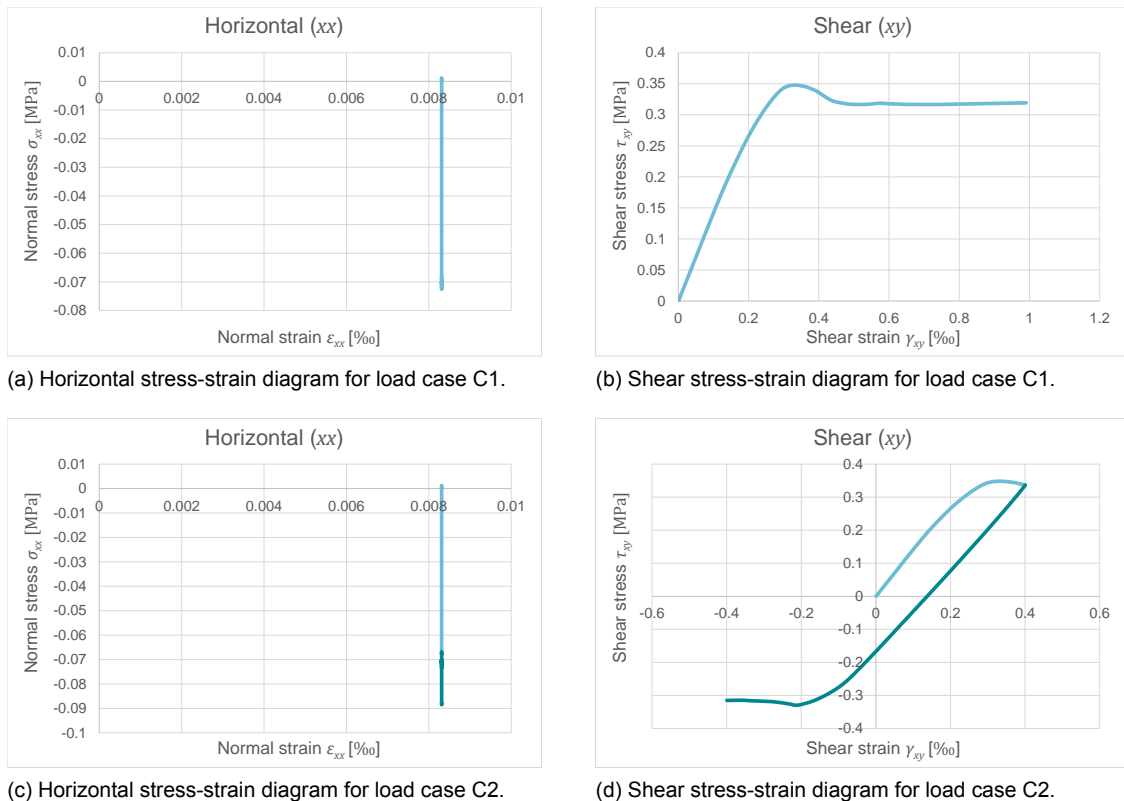
Figure 8.2: Stress-strain diagrams of the masonry unit cell model for load cases C1 shear loading (in blue) and C2 shear loading (in blue) and unloading (in teal) halfway through the softening.
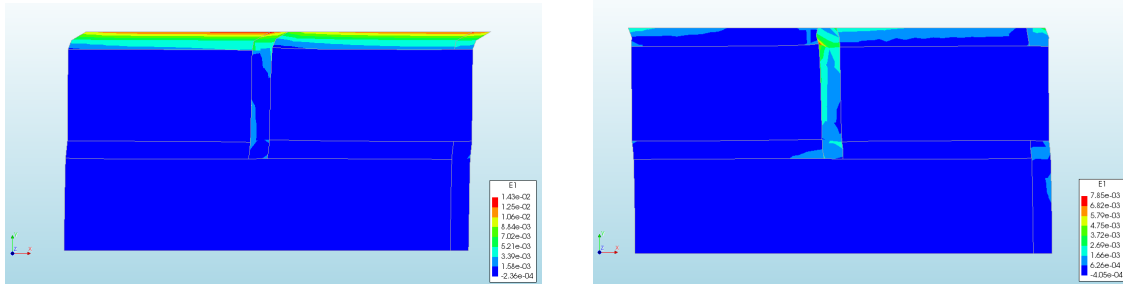
(a) Principle strain plot at the end of load case C1, at maximum positive shear strain.

(b) Principle strain plot at the end of load case C2, at maximum negative shear strain.

Figure 8.3: Principle strain plot of the masonry unit cell model at the end of load case C1 shear loading and at the end of load case C2 shear loading halfway through the softening. The deformation is magnified by a factor 100.
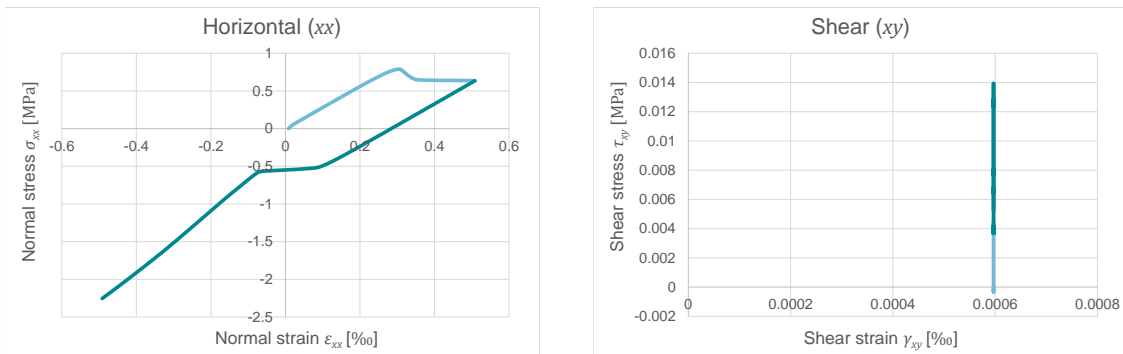
(a) Horizontal stress-strain diagram for load case DE.

(b) Shear stress-strain diagram for load case DE.

Figure 8.4: Stress-strain diagrams of the masonry unit cell model for load case DE, horizontal tensile loading (in blue) and unloading (in teal) to end with compression.
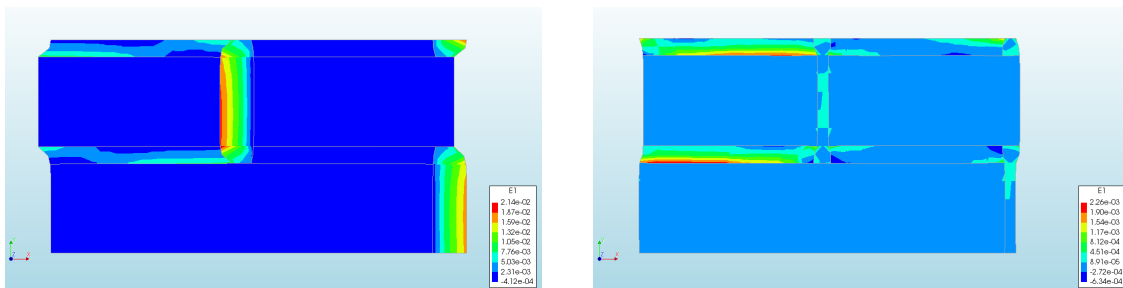
(a) Principle strain plot at the end of the loading of load case DE, at maximum horizontal tensile strain.

(b) Principle strain plot at the end of the unloading of load case DE, at maximum horizontal compressive strain.

Figure 8.5: Principle strain plot of the masonry unit cell model at the end of the (tensile) loading and at the end of the unloading of load case DE, horizontal tensile loading and unloading to end with compression. The deformation is magnified by a factor 100.
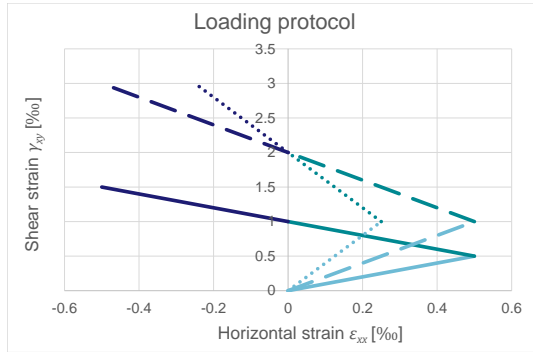
(a) Loading protocols applied, the solid line for load case G1a, the dashed line for load case G1b and the dotted line for load case G1c.
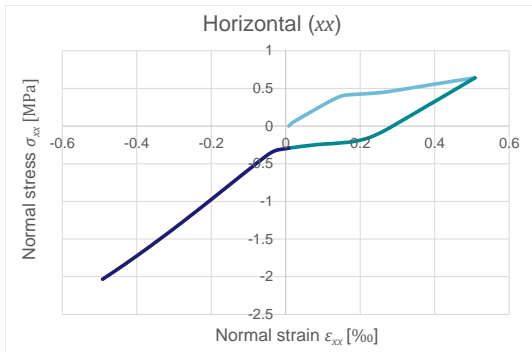
(b) Horizontal stress-strain diagram for load case G1a.
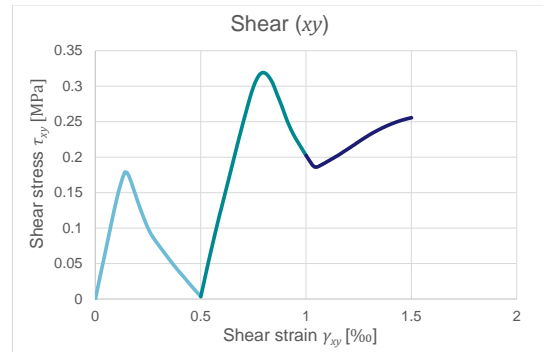
(c) Shear stress-strain diagram for load case G1a.
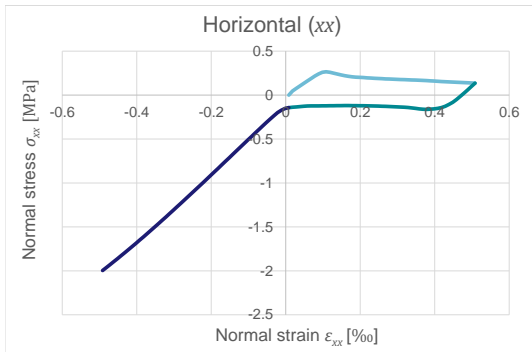
(d) Horizontal stress-strain diagram for load case G1b.
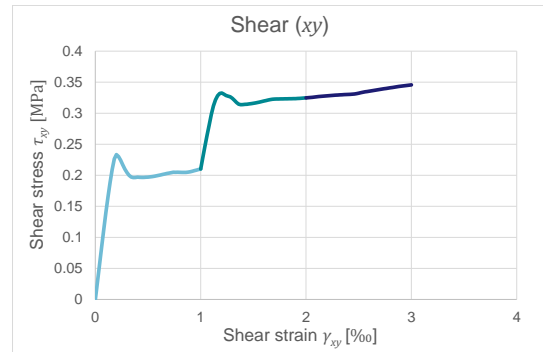
(e) Shear stress-strain diagram for load case G1b.
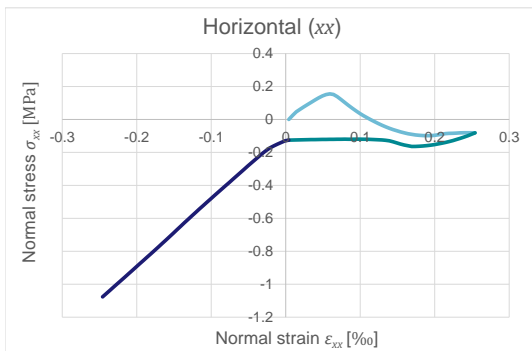
(f) Horizontal stress-strain diagram for load case G1c.
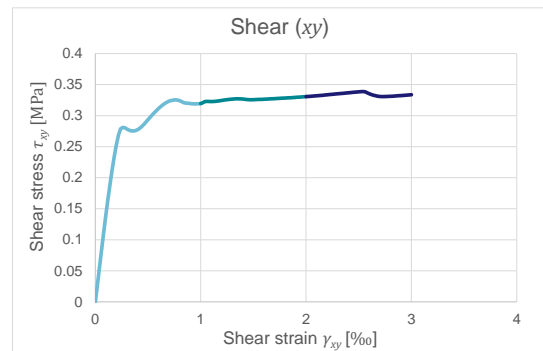
(g) Shear stress-strain diagram for load case G1c.

Figure 8.6: Stress-strain diagrams of the masonry unit cell model for load case G1, for three different ratios between the shear and tensile deformation. Colours correspond to the consecutive parts of the loading protocol applied.
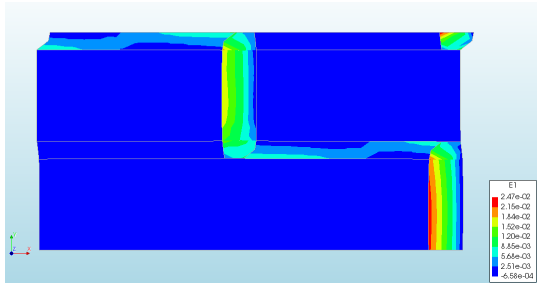
(a) Principle strain plot at the end of the first (blue) part of load case G1a, at maximum horizontal tensile strain.
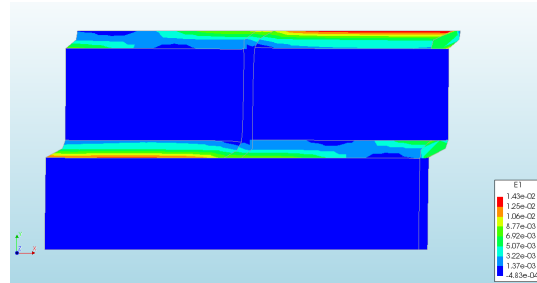
(b) Principle strain plot at the end of load case G1a, at maximum shear strain and maximum horizontal compressive strain.
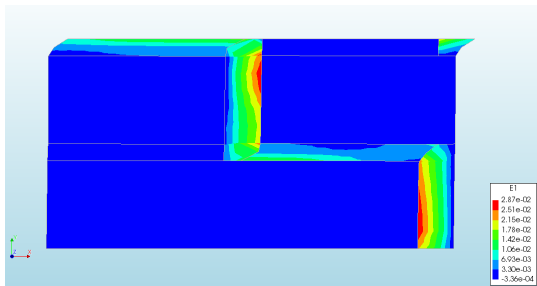
(c) Principle strain plot at the end of the first (blue) part of load case G1b, at maximum horizontal tensile strain.
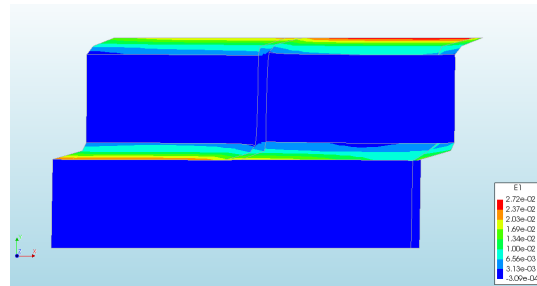
(d) Principle strain plot at the end of load case G1b, at maximum shear strain and maximum horizontal compressive strain.
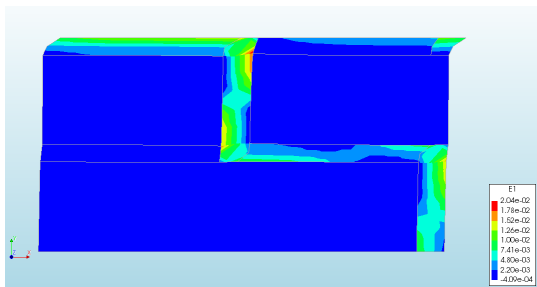
(e) Principle strain plot at the end of the first (blue) part of load case G1c, at maximum horizontal tensile strain.
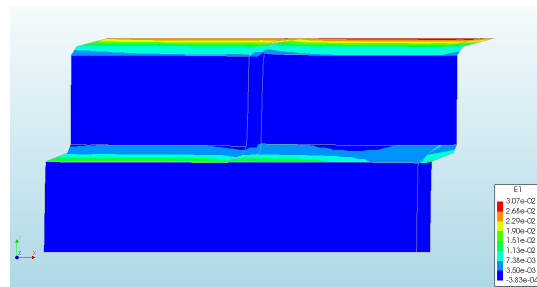
f) Principle strain plot at the end of load case G1c, at maximum shear strain and maximum horizontal compressive strain.

Figure 8.7: Principle strain plot of the masonry unit cell model at the end of the first (blue) part and at the end of load case G1, for three different ratios between the shear and tensile deformation. The deformation is magnified by a factor 100.
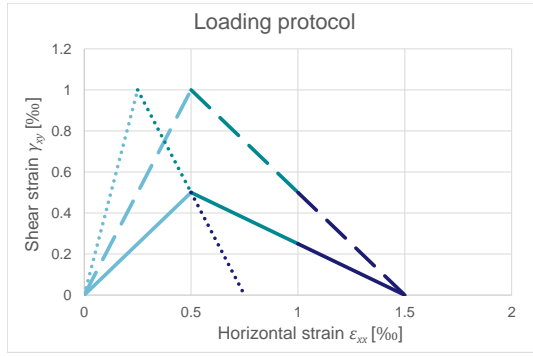
(a) Loading protocols applied, the solid line for load case G2a, the dashed line for load case G2b and the dotted line for load case G2c.
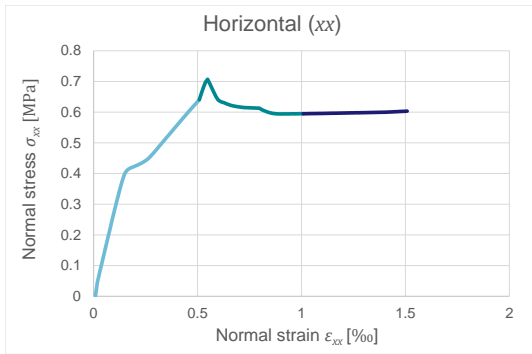
(b) Horizontal stress-strain diagram for load case G2a.
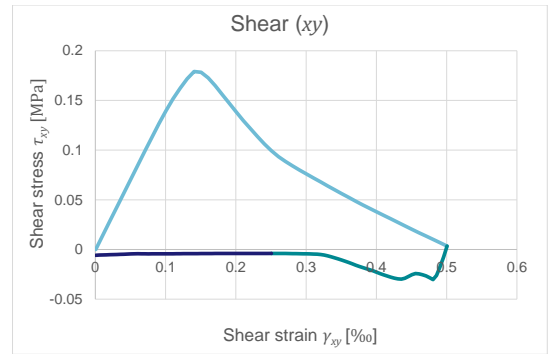
(c) Shear stress-strain diagram for load case G2a.
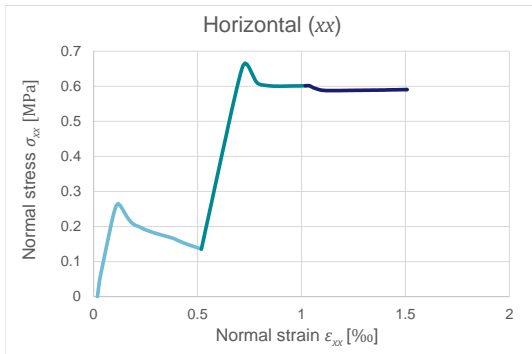
(d) Horizontal stress-strain diagram for load case G2b.
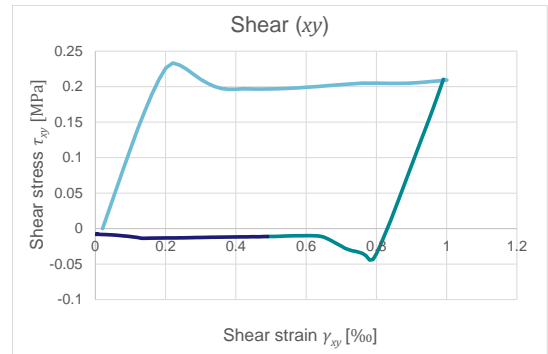
(e) Shear stress-strain diagram for load case G2b.
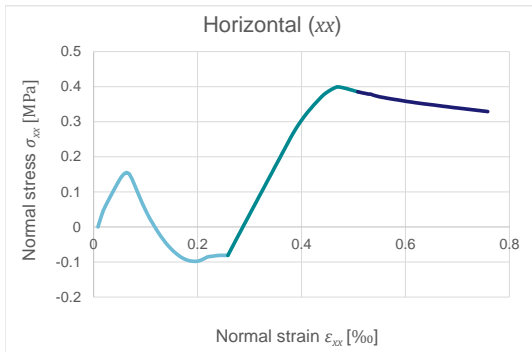
(f) Horizontal stress-strain diagram for load case G2c.
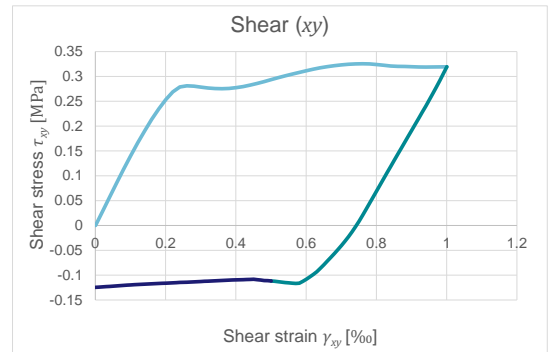
(g) Shear stress-strain diagram for load case G2c.

Figure 8.8: Stress-strain diagrams of the masonry unit cell model for load case G2, for three different ratios between the shear and tensile deformation. Colours correspond to the consecutive parts of the loading protocol applied.
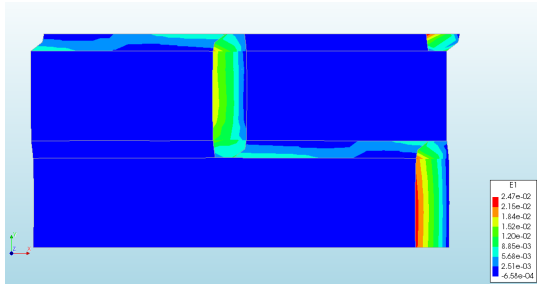
(a) Principle strain plot at the end of the first (blue) part of load case G2a, at maximum shear strain.
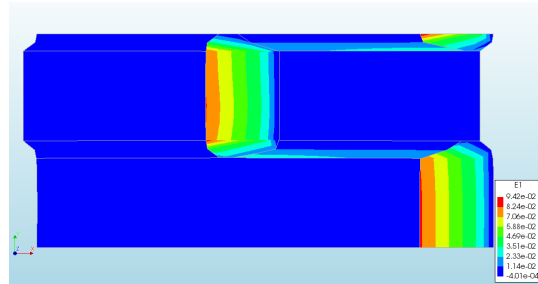
(b) Principle strain plot at the end of load case G2a, at maximum horizontal tensile strain and zero shear strain.
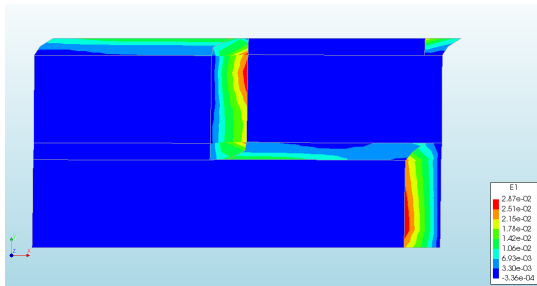
(c) Principle strain plot at the end of the first (blue) part of load case G2b, at maximum shear strain.
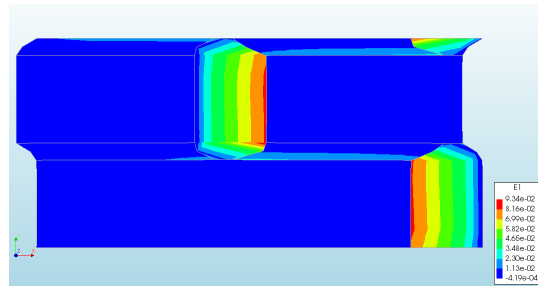
(d) Principle strain plot at the end of load case G2b, at maximum horizontal tensile strain and zero shear strain.
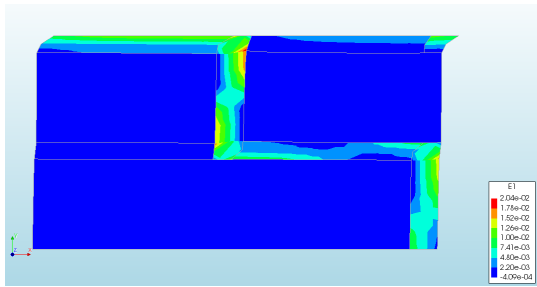
(e) Principle strain plot at the end of the first (blue) part of load case G2c, at maximum shear strain.
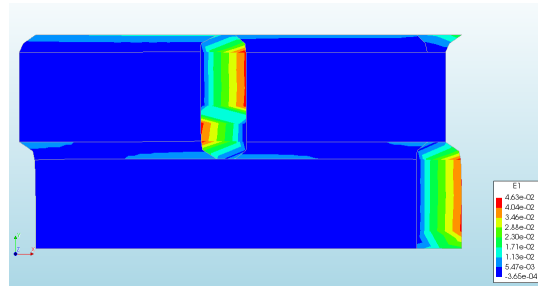
f) Principle strain plot at the end of load case G2c, at maximum horizontal tensile strain and zero shear strain.

Figure 8.9: Principle strain plot of the masonry unit cell model at the end of the first (blue) part and at the end of load case G2, for three different ratios between the shear and tensile deformation. The deformation is magnified by a factor 100.
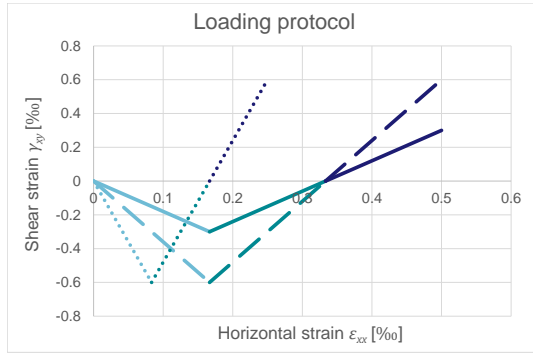
(a) Loading protocols applied, the solid line for load case G3a, the dashed line for load case G3b and the dotted line for load case G3c.
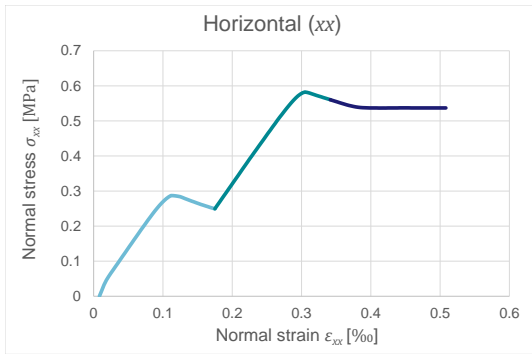
(b) Horizontal stress-strain diagram for load case G3a.
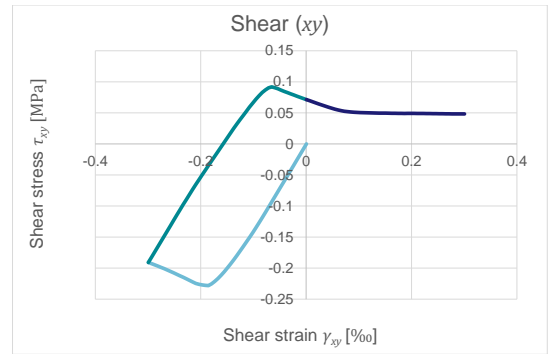
(c) Shear stress-strain diagram for load case G3a.
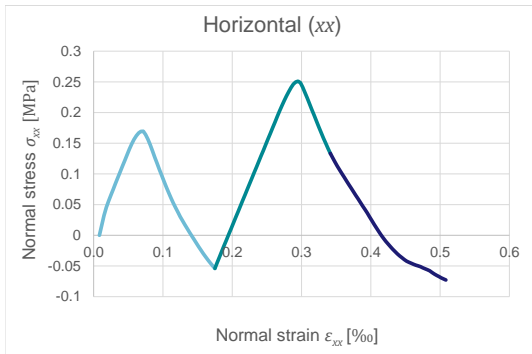
(d) Horizontal stress-strain diagram for load case G3b.
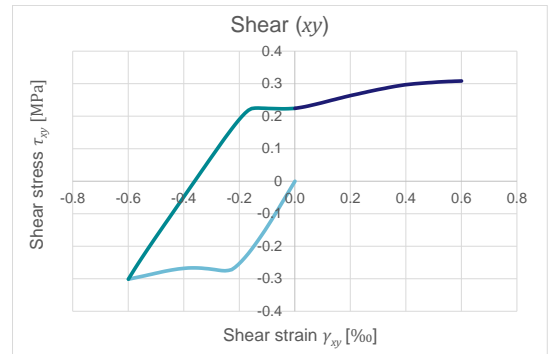
(e) Shear stress-strain diagram for load case G3b.
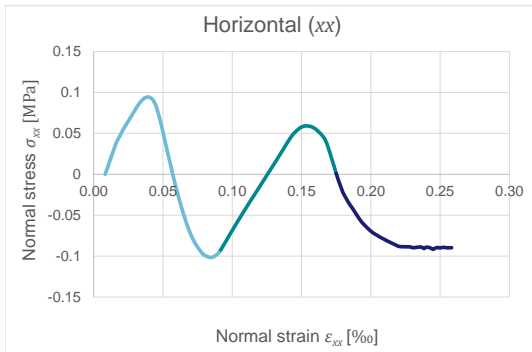
(f) Horizontal stress-strain diagram for load case G3c.
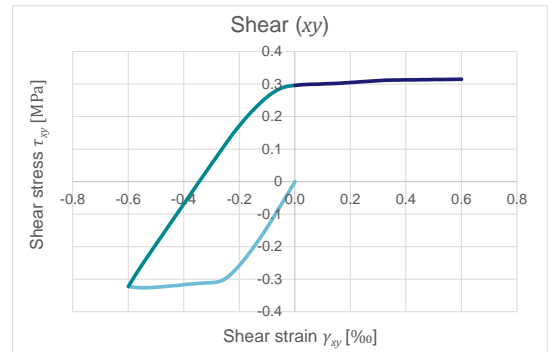
(g) Shear stress-strain diagram for load case G3c.

Figure 8.10: Stress-strain diagrams of the masonry unit cell model for load case G3, for three different ratios between the shear and tensile deformation. Colours correspond to the consecutive parts of the loading protocol applied.
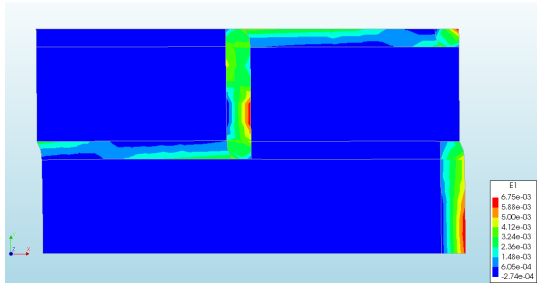
(a) Principle strain plot at the end of the first (blue) part of load case G3a, at maximum negative shear strain.
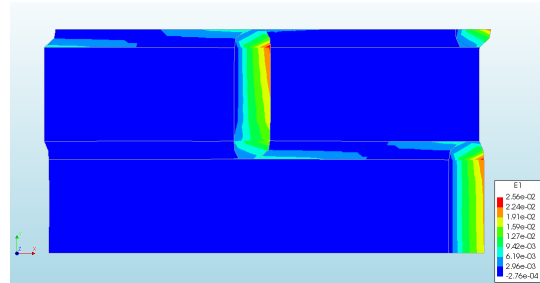
(b) Principle strain plot at the end of load case G3a, at maximum horizontal tensile strain and maximum positive shear strain.
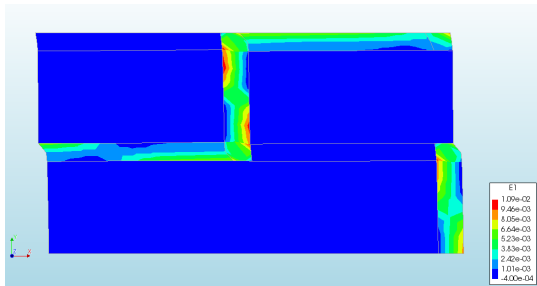
(c) Principle strain plot at the end of the first (blue) part of load case G3b, at maximum negative shear strain.
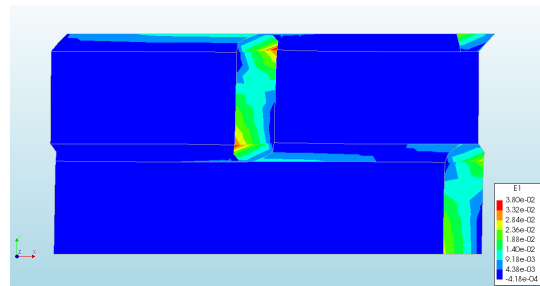
(d) Principle strain plot at the end of load case G3b, at maximum horizontal tensile strain and maximum positive shear strain.
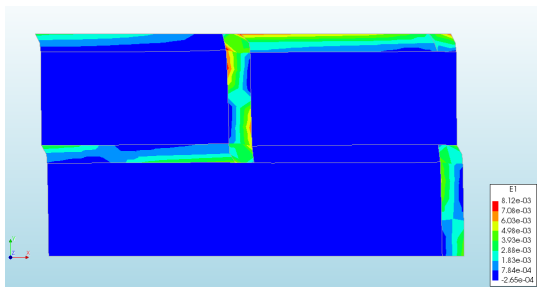
(e) Principle strain plot at the end of the first (blue) part of load case G3c, at maximum negative shear strain.
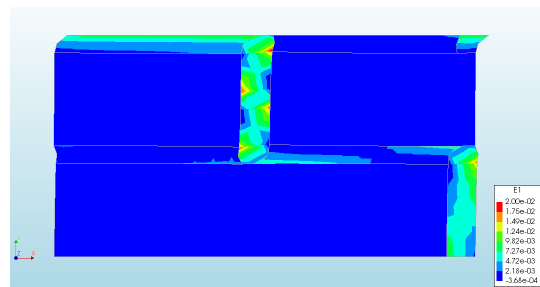
f) Principle strain plot at the end of load case G3c, at maximum horizontal tensile strain and maximum positive shear strain.

Figure 8.11: Principle strain plot of the masonry unit cell model at the end of the first (blue) part and at the end of load case G3, for three different ratios between the shear and tensile deformation. The deformation is magnified by a factor 100.

8.5. Discussion

The stress-strain diagrams and deformed shapes of the masonry unit cell model that were presented in the previous section will be discussed for each load case.

Shear Load Cases

The shear load cases C1 and C2 (Figure 8.2) show similar stress-strain diagrams as the Equivalent Shear Masonry Model (Figure 7.4(a) and (c)). Also, the model 'invents' small horizontal tensile stress and strain, in spite of the prescribed displacements. This is attributed to the Engineering Masonry Model used for the joints.

The deformed shapes (Figure 8.3) show that the failure mode of shear is sliding in the top bed joint.

Horizontal Tension Load Case

The horizontal tension load case DE (Figure 8.4) shows a similar stress-strain diagram to the Equivalent Shear Masonry Model (Figure 7.5(a)). The stress-strain diagram does, however, goes through the fourth quadrant. This is precisely what was expected before the simplification in Section 5.4 was made. This part of the material model could be refined. Also, the model 'invents' small shear stress and strain, in spite of the prescribed displacements. Again, this is attributed to the Engineering Masonry Model used for the joints.

The deformed shape (Figure 8.5(a)) shows that the failure mode of horizontal tension is a vertical merlon shaped crack.

Combined Load Cases

The shear load cases G1, G2 and G3 show similar stress-strain diagrams (Figures 8.6, 8.8 and 8.10) as the Equivalent Shear Masonry Model for some of the investigated ratios between the shear loading and the extension loading. Compare the results for load case G1b in Figure 8.6(d) and (e) to Figure 7.6(b) and (d), the results for load case G2b in Figure 8.8(d) and (e) to Figure 7.7(b) and (d), and the results for load case G3a in Figure 8.10(b) to (e) to Figure 7.8(b) and (d): they show clear resemblance. For the other ratios between the shear loading and the extension loading, the resemblance is less evident. The assumption that was made in Section 5.4 about the ratio between the shear stress and the horizontal tensile stress remaining the same during yielding, does not seem to hold.

Table 8.4 presents the deformation increment ratios between horizontal tension and shear loading $\Delta\varepsilon_{xx}/\Delta\gamma_{xy}$. It can be seen that the load phases for which the absolute value of the deformation increment ratio is closest to the height-width ratio of the diagonal staircase crack,[3] are the same load phases that show the best resemblance to the single element model results. The ratio between the shear stress (increment) and the horizontal tensile stress (increment) during combined softening and yielding seems to be related to the deformation increment ratio. The ratio between the shear stress and the horizontal tensile stress only remains unchanged if the absolute value of the deformation increment ratio is equal to the height-width ratio of the staircase crack.

Table 8.4: Deformation increment ratio $\Delta\varepsilon_{xx}/\Delta\gamma_{xy}$ for the combined load cases G. The first phase correspond to the blue parts of the loading protocols in Figures 8.6(a), 8.8(a) and 8.10(a), the second phase to the teal and purple parts.

	G1a	G1b	G1c	G2a	G2b	G2c	G3a	G3b	G3c
First phase	1.0	0.50	0.25	1.0	0.50	0.25	-0.67	-0.33	-0.17
Second phase	-1.0	-0.50	0.25	-2.0	-1.0	-0.50	0.67	0.33	0.17

Although the stress-strain diagrams are quite different for the three variants of each load case, the deformed shapes are very similar to each other. The deformed shapes of load case G1 (Figure 8.7) show that the failure mode of combined shear and horizontal tension is a diagonal stair case crack, that then evolves into shear sliding in both bed joints for shear and horizontal compression. The deformed shapes of load case G2 (Figure 8.9) again show that the failure mode of combined shear and horizontal tension is a diagonal stair case crack, that then evolves into a vertical merlon shaped crack when only horizontal tension remains. The deformed shapes of load case G3 (Figure 8.11) once more show that the failure mode of combined shear and horizontal tension is a diagonal stair case crack, that then evolves into a diagonal stair case crack in the other direction when only shear of the opposite sign remains.

---

[3]The height-width ratio of the expected staircase crack in the masonry unit cell model is $\tan\alpha = 120/220 = 0.55$.

<div style="text-align: right; font-size: 3em;">9</div>

Prediction of Shear Wall Experiment

This chapter presents a full scale finite element analysis of a shear wall using the Equivalent Shear Masonry Model, meant to approximate real life masonry laboratory tests.

9.1. Description of the Laboratory Experiments

The experimental shear wall tests that are simulated in this chapter are TUD-COMP-47 and TUD-COMP-48, both double clamped shear walls under light damage asymmetric cyclic horizontal loading. The walls are single wythe with a running bond. The materials are representative of existing masonry in the Groningen region, with solid clay bricks of approximately 210x100x50 mm and BM2 v2 mortar joints of approximately 10 mm thick. See the report of [9] for more detailed information.

9.2. Model Description

The experimental shear wall tests are simulated by a finite element analysis of a macro model using the Equivalent Shear Masonry Model, and for comparison also with the Engineering Masonry Model with the head joint option *Diagonal stair-case cracks*. The modelling is executed similarly to the macro model in [9, Chapter 4], that used the Engineering Masonry Model with the head joint option *Tensile strength head-joint defined by friction*. That report also presents a micro modelled analysis, whose approach is similar to the micro modelling approach in Chapter 8. The results of this Sections analysis can therefore be compared not only with each other and the experimental results, but also with the macro and micro model results from [9, Chapter 4].

Table 9.1: Element properties used in the shear wall model.

Model component	Element type	Integration scheme	Mesh size	Direction of local x-axis	Material Model
Masonry	CQ16M	High, i.e. Gauss 3x3	50x50 mm	Horizontal	*Equivalent Shear Masonry Model* or *Engineering Masonry Model – Diagonal stair-case cracks* respectively
Steel	CL9BE	High, i.e. Gauss 7	50 mm	n.a.	*Linear Elastic Isotropic*

The masonry wall is modelled as a two-dimensional rectangular sheet of 3050 mm wide and 2700 mm high, see Figure 9.1. This sheet is meshed with 50x50 mm second-order membrane elements (CQ16M) with a 100 mm thickness. The x-axis of these elements is aligned horizontally. The masonry material model is the Equivalent Shear Masonry Model for the first analysis and the Engineering Masonry Model with the *Diagonal stair-case cracks* option for the other analysis. This is summarized in Table 9.1. The material properties used are adopted from [9, Chapter 4] and are shown in Table 9.2.
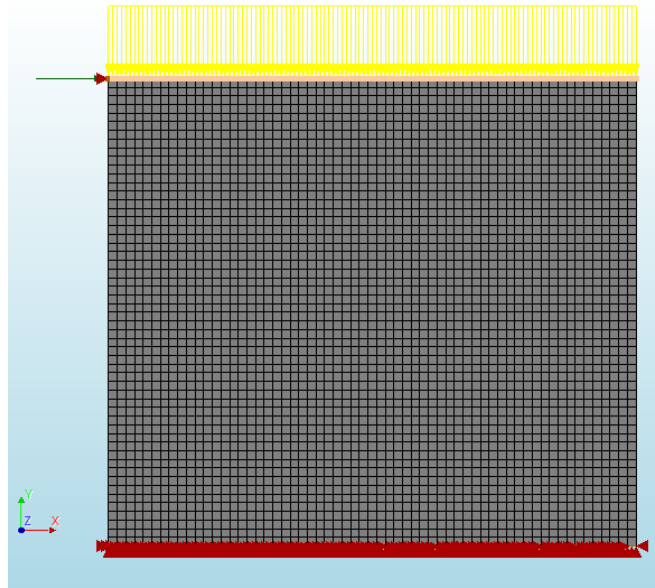
Figure 9.1: Mesh of the shear wall as modelled in Diana's graphical user interface. Visible are the masonry (grey), the translation supports (red triangles), the overload (yellow arrows), the prescribed displacement load (dark green arrow), the slave nodes of the vertical displacement tying of the top (light orange line) and its master node (dark orange dot). Not visible are the steel beams at the top and bottom and the rotation supports at the top and bottom.

Table 9.2: Material properties used for the masonry in the shear wall model.

Horizontal stiffness	E_x	2497	MPa
Vertical stiffness	E_y	3751	MPa
Shear stiffness	G_{xy}	1500	MPa
Tangent of friction angle	$\tan\varphi$	0.821979	[-]
Vertical tensile strength	f_{ty}	0.16	MPa
Tensile fracture energy	G_{ft}	11.3	N/m
Compressive strength	f_c	12.93	MPa
Compressive fracture energy	G_{fc}	35590	N/m
Compressive unloading factor	λ	1	[-]
Cohesion	c	0.17	MPa
Shear fracture energy	G_{fs}	209	N/m
Diagonal crack angle	α	0.5	rad
Factor strain at compressive strength	n	4	[-]
Crack band width[a]	h	0.05	m
Mass density	ρ	1624	kg/m^3
Crack bandwidth specification[b]		*Govindjee*	

[a] Used for the Equivalent Shear Masonry Model only.
[b] Used for the Engineering Masonry Model only.

Table 9.3: Material properties used for the steel beams in the shear wall model.

Young's modulus	E	210,000 MPa
Poisson's ratio	ν	0.30
Mass density	ρ	10^{-15} kg/m^3

At the top of the sheet, a HEB-600 steel beam is modelled using eccentric one-dimensional class III beam elements (CL9BE). An overload is applied to this top beam and the in-plane rotation is restrained here. Also, the vertical deformation is tied so the beam stays horizontal. A prescribed horizontal

displacement is applied to the top left corner. The material properties of the steel are given in Table 9.3.

At the bottom of the sheet, a HEB-300 steel beam is modelled similarly to the top beam. Both the vertical and horizontal translations and the in-plane rotation are restrained here.

9.3. Loading Protocol

The shear wall model was subsequently loaded by its own weight and an overload of 0.46 MPa, that represents both the weight of the test setup carried by the wall and the extra applied overload. Then a horizontal deformation load was applied to the top in time steps of 0.01 mm. The horizontal loading protocol is pictured in Figure 9.2. It consists of six cycles with increasing amplitudes, that each consist of three repetitions of a load that statically resembles the Zeerijp earthquake from January 2018. This an asymmetric cyclic load that combines larger and smaller peaks.
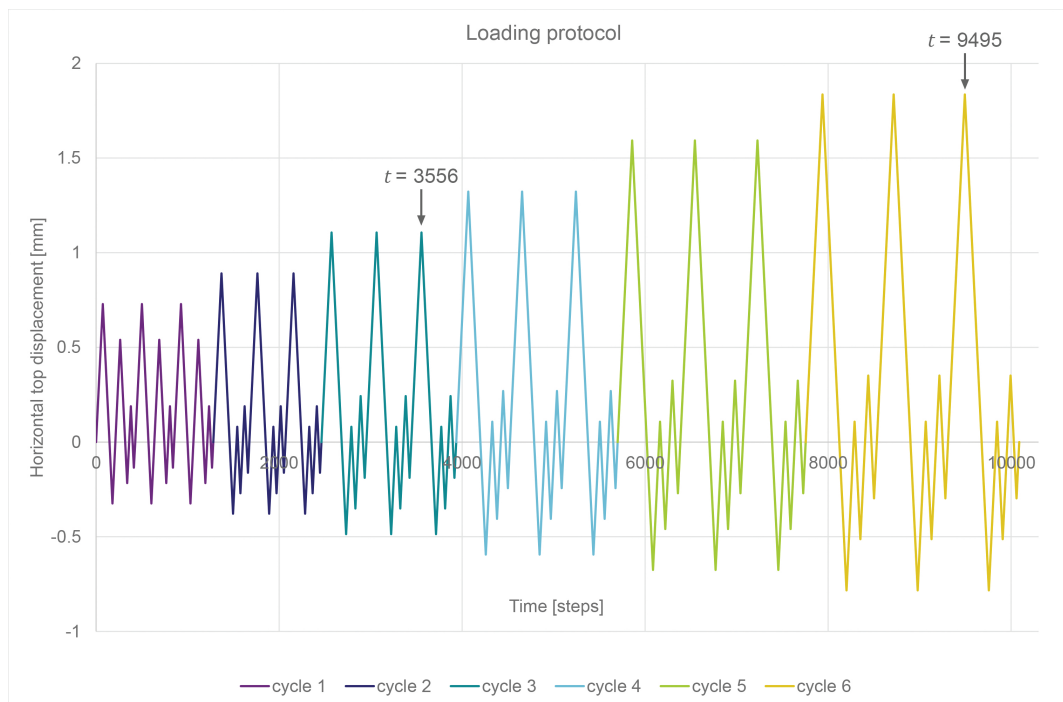
Figure 9.2: Horizontal loading protocol of the shear wall: six cycles of increasing amplitude, each consisting of three repetitions of a load that statically resembles the Zeerijp earthquake from January 2018. The last large drift peak of the first half of the loading $t = 3556$ and the final large drift peak of the loading protocol $t = 9495$ that will be referred to later are indicated.

9.4. Analysis Procedure

A non-linear static analysis was performed with a prescribed displacement load that changes over time. First, the self weight was applied in ten load steps. Subsequently the overload was applied, also in ten load steps. Then the prescribed displacement was applied. The regular Newton-Raphson iteration method was used, with a maximum number of iterations set at 100. Both the force and the displacement norm had to be satisfied, both with a tolerance of 0.01, though the analysis should continue when convergence was not reached.

9.5. Results

An important result of the finite element analysis is the overall force-deformation relations, given in the form of horizontal force-drift diagrams[1]. Figures 9.3, 9.4 and 9.5 show the horizontal force on the top versus the drift of the shear wall, as found in the experiments, with the Equivalent Shear Masonry Model and with the Engineering Masonry Model with *Diagonal stair-case cracks* option, respectively. Note that in the experiments, each cycle consisted of ten repetitions.

---
[1]The drift is equal to the horizontal top displacement divided by the height of the wall.
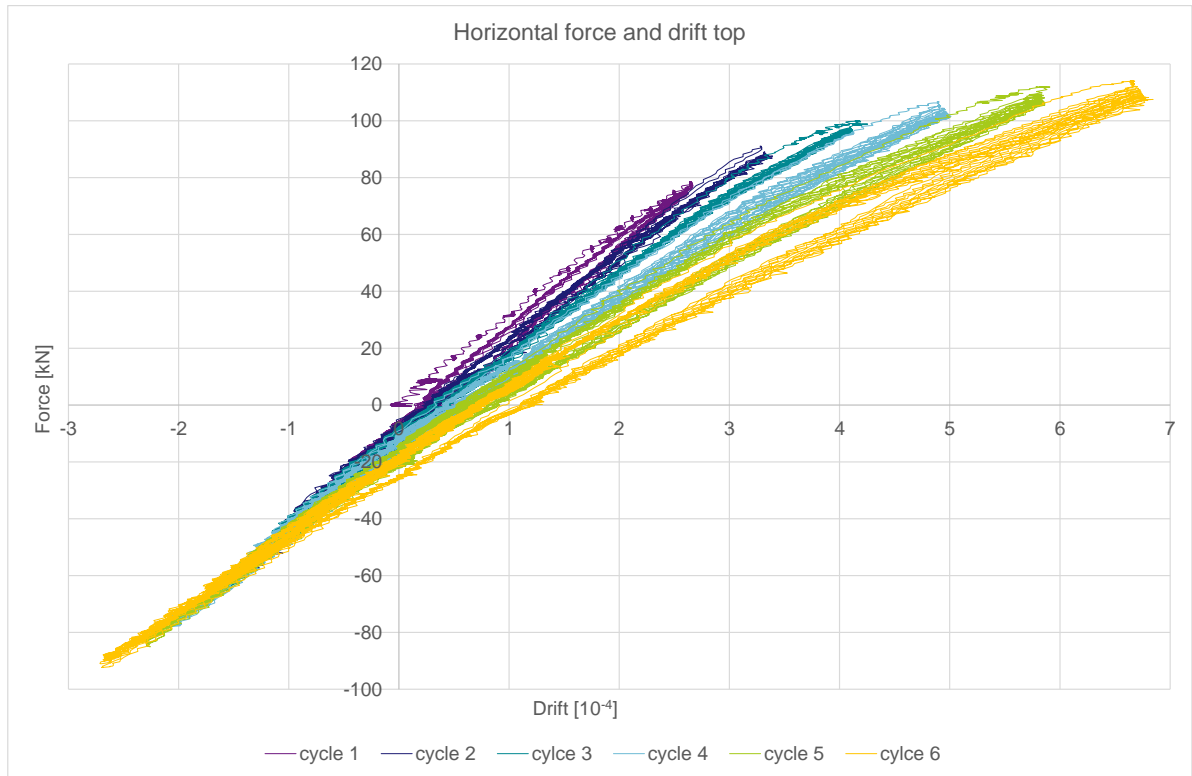
(a) of wall TUD-COMP-47.
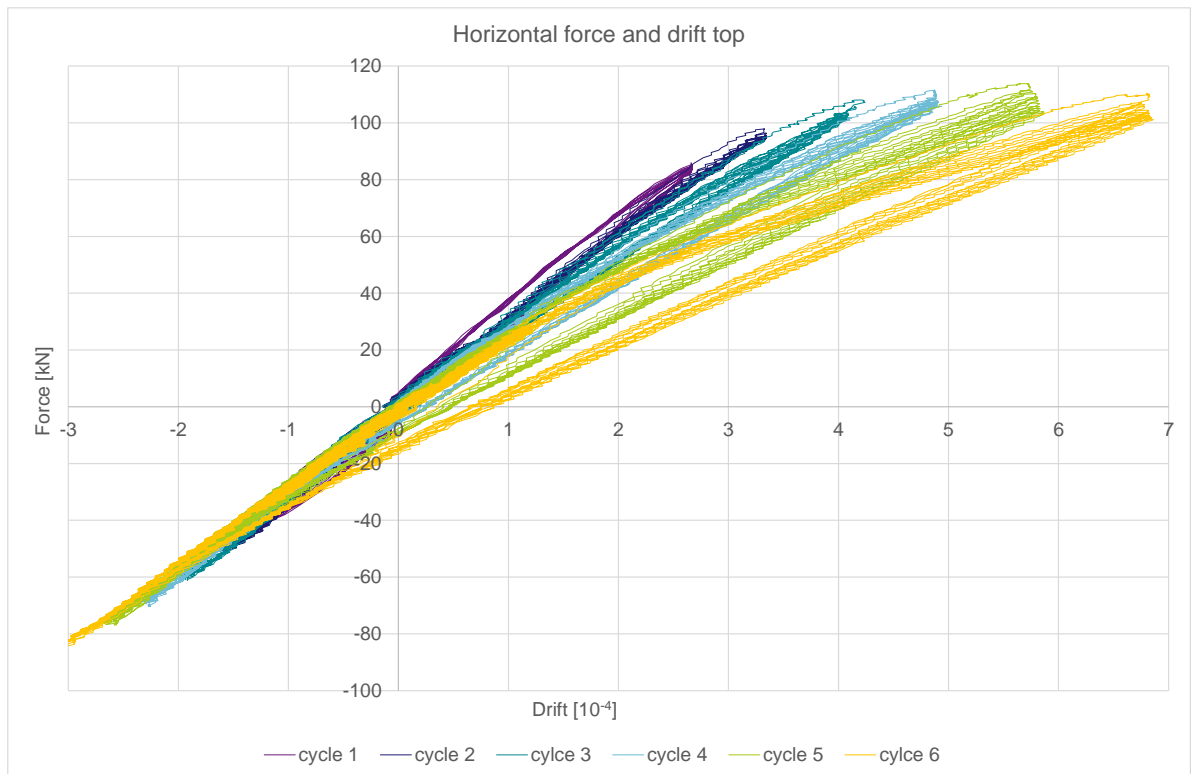
(a) of wall TUD-COMP-48.

Figure 9.3: Force-drift diagram of the experimental results, coloured per cycle. Data courtesy of [9].
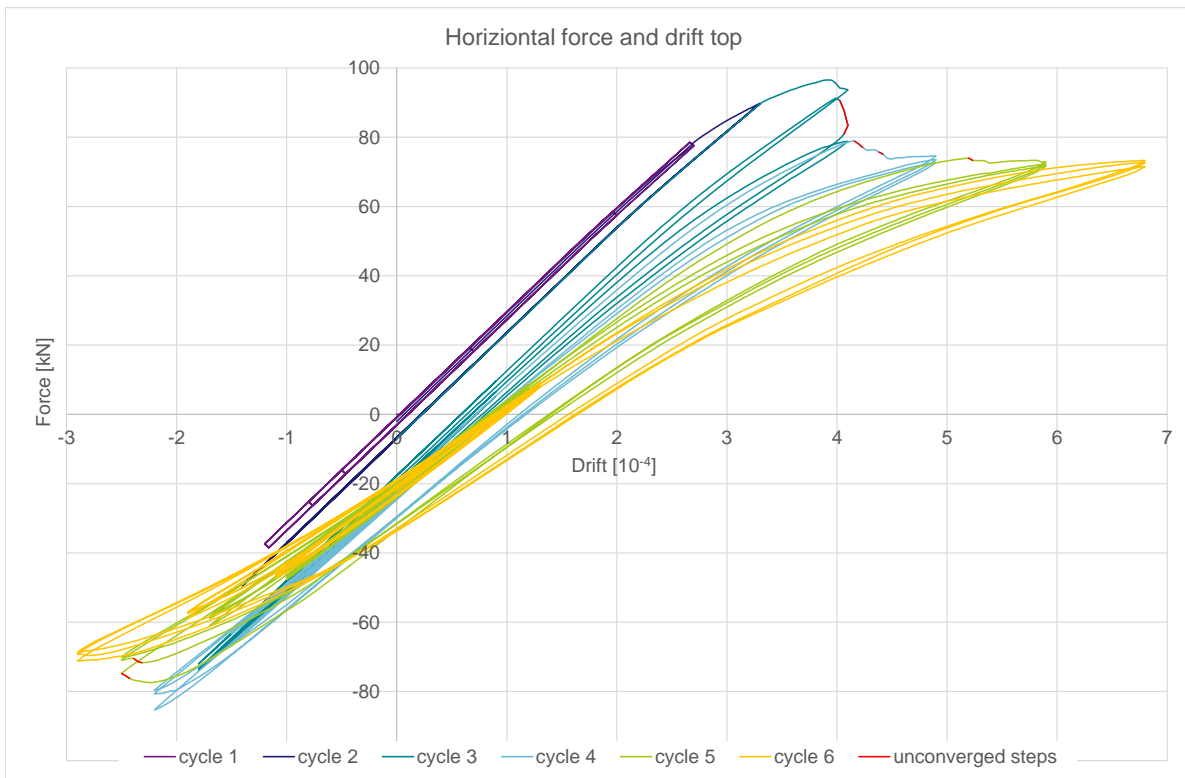
Figure 9.4: Force-drift diagram of the finite element analysis with the Equivalent Shear Masonry Model, coloured per cycle and with the unconverged steps marked in red.
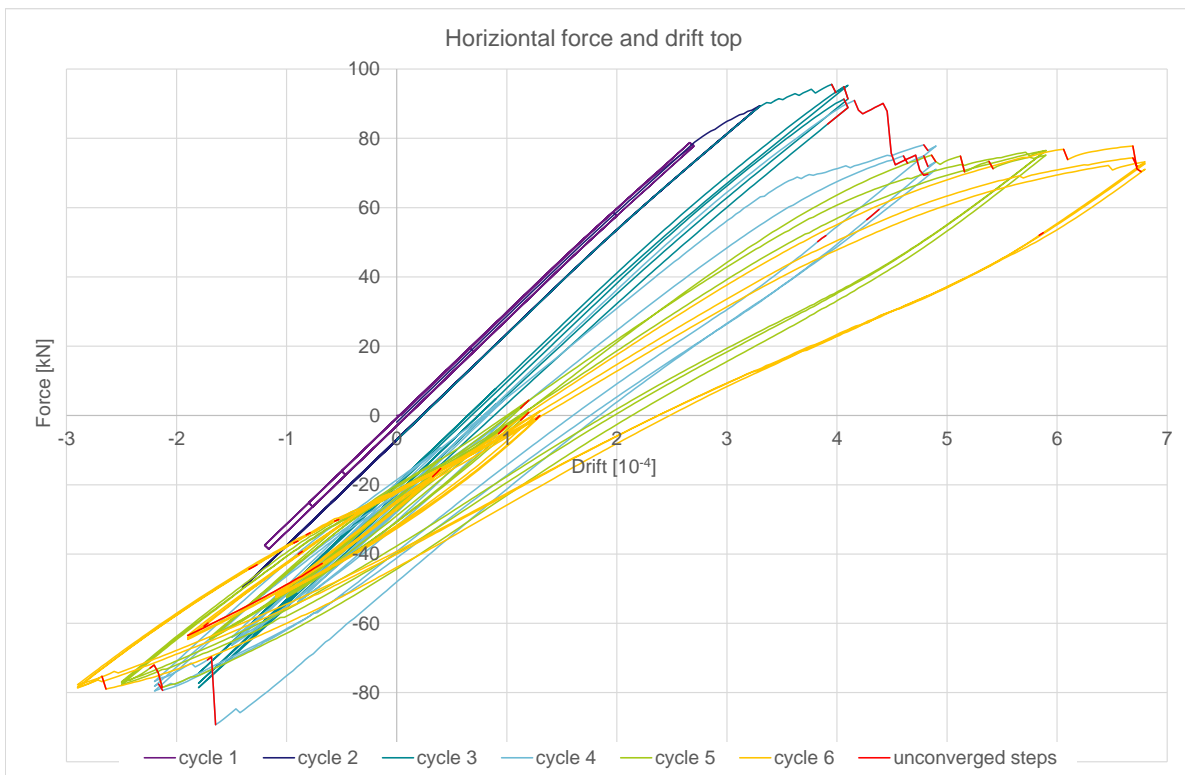
Figure 9.5: Force-drift diagram of the finite element analysis with the Engineering Masonry Model's *Diagonal stair-case cracks* option, coloured per cycle and with the unconverged steps marked in red.

The experimental force-drift diagrams (Figure 9.3) show that the initial behaviour is almost linear. The overall stiffness reduces over the consecutive cycles and the force-drift lines are slightly curved with a decreasing steepness. The behaviour to the left remains almost linear. Some permanent inelastic deformation is found, up to a drift of approximately 1‰. The peak forces reduce over the repetitions within each cycle, but are subsequently exceeded in the next cycle. The peak force is 114 kN. With the TUD-COMP-47, the peak force increases each cycle. With the TUD-COMP-48, the maximum is reached in cylce 5. The hysteresis loop is widest in the middle and small near the peak drift values. TUD-COMP-48 shows a significantly wider hysteresis loop than TUD-COMP-47.

The Equivalent Shear Masonry Model's force-drift diagram (in Figure 9.4) shows initial linear behaviour, followed by softening and then a residual plateau, both to the right and the left. The diagram is generally smooth. Permanent inelastic deformation is found, up to a drift of approximately 1.5‰. The peak forces reduce over the repetitions within each cycle, but are subsequently exceeded in the next cycle. The peak force is 96.5 kN, which is reached in cycle 3. The hysteresis loop has a similar width over its entire height.

The Engineering Masonry Model with *Diagonal stair-case cracks* option's force-drift diagram (in Figure 9.5) also shows initial linear behaviour, followed by softening and then a residual plateau, both to the right and the left. The diagram is partly smooth and partly serrated. Permanent inelastic deformation is found, up to a drift of approximately 2.5‰. The peak forces increase over the repetitions within each cycle. The peak force is 96.6 kN, which is reached in cycle 3. The hysteresis loop is smallest in the middle and wide near the peak drift values.

Convergence

The analysis with the Equivalent Shear Masonry Model had an average number of iterations per step of 6.8. 0.11% of these steps did not converge, see the red segments in Figure 9.4. The non-converging steps all occurred unaccompanied or in groups of two or three and all coincided with softening.

The analysis with the Engineering Masonry Model had an average number of iterations per step of 2.8. 0.95% of these steps did not converge, see the red segments in Figure 9.5. Most of the non-converging steps occurred unaccompanied or in groups of two, three or four, except two a long series of respectively 18 and 33 consecutive non-converging steps. Most of the non-converging steps also occurred during softening, but some others occurred during pre-peak loading or during unloading.

Peak Force Reduction

In the experiments, the force reached at the extreme drift of each cycle decreases with the repetitions. This peak force reduction is in the order of 10% over the ten repetitions of each cycle. The peak force reduction observed in the two finite element analysis are quantified in Table 9.4. The Equivalent Shear Masonry Model clearly displays reductions in the order of a few percent for the post-softening load cycles. The Engineering Masonry Model's *Diagonal stair-case cracks* option does not show any obvious peak force reduction. Instead, its peak forces rather seem to increase with each repetition.

Table 9.4: Peak force reduction (here negative) of the second and third repetitions of each cycle, given as the change relative to the force at the first peak of the cycle in question. The peak forces are considered at the extreme displacements to the right (positive displacement and force) and left (negative displacement and force) of each cycle.

			Cylce 1	Cylce 2	Cylce 3	Cylce 4	Cylce 5	Cylce 6
Equivalent Shear Masonry Model	right	2nd	-0.051%	-0.067%	-11%	-1.4%	-1.0%	-0.82%
		3rd	-0.076%	-0.13%	-16%	-2.5%	-1.8%	-2.4%
	left	2nd	+0.23%	+0.32%	+2.0%	-5.5%	-5.1%	-2.8%
		3rd	+0.34%	+0.53%	+2.7%	-6.6%	-6.2%	-3.5%
Engineering Masonry Model – *Diagonal stair-case cracks*	right	2nd	-0.051%	-0.10%	-4.1%	+9.4%	+1.7%	+2.3%
		3rd	-0.051%	-0.16%	-6.8%	+3.1%	+1.8%	+3.0%
	left	2nd	+0.26%	+0.26%	+3.8%	+3.6%	+1.1%	-0.3%
		3rd	+0.34%	+0.38%	+5.6%	+1.8%	+0.39%	-1.1%

Crack Pattern

The other important results of the finite element analysis are plots that provide insight into the failure mechanism and crack pattern. Figure 9.6 shows the crack patterns found in the experimental the TUD-COMP-47 and TUD-COMP-48 shear wall tests. To provide insight into the failure mechanism, these are given at two moments, at a large peak halfway trough the loading protocol and at the final large peak of the loading protocol. The diagonal crack segments follow the staircase paths through the head joints and bed joints. The diagonal cracked zones are steeper, at angles of approximately -55° and -45° with the bed joints.

(a) of TUD-COMP-47 at the last large drift peak of the first half of the loading protocol.

(b) of TUD-COMP-47 at the final large drift peak of the loading protocol.

(c) of TUD-COMP-48 at the last large drift peak of the first half of the loading protocol.

(d) of TUD-COMP-48 at the final large drift peak of the loading protocol.
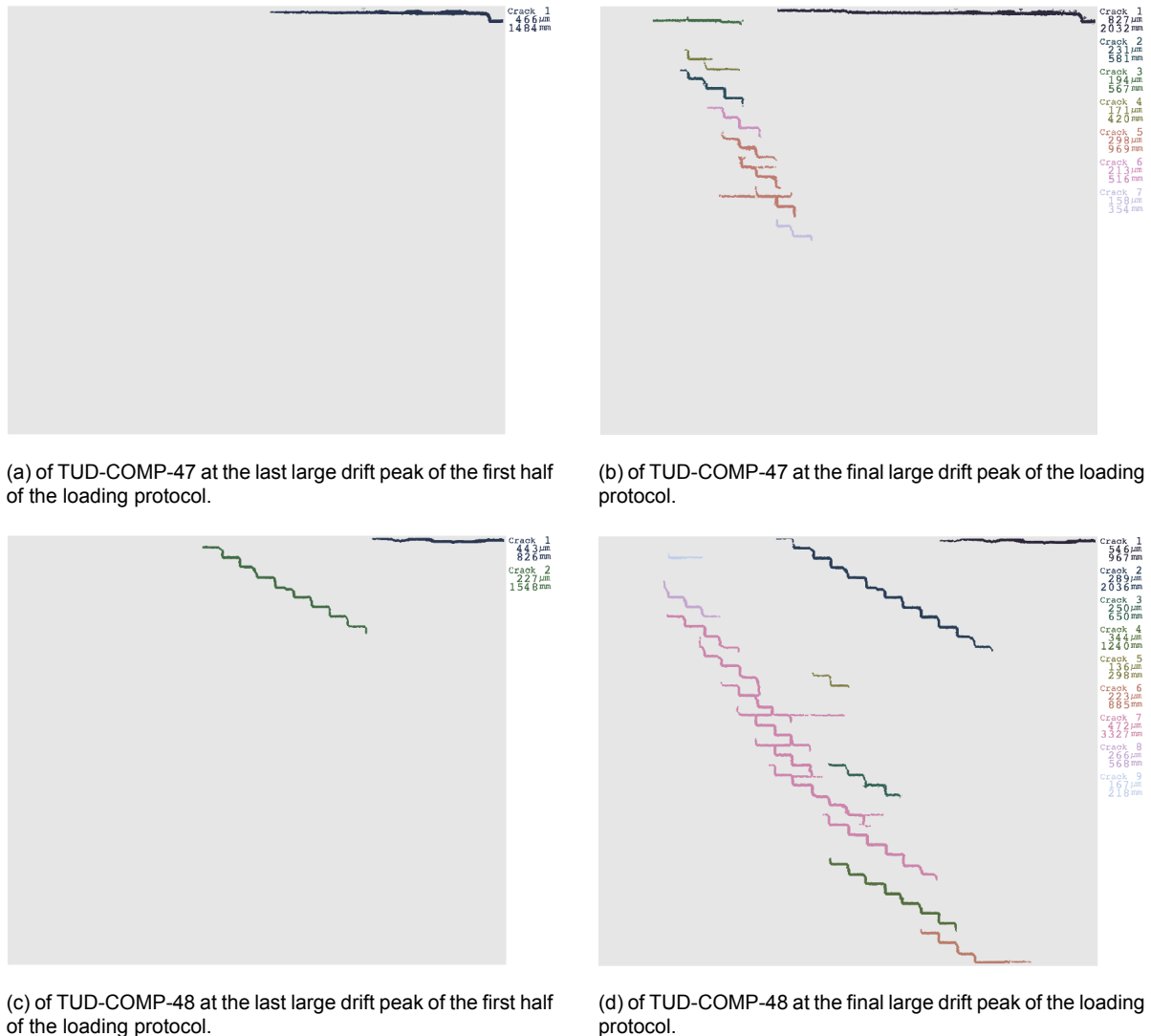
Figure 9.6: Cumulated crack patterns of the experimental shear wall tests. Courtesy of [9].

Three different types of finite element model outputs are included that each provide information about the crack pattern. These are the remaining cohesion, the crack width and the principle strain. The first two measures are insightful, but they are not generated in the same way for each of the two models. To allow for a fair comparison between the two models, the more fundamental measure of principle strain is displayed.

The cracks observed with the Equivalent Shear Masonry Model are at an angle of approximately $\pm 68°$ with the horizontal x-axis. The cracks observed with the Engineering Masonry Model's *Diagonal stair-case cracks* option are at an angle of approximately $\pm 74°$ with the horizontal x-axis.

The remaining cohesion is a useful model output to asses the cumulated damage, because it provides information about what points have at least once already reached the shear strength. Figure 9.7 presents cohesion plots of the analysis with the Equivalent Shear Masonry Model. The non-red points in these plots have reached their peak shear stress, peak horizontal tensile stress or peak combination of the two. Figure 9.8 presents cohesion plots of the analysis with the Engineering Masonry Model with the head joint option *Diagonal stair-case cracks*. The non-red points in these plots have reached their maximum shear stress. Points that have (only) reached their maximum diagonal stress are not represented here.

(a) at the last large drift peak of the first half of the loading protocol, at $t = 3556$.

(b) at the final large drift peak of the loading protocol, at $t = 9495$.
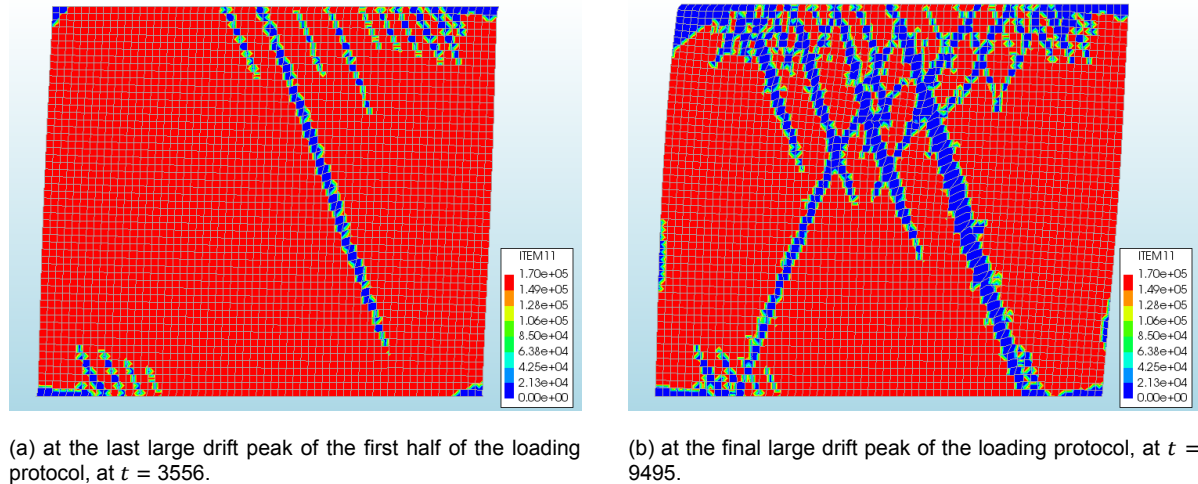
Figure 9.7: Cohesion (`USRSTA(11)`) plots of the finite element analysis with the Equivalent Shear Masonry Model. The red parts still behave linearly, the blue parts are post-softening. The deformation is magnified by a factor 100.

(a) at the last large drift peak of the first half of the loading protocol, at $t = 3556$.

(b) at the final large drift peak of the loading protocol, at $t = 9495$.
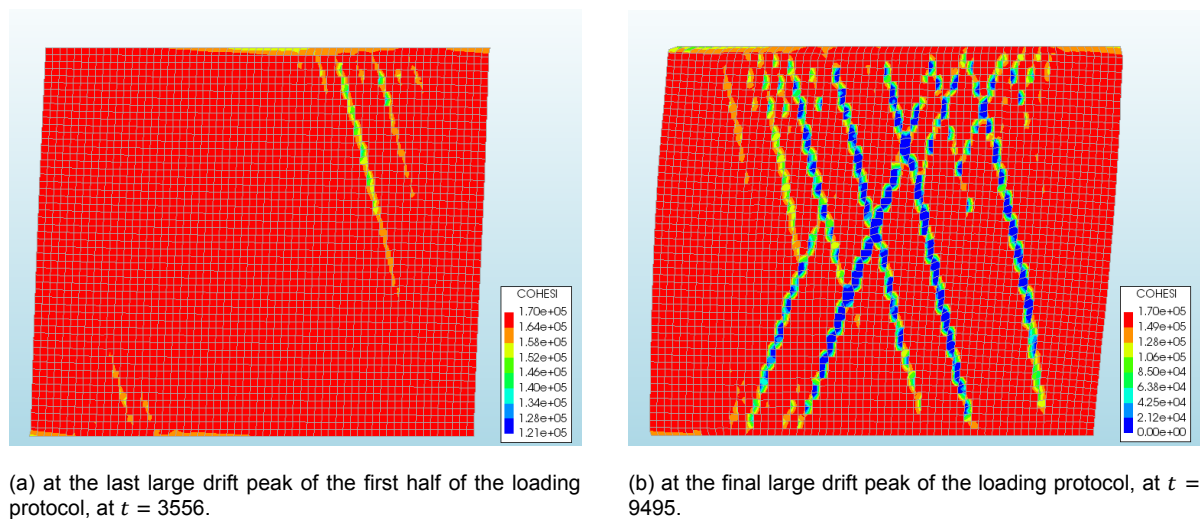
Figure 9.8: Cohesion plots of the finite element analysis with the Engineering Masonry Model's *Diagonal stair-case cracks* option. The red parts still behave linearly, the blue parts are post-softening. The deformation is magnified by a factor 100.

Another useful aspect is the crack width, that relates to the current deformed state of the model and can be straightforwardly compared with experimental results. Figure 9.9 presents crack width plots of the analysis with the Equivalent Shear Masonry Model. This crack width is the horizontal crack opening due to both shear and horizontal extension. Figure 9.10 presents crack width plots of the analysis with the Engineering Masonry Model with the head joint option *Diagonal stair-case cracks*. These crack widths are the deformations normal to and parallel to the prescribed crack direction α or $-\alpha$[2].

---

[2]Note that these crack widths are not related to the actual occurring crack direction.
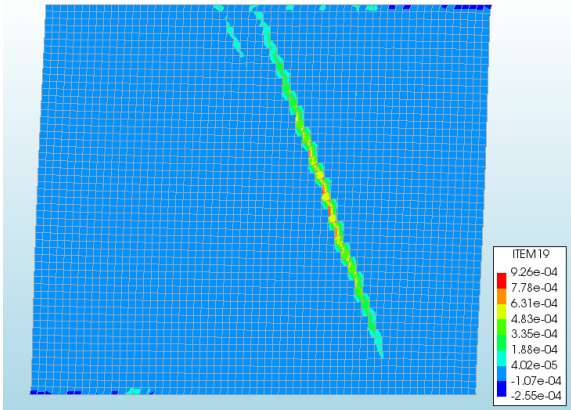
(a) at the last large drift peak of the first half of the loading protocol, at $t = 3556$.
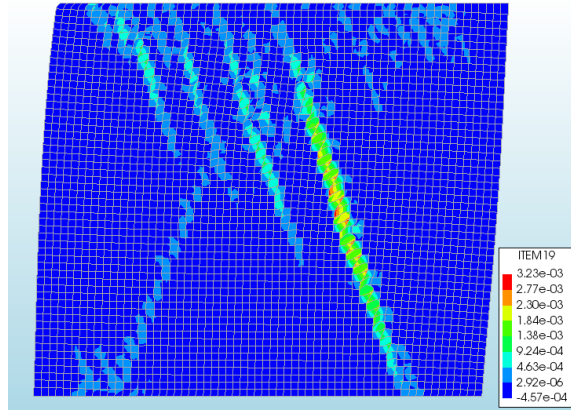
(b) at the final large drift peak of the loading protocol, at $t = 9495$.

Figure 9.9: Crack width (USRSTA(19)) plots of the finite element analysis with the Equivalent Shear Masonry Model. The crack widths presented are the horizontal crack opening due to shear and horizontal extension, as defined by Equation 6.4. The deformation is magnified by a factor 100.
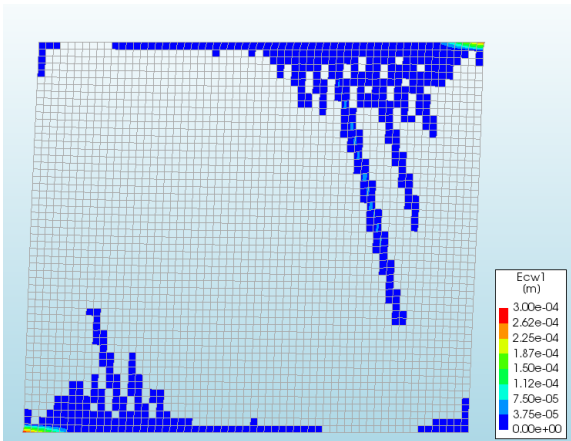
(a) at the last large drift peak of the first half of the loading protocol, at $t = 3556$.
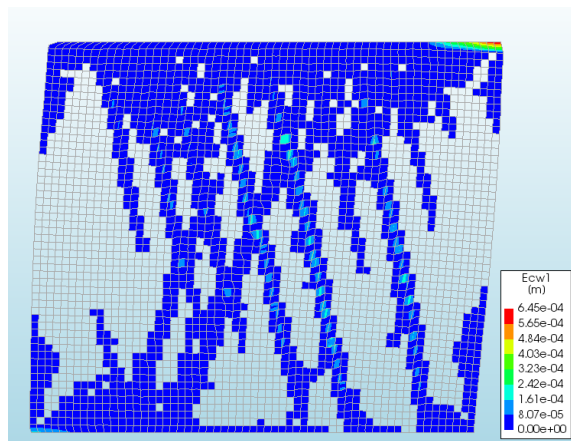
(b) at the final large drift peak of the loading protocol, at $t = 9495$.
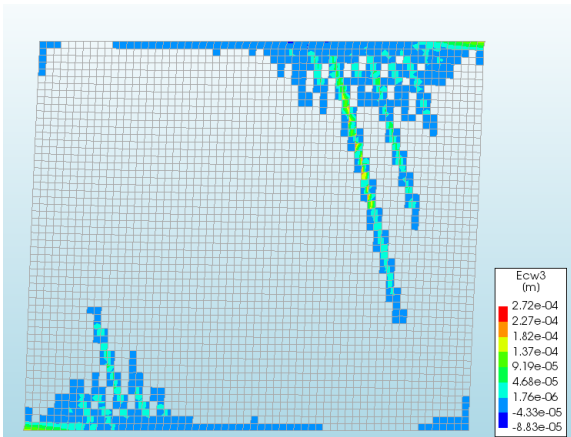
(c) at the last large drift peak of the first half of the loading protocol, at $t = 3556$.
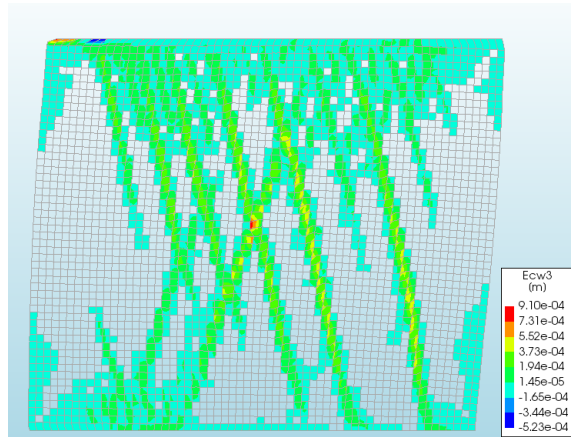
(d) at the final large drift peak of the loading protocol, at $t = 9495$.

Figure 9.10: Crack width plots of the finite element analysis with the Engineering Masonry Model's *Diagonal stair-case cracks* option. Presented are the crack widths normal (Ecw1) and parallel (Ecw3) to the prescribed diagonal crack direction α or $-\alpha$. The deformation is magnified by a factor 100.

When a good crack width output unavailable, the principle strain also gives a good indication of the current deformed shape. Because the reduction of the cohesion and the definition of the crack widths are different for the Equivalent Shear Masonry Model and the Engineering Masonry Model, Figures 9.11 and 9.12 give the principle strain plots for a fair comparison between the two.
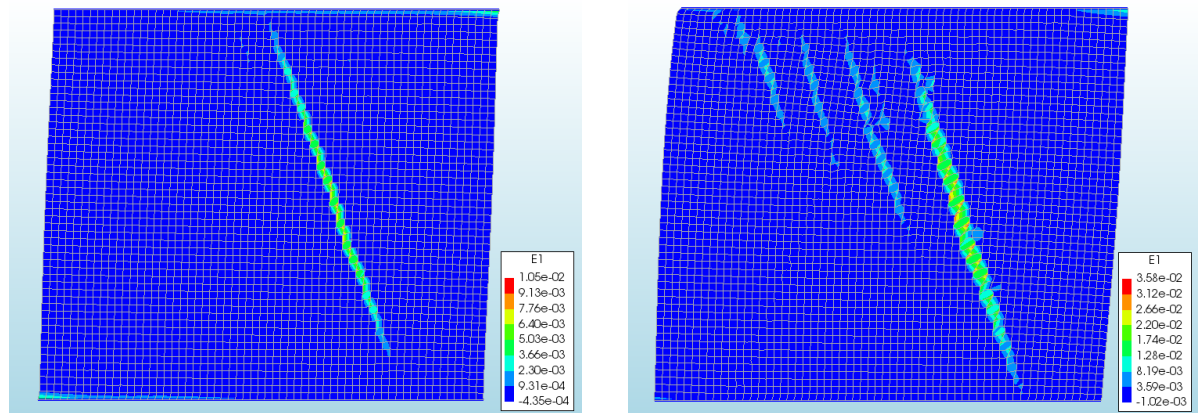
(a) at the last large drift peak of the first half of the loading protocol, at $t = 3556$.

(b) at the final large drift peak of the loading protocol, at $t = 9495$.

Figure 9.11: The principle strain plots of the finite element analysis with the Equivalent Shear Masonry Model. The deformation is magnified by a factor 100.
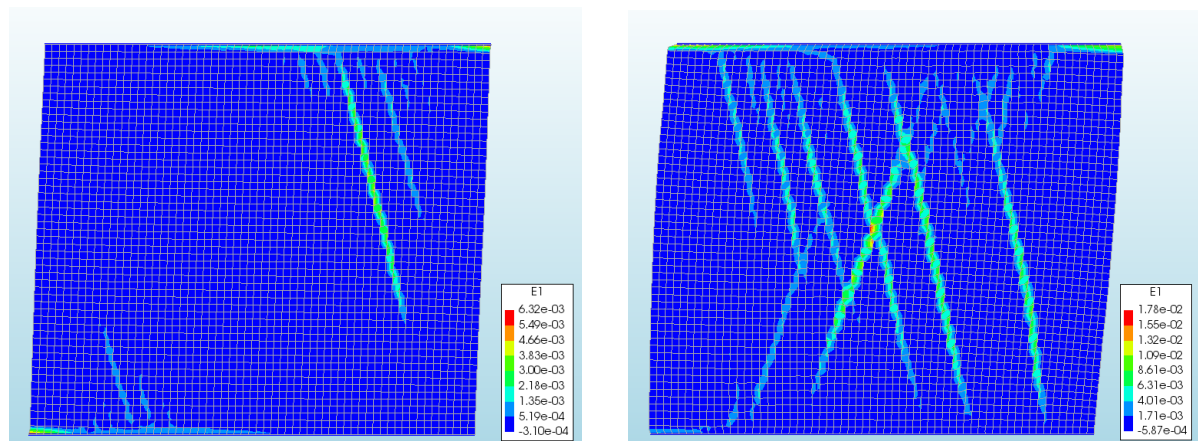
(a) at the last large drift peak of the first half of the loading protocol, at $t = 3556$.

(b) at the final large drift peak of the loading protocol, at $t = 9495$.

Figure 9.12: The principle strain plots of the finite element analysis with the Engineering Masonry Model's *Diagonal stair-case cracks* option. The deformation is magnified by a factor 100.

Additional Finite Element Results from Literature

For comparison, Figure 9.13(a) and (b) show the results of the macro models with the Equivalent Shear Masonry Model and with the Engineering Masonry Model with *Diagonal stair-case cracks* option for Figures 9.4 and 9.5 again, now compared with the experimental results. Figure 9.13(c) and (d) show the results of the micro model and of the macro model with the Engineering Masonry Model with *Tensile strength head-joint defined by friction* option, both from [9, Chapter 4]. Note that in the micro model, each cycle consisted of only one repetition rather than the three repetitions drawn in Figure 9.2.

The micro model's force-drift diagram (in Figure 9.13(c)) shows initial linear behaviour. The overall stiffness then reduces over the consecutive cycles and the force-drift lines are slightly curved with a decreasing steepness. The unloading is almost linear. The diagram is generally smooth. Permanent inelastic deformation is found, up to a drift of approximately 2‰. The peak forces increase over the
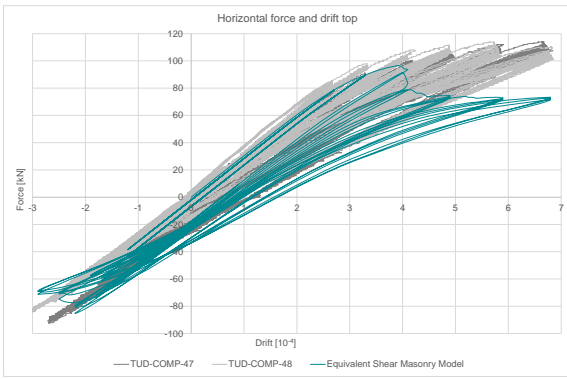
(a) of analysis of a macro model with the Equivalent Shear Masonry Model.
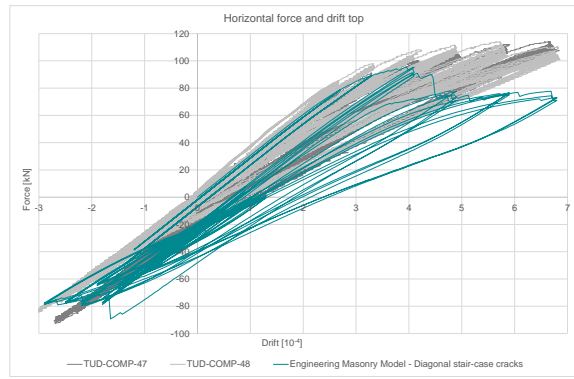
(b) of analysis of a macro model with the Engineering Masonry Model with *Diagonal stair-case cracks* option.
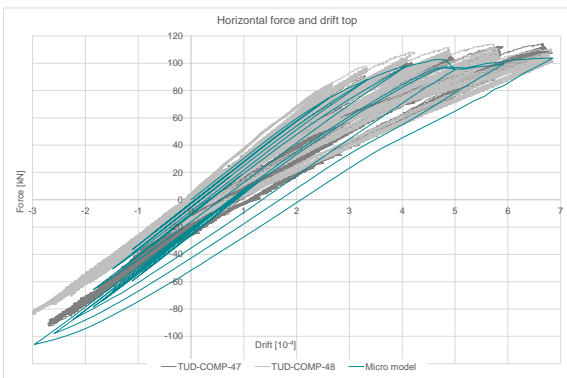
(c) of analysis of a micro model with linear elastic bricks and Engineering Masonry Model with *Direct input head-joint tensile strength* joints.
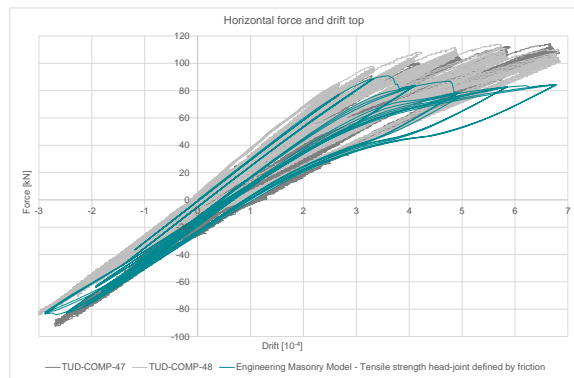
(d) of analysis of a macro model with the Engineering Masonry Model with *Tensile strength head-joint defined by friction* option.

Figure 9.13: Force-drift diagram of four finite element analyses of the shear walls TUD-COMP-47 and TUD-COMP-48, compared with the experimental results. Experimental data and analysis data of (c) and (d) courtesy of [9].

repetitions within each cycle. The peak force is 104 kN, which is reached in last cycle. The hysteresis loop has a constant width over its entire height.

The Engineering Masonry Model with *Tensile strength head-joint defined by friction* option's force-drift diagram (in Figure 9.13(d)) also shows initial linear behaviour, followed by slight softening and then a residual plateau on the right side. The behaviour to the left is almost linear. The diagram is generally smooth. Permanent inelastic deformation is found, up to a drift of approximately 1‰. The peak forces increase over the repetitions within each cycle. The peak force is 91.0 kN, which is reached in cycle 3. The hysteresis loop is small in the middle and to the left, but wide near the positive peak drift values.

Figure 9.14 presents cohesion plots of the micro model analysis. The red points in these plots have reached their peak shear stress. The cracked zone is at an angle of approximately -63° with the bed joints.

Figure 9.15 presents cohesion plots of the analysis with the Engineering Masonry Model's *Tensile strength head-joint defined by friction* option. The grey and black points in these plots have reached their peak shear stress. The cracks observed are at an angle of approximately ±71° with the horizontal x-axis.

(a) at the last large drift peak of the first half of the loading protocol.

(b) at the final large drift peak of the loading protocol.
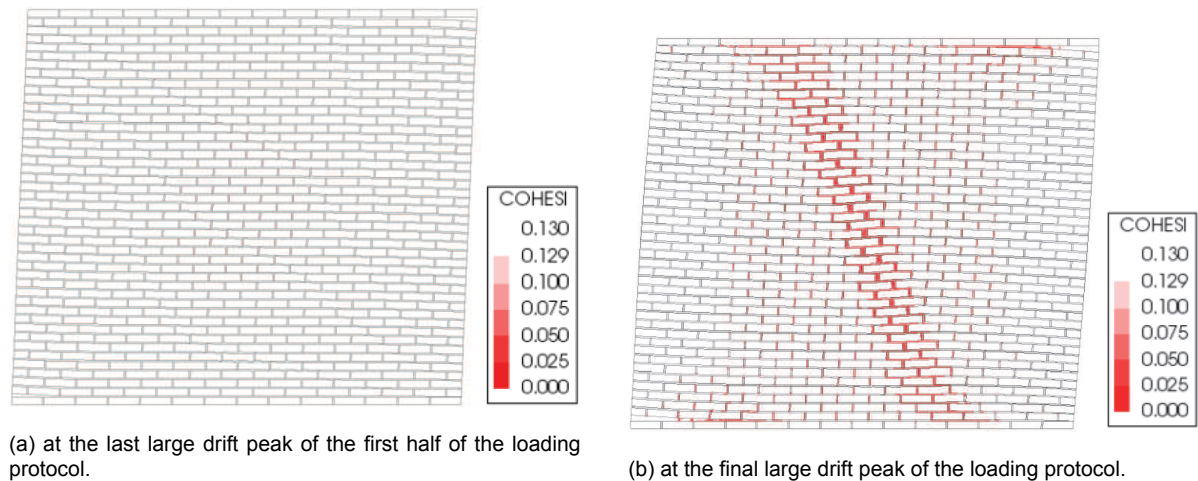
Figure 9.14: Cohesion plots of the micro model analysis. The white parts still behave linearly, the red parts are post-softening. The deformation is magnified by a factor 100. Images courtesy of [9].

(a) at the last large drift peak of the first half of the loading protocol, at $t = 3556$.

(b) at the final large drift peak of the loading protocol, at $t = 9495$.
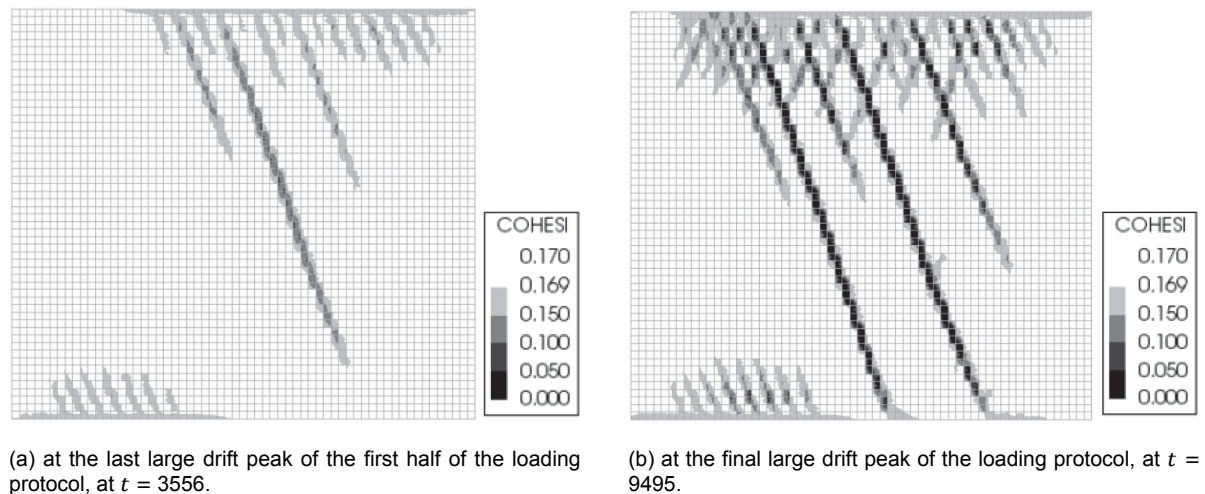
Figure 9.15: Cohesion plots of the finite element analysis with the Engineering Masonry Model's *Tensile strength head-joint defined by friction* option. The white parts still behave linearly, the black parts are post-softening. Images courtesy of [9].

9.6. Discussion

The results of the shear wall experiments and analyses presented in the previous Section are discussed and compared here.

Discussion of the Results Obtained with the Equivalent Shear Masonry Model
The force-drift diagram obtained with the Equivalent Shear Masonry Model (Figure 9.4) shows almost linear behaviour during the first two cycles. The second cycle shows plastic deformation on the positive side of the graph. The wall reaches its peak strength of 96.5 kN and then commences to soften. Over the fourth, fifth and sixth cycle, almost horizontal yielding is observed. During the fifth and sixth loop, the wall commences to soften on the negative side, too. The hysteresis loop has a slight S-shape and a similar width over its entire height. The peak forces are slightly reduced with each repetition in each cycle by a few percent, but are subsequently exceeded in the next cycle.

The crack width output `USRSTA(19)` gives some unwanted negative values, see Figure 9.9. Therefore, the principle strain is plotted for an alternative impression of the deformation, Figure 9.11. The crack pattern starts with two horizontal cracks at the top right and the bottom left. Then one large diagonal crack appears, later accompanied by some smaller diagonal cracks. The diagonal cracks are at an angle of approximately $\pm 68°$ with the horizontal x-axis.

Additionally, the cohesion plots in Figure 9.7 show that diagonal cracks have formed from the loading

in the other direction, too. The cohesion plots also show that the locations where the material has failed are more numerous than the locations where cracks actually open up.

Comparison with the Experimental Results

When the force-drift data obtained with the Equivalent Shear Masonry Model are compared with the experimental results, it is seen that the predicted peak force is too low. Therefore, the finite element model starts to soften and follow the residual plateau, where the real wall did not. Note that the model used the same material properties as in [9, Chapter 4] and the model was not calibrated to the experimental results. Increasing the shear strength parameters could improve this aspect. Compared to the TUD-COMP-48 results, the softening seems to be to steep. Increasing the shear fracture energy could improve this aspect.

The cracks found in the analysis are a little steeper than in reality. This could partially be due to mesh directional bias, the tendency of localisations to follow the mesh edges. Nonetheless, the localisation of the cracks is satisfactory. The peak force reduction over the repetitions of each cycle is of the same magnitude as observed in the experimental data. Furthermore, the softening, the residual plateau and the shape of the hysteresis loop do resemble test results of other shear walls that were loaded further, to more severe damage, for instance the LOWSTA, CS03, PMW2 and TUD-COMP-Q6 tests shown in [16]. Thus the model's ability to represent this kind of post-peak behaviour is regarded a positive characteristic.

Comparison with the Engineering Masonry Model's *Diagonal stair-case cracks* option

Compared to the Engineering Masonry Model with the *Diagonal stair-case cracks* option, the Equivalent Shear Masonry Model shows similar peak strength and softening characteristics. The shape of the hysteresis loop and the amount of inelastic deformation are slightly better. Moreover, the peak force reduction is more realistic.

The force-drift diagram of the Equivalent Shear Masonry Model is smoother. Also, the model has less convergence issues, less unconverged steps and significantly shorter series of consecutive unconverged steps. It does, however, need more iterations per step.

According to the principle strain plots in Figures 9.11 and 9.12, the cracks of both models are too steep, but the direction of the cracks of the Equivalent Shear Masonry Model is slightly better. Besides, its crack localisation is significantly better, featuring one major diagonal crack in the middle of the wall instead of numerous diagonal cracks

Comparison with the Two Other Finite Element Models from Literature

Compared to the macro model with the Engineering Masonry Model with the *Tensile strength head-joint defined by friction* option, the Equivalent Shear Masonry Model shows a lower strength and thus more softening and yielding. It shows more plastic deformation and a wider hysteresis loop. The peak force reduction is more in line with the experiments than with the Engineering Masonry Model. The cracks of both models are too steep, but the direction of the cracks of the Equivalent Shear Masonry Model is slightly better. Besides, its crack localisation is significantly better.

Compared to the micro model, the Equivalent Shear Masonry Model also shows a lower strength and thus more softening and yielding. The inelastic deformation is less and the hysteresis loop is narrower. The peak force reduction cannot be compared, because the micro model was only loaded with one repetition for each load cycle. The cracks of both models are too steep, but the direction of the cracks of the micro model is slightly better. The localization of the cracks of the micro model is most similar to the experimental results.

IV

Conclusions and Recommendations

10
Conclusions

The Equivalent Shear Masonry Model is an improvement of the Engineering Masonry Model that seems to model diagonal stair-case cracks better than that model's *Diagonal stair-case cracks* option.

Like the Engineering Masonry Model, the Equivalent Shear Masonry Model is an orthotropic material model for masonry that uses a smeared cracking approach. It adopts that model's constitutive relations for the behaviour normal to the bed joints and for the compressive behaviour normal to the head joints. However, the shear failure criterion and the tensile head joint failure options are replaced by a new failure criterion for diagonal staircase cracks.

This failure criterion, the equivalent shear failure criterion, evaluates both the shear stress and the tensile stress normal to the head joints. The combined constitutive relation is based on the Coulomb friction shear behaviour of the bed joints, thus hysteresis occurs in case of cyclic equivalent shear loading. Both the tensile strain and the shear strain directly contribute to the softening of the material.

The theoretical advantages of the Equivalent Shear Masonry Model over the Engineering Masonry Model's *Diagonal stair-case cracks* option are that the formulation is simpler and more true to the actual failure mechanism. A constitutive relation is defined for the diagonal cracking, opposed to just a maximum stress. This constitutive relation provides for hysteresis, inelastic deformation and softening due to the deformations of the diagonal crack.

The improved material model has been implemented as a Fortran subroutine to be used as a user supplied material model in Diana's finite element analysis software. This implementation has been verified for a single integration point for several load paths. These load paths consisted of loading, unloading and reloading; in vertical tension and compression, horizontal tension, shear and three combinations of shear and horizontal tension; all but the vertical ones while under a constant vertical pre-compression. For these cases, the code properly produced the intended material behaviour. Furthermore, for this single integration point model, the stress-strain relations of the Equivalent Shear Masonry Model were more consistent than those of the Engineering Masonry Model's *Diagonal stair-case cracks* option, which suffered sudden drops.

Next, a validation was made against a micro modelled unit cell for the same (combined) shear and horizontal extension load cases as before. This showed that the material model represents the masonry behaviour quite well, though some improvements are recommended. The connection between the horizontal tensile unloading and the compressive loading could be modelled more realistically and the division of the equivalent shear stress into the horizontal tensile stress and the shear stress should be investigated further.

Subsequently, the model was validated at structural level, against a laboratory experiment of shear wall under cyclic horizontal light damage loading. A macro model using the Equivalent Shear Masonry Model was analysed to approximate the experimental results. This showed promising characteristics. Though the diagonal cracks were still slightly too steep, their localisation was satisfactory. The force-drift diagram showed linear behaviour in the first cycles, then continued non-linear with some inelastic deformation, and then showed softening and a residual plateau in later cycles. The hysteresis loop had

a slight S-shape and a similar width over its entire height. The peak force was slightly reduced with each repetition in each cycle.

Compared to the Engineering Masonry Model's *Diagonal stair-case cracks* option, the model gave smoother results and had less convergence issues. However, it did need more iterations per step. Therefore it is recommended to adjust the 'tangent' shear stiffness returned by the code. The crack direction of the Equivalent Shear Masonry Model is slightly better and its crack localisation is much more realistic. Both models did not reach the experimental peak strength and showed a too steep softening regime, though calibration might be able to improve this. The peak force reduction of the Equivalent Shear Masonry Model was not matched by either the Engineering Masonry Model's *Diagonal stair-case cracks* option or its *Tensile strength head-joint defined by friction* option.

In the context of this thesis, only a limited amount validations could be done. The validity of these conclusions is therefore also limited to these specific load cases and applications. Further verification for other load cases is recommended, for instance the shear behaviour under a varying or even tensile overload. Also, further validation against different experiments is recommended, for instance slender shear walls that show rocking, window banks that suffer tensile bending failure and wide shear walls that are loaded much further than light damage.

In conclusion, the Equivalent Shear Masonry Model shows promising characteristics to model diagonal staircase cracking in masonry. It produces smooth force-displacement diagrams and has less convergence problems than the Engineering Masonry Model's *Diagonal stair-case cracks* option. It generates cracks that are less steep and more localized. The model is able to represent post-peak behaviour of shear walls and even displays peak force reduction. Therefore, it is recommended that the material model is developed further, so that hopefully one day it can be used in practice to provide more accurate masonry cracking predictions.

11

Recommendations

The following recommendations are made for the further development of the Equivalent Shear Masonry Model. It is recommended that the theory is eventually expanded for shell elements or even for three-dimensional solid elements. But first, the following improvements are proposed to the theory and its implementation, and the following further validation is proposed.

11.1. Recommended Improvements of the Theory

It is recommended that the two point of interest from Section 5.4 are further investigated. The connection from the horizontal tensile unloading to the compression behaviour could be modelled more realistically. A sophisticated description of this connection should be sought for.

Also, the ratio between the shear stress and the horizontal tensile stress during softening and yielding did not always remain the same, like assumed in Section 5.4. It seemed from the unit cell results that this ratio is related to the ratio between the respective strain increments and the height-width ratio of the expected diagonal crack. Study of more combinations of strain increments is needed to properly define this relation.

11.2. Recommended Improvements of the Code

As Figure 9.9 showed, the crack width output included in the Equivalent Shear Masonry Model subroutine gave undesired negative values. Some of the failure mechanism indicators in the `USRVAL`-array that were adopted directly from the `usrmat_quad2.f`-code also gave unexpected results. These minor issues should both be fixed.

Furthermore, it is recommended that the shear stiffness returned by the Equivalent Shear Masonry Model subroutine is adapted. As was described in Section 6.6, the shear stiffness returned by the material model is always the linear stiffness. The main advantage of this is that it always works, because be it loading, softening, yielding or unloading, this is always equal to or larger than the actual stiffness. During softening and yielding, however, the linear stiffness is quite far from the actual stiffness, so the model might need many iterations, what was reflected by the shear wall results in Section 9.5. Therefore, this choice of stiffness makes the model robust, but slow. Perhaps a more sophisticated choice is possible.

Though the real current tangent stiffness is not an option – because that is zero or negative during those phases–, a much smaller positive stiffness could be used, for instance 0.01 times the linear shear stiffness. This could, however, raise problems if the integration point wants to start to unload, because then the estimated stiffness is lower than the actual stiffness, which – as explained in Section 2.1.2 – gives convergence issues. To mitigate this, the linear stiffness could be used for the first and every tenth iteration of each step, in order to overcome the bifurcation point.

11.3. Recommended Further Validation

Last but not least, many further validations are required. This thesis only assessed the validity of the Equivalent Shear Masonry Model for a very limited amount of load cases and applications.

More load paths should be studied with a single element model, like simultaneous shear and horizontal tensile unloading, horizontal tensile and/or shear loading under a varying (also tensile) overload. These should then also be validated against the masonry unit cell model.

Post-diction calibration is proposed in order to improve the accuracy of the results of the shear wall model from Chapter 9. The material model should also be applied to different types of laboratory test, for instance slender shear walls that show rocking, window banks that suffer tensile bending failure and wide shear walls that are loaded much further than light damage.

Appendices

A
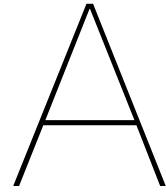
Overview of Symbols Used in Literature on the Engineering Masonry Model

This appendix gives an overview of the different names and symbols that are used in this thesis and in literature to describe the Engineering Masonry Model. It compares:

- the symbols used in this thesis,

- the symbols used in the *SAHC* conference paper *Computational modelling of masonry with a view to Groningen induced seismicity*,[14]

- the symbols used in the *DIANA Validation report for Masonry modelling*,[16]

- the symbols used in section 38.12 *Engineering Masonry Model* of the *Theory Manual* in the *DIANA User's Manual*,[6, Section 38.12]

- the arguments used in section 6.5 *Engineering Masonry Model* of the *Material Library* in the *DIANA User's Manual*,[5, Section 6.5]

- the arguments used in the Engineering Masonry Model subroutine `engmas.f`,[15] and

- the descriptions given in the graphical user interface *Diana Interactive Environment* of the *Diana* software.[4]

Table A.1: General symbols

This thesis	SAHC paper	Validation report	Theory Manual	Material Library	Code `engmas.f`	Diana Interactive Environment
E, E_x, E_y	E_i, E_x, E_y	E, E_x, E_y	E, E_x, E_y	`YOUNG`, ex, ey	`YNG`	Young's modulus, E x*, E y*
G_{xy}	G	G	G, G_{xy}	`SHRMOD`, gxy	`SHRM0`	Shear modulus, G xy*
h	h	h	h	`CRACKB`, h	`HCRCEM`	Crack band width
				`FAIFAC`, fac	`FAILIN`	Linearize material at failure
ρ			ρ			Mass density
σ	σ_i	σ	σ		`SIGMA`	
σ_0	σ_{0i}	σ_0	σ_0		`SIG0`	
ε	ε_i	ε	ε		`EPS`	
ε_0	ε_{0i}	ε_0	ε_0		`EPS0`	
$\Delta\varepsilon$	$\Delta\varepsilon_i$	$\Delta\varepsilon$	$\Delta\varepsilon$		`DEPS`	
τ	τ_{xy}	τ	τ		`SIGSHR`	
τ_0	τ_0	τ_0	τ_0		`SI0SHR`	
γ, γ_{xy}	γ_{xy}	γ	γ		`EPSSHR`	
$\Delta\gamma$	$\Delta\gamma_{xy}$	$\Delta\gamma$	$\Delta\gamma$		`DEPSHR`	

Table A.2: Symbols used to describe the tensile behaviour

This thesis	SAHC paper	Validation report	Theory Manual	Material Library	Code `engmas.f`	Diana Interactive Environment
f_t	f_{ti}, f_{t1}, f_{t2}	f_t, ft_x, ft_y	f_t	`TENSTR`, fty, ftx	`TSTR`	Tensile strength
$\sigma_{t,ref}$	σ_{ti}	$\sigma_{rf}, \sigma_{rf,tensile}$	σ_{rf}		`SIGRF(1)`	
$\alpha_{t,ref}$	ε_{ti}	$\alpha_{tensile}, \alpha_{tension}$	$\alpha_{tensile}$		`ALPHA(1)`	
$\varepsilon_{t,u}$	ε_{uti}	ε_{ult}	ε_{ult}		`EPSULT`	
G_{ft}	G_{fti}	G_{ft}, Gft	G_{ft}	`GFI`, $gf1$	`GFT`	Fracture energy in tension*
			$f_{t,unl}$	`RESTST`, $sigres$	`RESTST`	Residual tensile strength[a]
			$f_{tx,\min}$			Minimum tensile strength head-joint*[b]

[a] The residual tensile strength is asked for when the head joint failure option *Diagonal stair-case cracks* is chosen.
[b] The minimal tensile strength is asked for when the head joint failure option *Tensile strength head-joint defined by friction* is chosen. What is meant is actually the minimal masonry tensile strength in the direction normal to the head joints.

Table A.3: Symbols used to describe the compressive behaviour

This thesis	SAHC paper	Validation report	Theory Manual	Material Library	Code `engmas.f`	Diana Interactive Environment
f_c	f_{ci}	$f_c, -f_c, fc$	$f_c, -f_c$	COMSTR, fc	FC	Compressive strength*
$\sigma_{c,ref}$	σ_{ci}	$\sigma_{rf}, \sigma_{rf,compressive}$	σ_{rf}		SIGRF(2)	
$\alpha_{c,ref}$	ε_{ci}	α_{comp}	α_{comp}		ALPHA(2)	
$\varepsilon_{c,u}$	ε_{uci}	ε_{ult}	ε_{ult}		EPSULC	
ε_p	ε_{pi}	ε_{peak}	ε_{peak}		EPSCP	
G_{fc}	G_{fci}	G_c, Gfc	G_c	GC, gc	GFC	Fracture energy in compression*
ε^*					ESTAR	
n	n_i	n	n	EPSCFA, n	EPSCFA	Factor to strain at compressive strength*
λ	$\lambda, (1-\lambda)^c$	$\lambda, (1-\lambda)^c$	$\lambda, (1-\lambda)^c$	UNLFAC, $lambda$	UNLFAC	Unloading factor, 1=secant, 0=linear*

[c] In these three sources, the formulas and the visuals attribute dissimilar meanings to λ.

Table A.4: Symbols used to describe the shear behaviour

This thesis	SAHC paper	Validation report	Theory Manual	Material Library	Code `engmas.f`	Diana Interactive Environment
τ_{max}	τ_{max}	τ_{max}	τ_{max}		TAUMAX	
c	c	c, C	c	COHESI, ch	COH0	Cohesion*
φ	φ	φ, ϕ, Φ	ϕ	PHI, phi	PHIANG	Friction angle*
σ_{yy}	σ_{yy}	σ_{yy}	σ_{yy}		SIGMA(2)	
γ_u	γ_{ult} [d]	γ_{ult}	γ_{ult}		SHRULT	
γ_p						
G_{fs}	G_{fs}	G_{fs}, Gfs	G_{fs}	GFS, gfs	GFS	Fracture energy in shear
γ_{cum}	γ_{cum}	γ_{cum}	γ_{cum}		CUMSHR	
					OOPSHR	Out of plane shear failure

[d] In this source γ_{ult} is defined as the total shear strain at the end of the softening regime, so $\gamma_{ult} = \gamma_p + \gamma_u$.

Table A.5: Symbols used to describe the diagonal behaviour

This thesis	SAHC paper	Validation report	Theory Manual	Material Library	Code engmas.f	Diana Interactive Environment
$f_{t\alpha}$	$f_{t\alpha}$	$f_{t\alpha}$	$f_{t\alpha}$		FTALPH	
f_{tx}	f_{t1}, f_{tx}	f_{tx}	f_{tx}		FT(1)	Head-joint tensile strength*
f_{ty}	f_{t2}, f_{ty}	f_{ty}	f_{ty}		FT(2)	Bed-joint tensile strength*
α	α	$\theta, \Theta, (\alpha)$[e]	α	DIAANG, $alpha$	DIAANG	Angle between stepped diagonal crack and bed-joint*
β	β[f]					

[e] The angle α is not defined as such in this source, but it is used in the formula for $f_{t\alpha}$.
[f] In this source β is defined as either β_1 or β_2, with the formula $\beta = \frac{\pi}{2} \pm \alpha$.

B

Fortran Code of User Supplied Subroutine `usrmat_eqshma.f`

Listing B.1: The user supplied subroutine written for the Equivalent Shear Masonry Model `usrmat_eqshma.f`

```fortran
1 CDEC$ ATTRIBUTES DLLEXPORT::USRMAT
2      SUBROUTINE USRMAT( EPS0, DEPS, NS, AGE0, DTIME, TEMP0, DTEMP,
3    $                    ELEMEN, INTPT, COORD, SE, ITER, USRMOD, USRVAL
        ,
4    $                    NUV, USRSTA, NUS, USRIND, NUI, SIGMA, STIFF )
5 C..................................................................
6 C$DDOC
7 C$DDOC    User-supplied subroutine for general nonlinear behaviour.
8 C$DDOC    Return updated stress and tangential stiffness matrix.
9 C$DDOC
10 C$DDOC ARGUMENTS:
11 C$DDOC    EPS0   D() In    - Strain vector at start of increment.
12 C$DDOC    DEPS   D() In    - Total strain increment.
13 C$DDOC    NS     I   In    - Number of stress components
14 C$DDOC    AGE0   D   In    - Age of element.
15 C$DDOC    DTIME  D   In    - Total time increment.
16 C$DDOC    TEMP0  D   In    - Temperature.
17 C$DDOC    DTEMP  D   In    - Total temperature increment.
18 C$DDOC    ELEMEN I   In    - Current element number.
19 C$DDOC    INTPT  I   In    - Current integration point number.
20 C$DDOC    COORD  D() In    - Coordinates of integration point.
21 C$DDOC    SE     D() In    - Elastcity matrix.
22 C$DDOC    ITER   I   In    - Current iteration number.
23 C$DDOC    USRMOD C   In    - User model name.
24 C$DDOC    USRVAL D() In    - User parameters.
25 C$DDOC    NUV    I   In    - Number of user parameters.
26 C$DDOC    USRSTA D() InOut - User state variables at start of increment
      .
27 C$DDOC                       Should be updated at output.
28 C$DDOC    NUS    I   In    - Number of user state variables.
29 C$DDOC    USRIND I() InOut - User indicators at start of increment.
30 C$DDOC                       Should be updated at output.
31 C$DDOC    NUI    I   In    - Number of user state indicators.
32 C$DDOC    SIGMA  D() InOut - Total stress at start of increment.
33 C$DDOC                       Current stress at output.
34 C$DDOC    STIFF  D() InOut - Previous tangent stiffness.
```

```
35 C$DDOC                        Current tangent stiffness at output.
36 C
     ...........................................................................
37 C...   LIST OF SYMBOLS
38        INTEGER           MSTR,   MOPCRK,   MCR
39        PARAMETER       ( MSTR=6, MOPCRK=4, MCR=3 )
40        DOUBLE PRECISION STFFAC,         SHRFAC,        SHRF
41        PARAMETER       ( STFFAC=0.0001D0, SHRFAC=0.01D0, SHRF=1.2D0 )
42 C
43        DOUBLE PRECISION DPMPAR
44        LOGICAL           XSGTC
45 C
46        INTEGER           NS, ELEMEN, INTPT, ITER, NUV, NUS, NUI,
47       $                  USRIND(NUI)
48        DOUBLE PRECISION EPS0(NS), DEPS(NS),
49       $                  COORD(3), USRVAL(NUV), USRSTA(NUS),
50       $                  SIGMA(NS), STIFF(NS,NS), SE(NS,NS)
51        CHARACTER*6       USRMOD
52 C
53        INTEGER           I, NCRACK, NOPCRK, NUMCR(3), CRACKS(2), IDIR(2),
54       $                  ISCRK(6), ICRACK, NCR, FRCFAI, SHRCRK, FAIMEC
55        DOUBLE PRECISION YOUN(3), SIG0(MSTR), GFT(2), GFC(2), HCRAC,
56       $                  FT(2), FC(2), EPS(MSTR), ALPHA(2), UNLFAC,
57       $                  TANPHI,  EPSULT(2), EPSULC, SIGRF(2), COH0,
58       $                  ELAXES(3,3), EPSCR(MCR*MOPCRK), GFS,
59       $                  SIGCR(MCR*MOPCRK), SHRMOD, TAUMAX, YOUN0(2),
60       $                  CRAXES(MCR*MCR), SHRULT,
61       $                  COH1, EPSP(MSTR), SHRMAX, SIGSHR, EPSSHR,
62       $                  DEPSHR, SI0SHR, SHRM0,
63       $                  EPSCP(2), EPSCFA(2), ESTAR,
64       $                  N, TAUEQ, SHRMEQ, EPSHEQ, DEPSEQ, RATIO
65 C
66        CHARACTER*6       STRTYP
67        LOGICAL           MEMBRA, SHELL, CRACKD, CRCKED, CRSHED, CRUSHD
68
69 C
70 C...   RETRIEVING DATA FROM USER VALUES
71        YOUN(1) = USRVAL(1)
72        YOUN(2) = USRVAL(2)
73        CALL RMOVE( YOUN, YOUN0, 2 )
74        SHRM0   = USRVAL(3)
75        SHRMOD  = SHRM0
76        TANPHI  = USRVAL(4)
77        FT(1)   = USRVAL(5)
78        FT(2)   = USRVAL(6)
79        GFT(1)  = USRVAL(7)
80        GFT(2)  = USRVAL(8)
81        FC(1)   = USRVAL(9)
82        FC(2)   = USRVAL(10)
83        GFC(1)  = USRVAL(11)
84        GFC(2)  = USRVAL(12)
85        UNLFAC  = USRVAL(13)
86        COH0    = USRVAL(14)
87        GFS     = USRVAL(15)
88        ANGLE0  = USRVAL(16)
```

```
 89        EPSCFA(1) = USRVAL(17)
 90        EPSCFA(2) = USRVAL(18)
 91        HCRAC   = USRVAL(19)
 92 C
 93 C... UPDATING STRAIN AND STRESS
 94        CALL UVPW( EPS0, DEPS, NS, EPS )
 95        CALL RMOVE( SIGMA, SIG0, NS )
 96           NCR = 2
 97           CALL GTC( '../ELAXES', ELAXES, 9 )
 98           CALL RMOVE( ELAXES(1,1), CRAXES(1), NCR )
 99           CALL RMOVE( ELAXES(1,2), CRAXES(NCR+1), NCR )
100           SI0SHR = SIG0(3)
101           EPSSHR = EPS(3)
102           DEPSHR = DEPS(3)
103        SIGMA(1) = SIG0(1) + YOUN0(1)*DEPS(1)
104        SIGMA(2) = SIG0(2) + YOUN0(2)*DEPS(2)
105        SIGSHR = SI0SHR + SHRM0*DEPSHR
106 C
107 C... AT THE BEGINNING OF THE STEP THE PARAMETER FAIMEC (RELATED TO THE
        FAILURE MECHANISM) IS SET TO ZERO
108        FAIMEC = 0
109 C... INITIALIZE CRACK INDICATORS, COUNTERS, OUTPUT
110        FRCFAI = USRIND(5)
111        CRCKED = .FALSE.
112        CRSHED = .FALSE.
113        NCRACK = 0
114        NOPCRK = 0
115        CALL ISET( 0, NUMCR, 3 )
116        CALL RSET( 0.D0, EPSCR, NCR*MOPCRK )
117        CALL RSET( 0.D0, SIGCR, NCR*MOPCRK )
118        CALL ISET( 0, ISCRK, 6 )
119 C
120 C... THE TENSILE AND COMPRESSIVE BEHAVIOUR OF THE ELEMENT IS EVALUATED
121        DO 100, I = 1, 2
122           ALPHA(1) = USRSTA(I)
123           ALPHA(2) = USRSTA(I+2)
124           SIGRF(1) = USRSTA(I+4)
125           SIGRF(2) = USRSTA(I+6)
126           CRACKD   = USRIND(I)   .EQ. 1
127           CRUSHD   = USRIND(I+2) .EQ. 1
128          IF ( EPS(I) .GT. 0.D0 .AND. I .EQ. 2) THEN
129 C...         ELEMENT IN VERTICAL TENSION
130             IF ( EPS(I) .GT. FT(I)/YOUN0(I) ) THEN
131 C...           IF THE STRAIN IS LARGER THAN THE ELASTIC LIMIT IN
      TENSION THE PARAMETER FAIMEC IS INCREASED OF 1 OR 2 (ACCORDING TO
      THE DIRECTION)
132                FAIMEC = FAIMEC + I
133             END IF
134             EPSULT(I) = 2.D0*GFT(I)/HCRAC/FT(I)
135             EPSULT(I) = MAX( EPSULT(I) , FT(I)/YOUN0(I) )
136             IF ( EPS(I) .GT. ALPHA(1) ) THEN
137 C...           NEW TENSILE EXTREME
138                ALPHA(1) = EPS(I)
139                IF ( EPS(I) .GT. EPSULT(I) ) THEN
140                   SIGMA(I) = EPS(I)*STFFAC
141                   CRACKD = .TRUE.
```

```fortran
142                 ELSE IF ( EPS(I) .GT. FT(I)/YOUN0(I) ) THEN
143                     SIGMA(I) = FT(I)*(1.D0 - (EPS(I)-FT(I)/YOUN0(I))/
144      $                        (EPSULT(I)-FT(I)/YOUN0(I)))
145                     CRACKD = .TRUE.
146                 ELSE
147                     SIGMA(I) = EPS(I)*YOUN0(I)
148                 END IF
149                 SIGRF(1) = SIGMA(I)
150                 IF ( ITER .EQ. 0 ) THEN
151                     YOUN(I) = YOUN0(I)
152                 ELSE
153                     YOUN(I) = MAX( STFFAC*YOUN0(I), SIGRF(1)/ALPHA(1) )
154                 END IF
155             ELSE IF ( ABS(ALPHA(1)) .GT. 1.D+6*DPMPAR(1) ) THEN
156 C...          TENSILE UNLOADING AND RELOADING
157                 SIGMA(I) = EPS(I)*SIGRF(1)/ALPHA(1)
158                 IF ( ITER .EQ. 0 ) THEN
159                     YOUN(I) = YOUN0(I)
160                 ELSE
161                     YOUN(I) = MAX( STFFAC*YOUN0(I), SIGRF(1)/ALPHA(1) )
162                 END IF
163             ELSE
164                 SIGMA(I) = YOUN0(I) * EPS(I)
165                 YOUN(I) = YOUN0(I)
166             END IF
167         ELSE IF ( EPS(I) .LE. 0.D0 ) THEN
168 C...      ELEMENT IN COMPRESSION
169             IF ( EPS(I) .LT. -FC(I)/YOUN0(I) ) THEN
170 C...          IF THE STRAIN IS LARGER THAN THE ELASTIC LIMIT IN
      COMPRESSION THE PARAMETER FAIMEC IS INCREASED OF 4 OR 8 (ACCORDING
      TO THE DIRECTION)
171                 FAIMEC = FAIMEC + 4 * I
172             END IF
173             IF ( EPS(I) .LT. ALPHA(2) ) THEN
174 C...          NEW COMPRESSIVE EXTREME
175                 ALPHA(2) = EPS(I)
176 C...          SEQUENCE OF 3RD ORDER AND PARABOLIC
177                 ESTAR = FC(I)/YOUN0(I)
178                 EPSCP(I) = EPSCFA(I)*ESTAR
179                 N = EPSCFA(I)
180                 EPSULC = EPSCP(I) + 2.D0*GFC(I)/(HCRAC*FC(I))-
181      $              (3.D0*N+4.D0)*FC(I)/(6.D0*N*YOUN0(I)) -
182      $              2.D0*FC(I)*(7.D0*N**3.D0-9.D0*N**2.D0+2)/
183      $              (3.D0*YOUN0(I)*N*(3.D0*N-2))
184                 EPSULC = MAX( EPSULC, EPSCP(I) )
185                 EPS(I) = -EPS(I)
186                 IF      ( EPS(I) .LT. ESTAR ) THEN
187                     SIGMA(I) = (-2.D0+N)/(3.D0*N-2.D0)*
188      $                  YOUN0(I)**3.D0/FC(I)**2.D0*EPS(I)**3.D0 -
189      $                  (3.D0*N**2.D0-6.D0*N+2.D0)/(N*(3.D0*N-2.D0))*
190      $                  YOUN0(I)**2.D0/FC(I)*EPS(I)**2.D0 +
191      $                  YOUN0(I)*EPS(I)
192                     CRUSHD = .TRUE.
193                 ELSE IF ( EPS(I) .LT. EPSCP(I) ) THEN
194                     SIGMA(I) = -2.D0/(N*(3.D0*N-2.D0))*
195      $                  YOUN0(I)**2.D0/FC(I)*EPS(I)**2.D0 +
```

```fortran
196     $                  4.D0/(3.D0*N-2.D0)*YOUN0(I)*EPS(I)+
197     $                  (-2.D0+N)/(3.D0*N-2)*FC(I)
198                    CRUSHD = .TRUE.
199                ELSE IF ( EPS(I) .LT. EPSULC ) THEN
200                    SIGMA(I) = FC(I)*(EPS(I)-EPSULC)/(EPSCP(I)-EPSULC)
201                    SIGMA(I) = MAX( SIGMA(I), 0.1D0*FC(I) )
202                    CRUSHD = .TRUE.
203                ELSE
204                    SIGMA(I) = 0.1D0*FC(I)
205                    CRUSHD = .TRUE.
206                END IF
207                SIGMA(I) = -SIGMA(I)
208                EPS(I)   = - EPS(I)
209                SIGRF(2) = SIGMA(I)
210                IF ( ITER .EQ. 0 ) THEN
211                    YOUN(I) = YOUN0(I)
212                ELSE
213                    YOUN(I) = MAX( STFFAC*YOUN0(I), SIGRF(2)/ALPHA(2) )
214                END IF
215            ELSE IF ( EPS(I) .LT. EPS0(I) ) THEN
216 C...          COMPRESSIVE RELOADING
217                IF ( ABS( ALPHA(2)-EPS0(I) ) .LT. 1.D+6*DPMPAR(1) ) THEN
218                    SIGMA(I) = SIG0(I) + YOUN0(I)*DEPS(I)
219                ELSE
220                    SIGMA(I) = SIG0(I)+DEPS(I)*(SIGRF(2)-SIG0(I))/
221     $                        (ALPHA(2)-EPS0(I))
222                END IF
223                IF ( ITER .EQ. 0 .OR.
224     $               ABS( ALPHA(2) ) .LT.  1.D+6*DPMPAR(1) ) THEN
225                    YOUN(I) = YOUN0(I)
226                ELSE
227                    YOUN(I) = MAX( STFFAC*YOUN0(I), SIGRF(2)/ALPHA(2) )
228                END IF
229            ELSE IF( ALPHA(2) .EQ. 0 ) THEN
230                SIGMA(I) = 0.D0
231            ELSE
232 C...          COMPRESSIVE UNLOADING
233                IF ( EPS(I) .LT.
234     $               ALPHA(2)-(1.D0-UNLFAC)*SIGRF(2)/YOUN0(I) ) THEN
235                    SIGMA(I) = SIGRF(2)+YOUN0(I)*(EPS(I)-ALPHA(2))
236                ELSE
237                    SIGMA(I) = EPS(I)*UNLFAC*SIGRF(2)/
238     $                        (ALPHA(2)-(1.D0-UNLFAC)*SIGRF(2)/YOUN0(I))
239                END IF
240                IF ( ITER .EQ. 0 .OR.
241     $               ABS( DEPS(I) ) .LT. 1.D+6*DPMPAR(1) ) THEN
242                    YOUN(I) = YOUN0(I)
243                ELSE
244                    YOUN(I) = MAX( STFFAC*YOUN0(I),
245     $                        (SIGMA(I)-SIG0(I))/DEPS(I) )
246                END IF
247            END IF
248        END IF
249        IF ( CRACKD ) THEN
250            USRIND(I) = 1
251            NCRACK = NCRACK + 1
```

```fortran
252                IDIR(NCRACK) = I
253                NUMCR(NCRACK) = NCRACK
254                IF ( EPS(I) .GT. 0.D0 ) THEN
255                   NOPCRK = NOPCRK + 1
256                   ISCRK(NCRACK) = 2
257                ELSE
258                   ISCRK(NCRACK) = -2
259                END IF
260             END IF
261             IF ( CRUSHD ) USRIND(I+2) = 1
262             USRSTA(I)   = ALPHA(1)
263             USRSTA(I+2) = ALPHA(2)
264             USRSTA(I+4) = SIGRF(1)
265             USRSTA(I+6) = SIGRF(2)
266             CRCKED = CRCKED .OR. CRACKD
267             CRSHED = CRSHED .OR. CRUSHD
268       100 CONTINUE
269
270
271 C...   SHEAR RETENTION
272 C
273 C...   FRICTIONAL CRITERION
274       SHRMAX = USRSTA(9)
275       COH1 = USRSTA(11)
276       IF ( EPS(1) .GT. 0.D0 ) THEN
277 C...      COMBINATION OF SHEAR AND HORIZONTAL TENSION
278          IF ( SIGSHR .LT. 0.D0 ) THEN
279             SIGSHR = -SIGSHR
280             SI0SHR = -SI0SHR
281             EPSSHR = -EPSSHR
282             DEPSHR = -DEPSHR
283             I = 1
284          ELSE
285             I = 0
286          END IF
287          EPSHEQ = EPSSHR + EPS(1)/TAN(ANGLE0)
288          IF ( USRSTA(18) .EQ. 0.D0 ) THEN
289 C...         PRE-PEAK
290             IF ( EPSHEQ .LT. 1.D+6*DPMPAR(1) ) THEN
291                SHRMEQ = SHRM0
292             ELSE
293                SHRMEQ = ( SHRM0*EPSSHR + YOUN0(1)*EPS(1)*TAN(ANGLE0) )
294     $                      / EPSHEQ
295             END IF
296          ELSE
297 C...         POST-PEAK
298             SHRMEQ = USRSTA(18)
299          END IF
300          SHRULT = 2.D0*GFS/(HCRAC*COH0)-COH0/SHRMEQ
301          IF ( SHRULT .GT. 1.D+6*DPMPAR(1) ) THEN
302             COH1 = COH0*(SHRULT-SHRMAX)/SHRULT
303             COH1 = MAX( 0.D0, COH1 )
304          ELSE IF ( SHRMAX .EQ. 0.D0 ) THEN
305 C...         GFS TOO SMALL, PRE-PREAK
306             COH1 = COH0
307          ELSE
```

```fortran
308 C...          GFS TOO SMALL, POST-PEAK
309                COH1 = 0.D0
310             END IF
311             IF ( CRCKED ) COH1 = 0.D0
312             TAUMAX   = MAX(0.D0, COH1-SIGMA(2)*TANPHI)
313             SIGSHR   = MIN( SIGSHR, TAUMAX )
314             SIGMA(1) = MIN( MAX(SIGMA(1),0.D0) , TAUMAX/TAN(ANGLE0))
315             TAUEQ    = SIGSHR + SIGMA(1)*TAN(ANGLE0)
316             IF ( ABS(TAUEQ) .GE. TAUMAX ) THEN
317                FAIMEC = FAIMEC + 16
318                IF ( DEPS(1) .LT. 0.D0 ) THEN
319 C...             SHEAR LOADING, TENSILE UNLOADING
320                   SIGSHR = TAUMAX - SIGMA(1)*TAN(ANGLE0)
321                ELSE IF ( SIGSHR*SI0SHR .LT. 0.D0 ) THEN
322 C...             TENSILE LOADING, SHEAR UNLOADING TO ZERO
323                   SIGSHR = 0.D0
324                   SIGMA(1) = TAUMAX/TAN(ANGLE0)
325                ELSE IF ( DEPSHR .LT. 0.D0 )   THEN
326 C...             TENSILE LOADING, SHEAR UNLOADING
327                   SIGMA(1) = (TAUMAX - SIGSHR)/TAN(ANGLE0)
328                ELSE
329 C...             SIMULTANEOUS SHEAR AND TENSILE LOADING
330                   IF ( ( SIG0(1)*TAN(ANGLE0) + SI0SHR )
331      $                            .LT. 1.D+6*DPMPAR(1) ) THEN
332                      RATIO = 0.5D0
333                   ELSE
334                      RATIO = SI0SHR / (SIG0(1)*TAN(ANGLE0) + SI0SHR)
335                   END IF
336 C...             RATIO BETWEEN SHEAR AND HORIZONTAL TESNION IS MAINTAINED
        DURING SOFTENING AND YIELDING
337                   SIGSHR   = RATIO*TAUMAX
338                   SIGMA(1) = (1.D0 - RATIO)*TAUMAX/TAN(ANGLE0)
339                END IF
340                USRSTA(18) = SHRMEQ
341 C...          SHRMEQ IS KEPT CONSTANT AFTER PEAK
342                DEPSEQ = DEPSHR + DEPS(1)/TAN(ANGLE0)
343                SHRMAX = SHRMAX + ABS( DEPSEQ )
344                FRCFAI = 1
345             END IF
346             IF ( I .EQ. 1 ) SIGSHR = -SIGSHR
347          ELSE
348 C...      SHEAR WITHOUT HORIZONTAL TENSION
349             TAUEQ = ABS(SIGSHR)
350             IF ( USRSTA(18) .EQ. 0.D0 ) THEN
351 C...          PRE-PEAK
352                SHRMEQ = SHRM0
353             ELSE
354 C...          POST-PEAK
355                SHRMEQ = USRSTA(18)
356             END IF
357             SHRULT = 2.D0*GFS/(HCRAC*COH0)-COH0/SHRMEQ
358             IF ( SHRULT .GT. 1.D+6*DPMPAR(1) ) THEN
359                COH1 = COH0*(SHRULT-SHRMAX)/SHRULT
360                COH1 = MAX( 0.D0, COH1 )
361             ELSE IF ( SHRMAX .EQ. 0.D0 ) THEN
362                COH1 = COH0
```

```fortran
363             ELSE
364                COH1 = 0.D0
365             END IF
366             IF ( CRCKED ) COH1 = 0.D0
367             TAUMAX =  MAX(0.D0, COH1-SIGMA(2)*TANPHI)
368             IF      ( ABS(SIGSHR) .GT.  TAUMAX ) THEN
369 C...          IF THE SHEAR STRESS IS LARGER THAN THE LIMIT THE PARAMETER
    FAIMEC IS INCREASED OF 16
370                FAIMEC = FAIMEC + 16
371                IF ( SIGSHR .GT.  TAUMAX ) SIGSHR =  TAUMAX
372                IF ( SIGSHR .LT. -TAUMAX ) SIGSHR = -TAUMAX
373                USRSTA(18) = SHRMEQ
374                EPSHEQ = ABS(EPSSHR)
375                SHRMAX = SHRMAX + ABS( DEPSHR )
376                FRCFAI = 1
377             END IF
378          END IF
379          IF ( USRSTA(18) .NE. 0.D0 ) USRSTA(19) =
380      $                              (EPSHEQ-TAUMAX/SHRMEQ)*HCRAC
381       USRSTA(9)  = SHRMAX
382       USRSTA(11) = COH1
383 C
384 C
385          CALL RSET( 0.D0, STIFF, NS*NS )
386          STIFF(1,1) = YOUN(1)
387          STIFF(2,2) = YOUN(2)
388          STIFF(3,3) = SHRMOD
389          SIGMA(3)   = SIGSHR
390          CALL RSET( 0.D0, EPSP, 4 )
391          IF ( USRIND(1) .EQ. 1 ) EPSP(2) = MAX( 0.D0, EPS(1)*HCRAC )
392          IF ( USRIND(2) .EQ. 1 ) EPSP(1) = MAX( 0.D0, EPS(2)*HCRAC )
393       USRIND(5) = FRCFAI
394
395       USRSTA(10) = DBLE( FAIMEC )
396       USRSTA(12) = DBLE( FRCFAI )
397       USRSTA(13) = TAUEQ/TAUMAX
398       IF ( CRSHED ) USRSTA(14) = 1.D0
399       USRSTA(15) = DBLE( USRIND(1) )
400       USRSTA(16) = DBLE( USRIND(2) )
401       USRSTA(17) = TAUMAX
402 C
403 C...  POST PROCESSING ITEMS
404       CALL PTL( 'ISCRK', ISCRK, 6 )
405       IF ( CRCKED ) THEN
406 C...     WRITE POSTPROCESSING STUFF FOR CRACKS
407          CRACKS(1) = NCRACK
408          CRACKS(2) = NOPCRK
409          DO 400, ICRACK = 1, NCRACK
410             CALL PTXL( 'CRACK/ICRDIR', ICRACK, IDIR(ICRACK), 1 )
411             CALL PTXL( 'CRACK/AXES',   ICRACK, CRAXES, NCR*NCR )
412             EPSCR((ICRACK-1)*NCR+1) = MAX( 0.D0, EPS(IDIR(ICRACK))   )
413             SIGCR((ICRACK-1)*NCR+1) = MAX( 0.D0, SIGMA(IDIR(ICRACK)) )
414                EPSCR((ICRACK-1)*NCR+2) = EPS(3)
415                SIGCR((ICRACK-1)*NCR+2) = SIGMA(3)
416   400     CONTINUE
417 C
```

```
418            CALL PTL( 'CRACKS', CRACKS, 2 )
419            CALL PTL( 'NUMCR',  NUMCR,  3 )
420            CALL PTL( 'EPSCR',  EPSCR, NCR*MOPCRK )
421            CALL PTL( 'SIGCR',  SIGCR, NCR*MOPCRK )
422         END IF
423 C
424         END
```
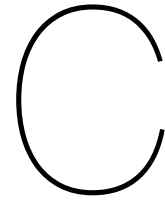
Exemplary Input Files for the Single Element Model Analysis

Listing C.1: The `.dat`-file used for the single element model analysis with the Equivalent Shear Masonry Model for load case G1

```
: Diana Datafile written by Diana 10.2
'DIRECTIONS'
   1   1.00000E+00    0.00000E+00    0.00000E+00
   2   0.00000E+00    1.00000E+00    0.00000E+00
   3   0.00000E+00    0.00000E+00    1.00000E+00
'MODEL'
DIMENS "2D"
GRAVDI 2
GRAVAC  -9.81000E+00
'COORDINATES'
   1   1.00000E-01    1.00000E-01    0.00000E+00
   2   1.00000E-01    0.00000E+00    0.00000E+00
   3   0.00000E+00    0.00000E+00    0.00000E+00
   4   0.00000E+00    1.00000E-01    0.00000E+00
'MATERI'
   1 USRMAT
     YOUNG    3.40000E+09
     POISON   0.00000E+01
     USRVAL   2.20000E+09    3.40000E+09    1.30000E+09    6.84137E-01
              1.00000E+05    1.00000E+05    5.00000E+00    5.00000E+00
              1.40000E+07    1.40000E+07    2.00000E+04    2.00000E+04
              3.00000E-01    1.50000E+05    5.00000E+00    0.50000E+00
              4.00000E+00    4.00000E+00    1.00000E-01
     USRSTA   0.00000E+00    0.00000E+00    0.00000E+00    0.00000E+00
              0.00000E+00    0.00000E+00    0.00000E+00    0.00000E+00
              0.00000E+00    0.00000E+00    0.00000E+00    0.00000E+00
              0.00000E+00    0.00000E+00    0.00000E+00    0.00000E+00
              0.00000E+00    0.00000E+00
     USRIND 0 0 0 0 0
     ASPECT
'GEOMET'
   1 GCNAME  SHEET
     GEOMDL  MEMBRA
     XAXIS    1.00000E+00    0.00000E+00    0.00000E+00
     THICK    1.00000E-01
```

```
'DATA'
   1 INTEGR REDUCE
'ELEMENTS'
SET  "Sheet 1"
CONNECT
   1 Q8MEM  2 1 4 3
MATERIAL 1
GEOMETRY 1
DATA 1
'LOADS'
CASE 1
NAME "overload"
ELEMEN
1    EDGE   KSI2
     FORCE   -4.00000E+04
     DIRECT 2
CASE 2
NAME "shear"
DEFORM
4    TR 1   1.00000E-01
CASE 3
NAME "horizontal extension"
DEFORM
2    TR 1   1.00000E-01
'SUPPOR'
NAME "support bottom"
/ 2 3 / TR 2
/ 2 3 / TR 1
NAME "support top"
4    TR 1
'TYINGS'
NAME "tying top right node"
FIX TR 1
   1  4 TR 1  1.
      2 TR 1  1.
EQUAL TR 2
1     4
'TIMELO'
LOAD 2
TIMES   0.00000E+00   1.50000E+02 /
FACTOR   0.00000E+00   1.50000E-03 /
LOAD 3
TIMES   0.00000E+00   0.50000E+02   1.50000E+02 /
FACTOR   0.00000E+00   0.50000E-03  -0.50000E-03 /
'END'
```

Listing C.2: The `.dcf`-file used for the single element model analysis with the Equivalent Shear Masonry Model for load case G1

```
*FILOS
INITIA
*INPUT
*FORTRAN
 USE "usrmat_eqshma.dll"
*NONLIN LABEL="Structural nonlinear"
  BEGIN EXECUT
    TEXT "application overload"
```

```
    BEGIN LOAD
      LOADNR 1
      STEPS EXPLIC SIZES 0.100000(10)
    END LOAD
    ITERAT METHOD NEWTON
  END EXECUT
  BEGIN EXECUT
    TEXT "application shear"
    TIME STEPS EXPLIC SIZES 1.00000(150)
    BEGIN ITERAT
      MAXITE 50
      METHOD NEWTON
      BEGIN CONVER
        FORCE CONTIN
        DISPLA CONTIN
      END CONVER
    END ITERAT
  END EXECUT
  SOLVE PARDIS
  BEGIN OUTPUT
    TEXT "Output"
    TABULA
    LAYOUT LINPAG 0
    SELECT STEPS ALL /
    BEGIN STRAIN
      BEGIN TOTAL
        BEGIN GREEN
          BEGIN GLOBAL
            XX YY ZZ XY YZ ZX
            INTPNT
          END GLOBAL
        END GREEN
      END TOTAL
    END STRAIN
    BEGIN STRESS
      BEGIN TOTAL
        BEGIN CAUCHY
          BEGIN GLOBAL
            XX YY ZZ XY YZ ZX
            INTPNT
          END GLOBAL
        END CAUCHY
      END TOTAL
    END STRESS
    STATUS CRACK
    STATUS USER
  END OUTPUT
*END
```

Bibliography

[1] *Application Example of an User-supplied DLL in DIANA 9.5 / 9.6*.

[2] `usrmat_quad2.f`. User supplied subroutine.

[3] DIANA FEA BV. User's Manual – Release 10.2, Analysis Procedures, 2017. `https://dianafea.com/manuals/d102/Diana.html`.

[4] DIANA FEA BV. Diana - Finite Element Analysis - Release 10.2, 2017. Software. Retrieved from `https://dianafea.com/content/sales`.

[5] DIANA FEA BV. User's Manual – Release 10.2, Material Library, 2017. `https://dianafea.com/manuals/d102/Diana.html`.

[6] DIANA FEA BV. User's Manual – Release 10.2, Theory Manual, 2017. `https://dianafea.com/manuals/d102/Diana.html`.

[7] S. Jafari and R. Esposito. Material tests for the characterisation of replicated solid clay brick masonry. Technical report, Delft University of Technology, August 2017. Report number C31B67WP1-12, version 01.

[8] P. Korswagen, M. Longo, E. Meulman, and C. Van Hoogdalem. Damage sensitivity of Groningen masonry structures – Experimental and computational studies. Technical report, November 2017. Report number C31B69WP0-11, Final report, version 1.0.

[9] P. Korswagen, M. Longo, and E. Meulman. Damage sensitivity of Groningen masonry structures – Experimental and computational studies – Stream 2 – Part 1. Technical report, 26 June 2019. Report number C31B69WP0-14, ongoing, version 1.0.

[10] P.A. Korswagen, M. Longo, E. Meulman, and J.G. Rots. Crack initiation and propagation in unreinforced masonry specimens subjected to repeated in-plane loading during light damage. *Bulletin of Earthquake Engineering*, 17(8):4651–4687, Aug 2019.

[11] P.J.B.B. Lourenço. *Computational Strategies for Masonry Structures*. PhD thesis, Technische Universiteit Delft, February 1996.

[12] G. Ravenshorst and F. Messali. In-plane tests on replicated masonry walls. Physical testing and modelling – Masonry structures. Technical report, Delft University of Technology, 27 May 2016. Final report.

[13] J.G. Rots. Private converstations, February 2018.

[14] J.G. Rots, F. Messali, R. Esposito, S. Jafari, and V. Mariani. Computational modelling of masonry with a view to Groningen induced seismicity. In *Structural Analysis of Historical Constructions. Anamnesis, diagnosis, therapy, control. Proceedings of the 10th International Conference on Structural Analysis of Historical Constructions (SAHC, Leuven, Belgium, 13-15 September 2016)*. "Structural Mechanics, Civil Engineering and Geosciences, TU Delft, Delft, Netherlands", 2016.

[15] G. Schreppers. `engmas.f`, February 2016. Material subroutine. TNO DIANA BV.

[16] G.M.A. Schreppers, A. Garofano, F. Messali, and J.G. Rots. Diana Validation report for Masonry modelling. Technical report, DIANA FEA BV and TU Delft, February 2017. DIANA FEA report 2016-DIANA-R1601, TU Delft Structural Mechanics CiTG report CM-2016-17.

[17] L.J. Sluys. Computational methods in nonlinear solid mechanics (CIE5142), 23 April - 13 June 2014. Lecture serie.

[18] R. van der Pluijm. Material properties of masonry and its components under tension and shear. In *Proc. 6th Canadian Masonry Symposium*, pages 675–686, 1992.

[19] G.N. Wells. The finite element method: An introduction, 2011.

[20] A. Wolthers, K. Palacio, and G. Schreppers. *User-supplied Subroutines*. TNO DIANA BV, February 2011.